

Bacterial Streamer Formation in Porous Media

by

Mahtab Hassanpourfard

A thesis submitted in partial fulfillment of the requirements for the degree of

Doctor of Philosophy

in

Chemical Engineering

Department of Chemical and Materials Engineering  
University of Alberta

© Mahtab Hassanpourfard, 2017

## **Abstract**

One of the central puzzles concerning the interaction of low Reynolds number ( $Re \ll 1$ ) fluid transport with bacterial biomass is the formation of filamentous structures called bacterial streamer. Bacterial streamers can be tethered at one or both ends to solid surfaces, while the rest of the structure is suspended in liquid. Bacterial streamer formation in low  $Re$  fluid transport is of significant technological and biomedical interest due to relevance to a wide variety of critical operating scenarios including clogging of biomedical devices such as heart stents, catheters, porous media, and water filtration systems. In the present study, we investigate formation and temporal evolution of biofilm-mediated streamers. These streamers form from deformation of pre-formed biofilm on a surface after several hours of injecting bacterial solution into the microfluidic device. Once the streamers form, they accelerate the clogging by accruing more biomass from the injected flow. Our experiments, carried out in a microfluidic device, rely on fluorescence microscopy techniques. Our microfluidic device consists of an array of micro-posts, which was fabricated using soft-lithography. Detailed procedures for experimentation with the microfluidic device are also presented in this study.

We report our discovery of a new kind of low  $Re$  bacterial streamers, which appear from pre-formed bacterial flocs. In sharp contrast to the biofilm-mediated streamers, these streamers form over extremely small timescales (less than a second). We demonstrate that floc-mediated streamers form when a freely-moving floc adheres to the micropillar's wall and gets rapidly sheared by the background flow. We also show that, at their inception, the deformation of the flocs is dominated by recoverable large strains indicating significant

elasticity. These strains subsequently increase tremendously to produce filamentous streamers. Interestingly, we find that these fully formed streamers are not static structures and show viscous response at time scales larger than their formation time scales. We also show that such novel streamer formation can lead to rapid clogging of microfluidic devices.

Thereafter, the clogging dynamics of bacterial biomass that accumulated in the device due to the formation of bacterial streamers is investigated. Particularly, we find the existence of a distinct clogging front which advances via pronounced ‘stick-slip’ of the viscoelastic bacterial biomass over the solid surface of the micro pillar. Thus, the streamer, the solid surface, and the background fluidic media define a clear three-phase front influencing these advancing dynamics. Interestingly, we also find that once the clogging becomes substantial, contrary to a static homogenous saturation state, the clogged mimic exhibits an instability phenomena marked by localized streamer breakage and failure leading to extended water channels throughout the mimic. These findings have implications for design and fabrication of biomedical devices, and membrane-type systems such as porous balloon catheters, porous stents, and filtration membranes prone to bacteria induced clogging as well as understanding bacterial growth and proliferation in natural porous media such as soil and rocks.

Finally, we study the impact of nanoparticles as antibacterial agents to combat biofilm formation. In our work, we use  $\text{Mg(OH)}_2$  nano-platelets to inhibit the growth of planktonic bacteria, and consequently biofilm and bacterial streamer formation. The results demonstrate that depending on the concentration of  $\text{Mg(OH)}_2$  nano-platelets in the solution they can act as an

antibacterial or a bacteriostatic agent for *Pseudomonas fluorescens* as a model organism for biofilm formation. Furthermore, they can inhibit streamer formation in the microfluidic devices.

## **Preface**

Chapter 2 of this thesis has been published as Hassanpourfard, Mahtab, Xiaohui Sun, Amin Valiei, Partha Mukherjee, Thomas Thundat, Yang Liu, and Alope Kumar. "Protocol for biofilm streamer formation in a microfluidic device with micro-pillars." *JoVE (Journal of Visualized Experiments)* 90 (2014): e51732-e51732. I was responsible for performing the experiments (including chip fabrication, bacterial culture, and microfluidic experiments), results analysis, manuscript composition, and revising the video scripts. I also was involved in the video shoot. Xiaohui Sun was involved in bacterial solution preparation and manuscript composition. Amin Valiei helped with microfluidic experiments. Partha Mukherjee helped with Comsol simulation. Thomas Thundat and Yang Liu were supervisory authors. Alope Kumar was supervisory author who was involved with concept formation, results analysis, manuscript composition, and revising the video scripts. He was also involved in the video shoot. All the authors contributed to the reviewing of the manuscript.

Chapter 3 of this thesis has been published as Hassanpourfard, Mahtab, Zahra Nikakhtari, Ranajay Ghosh, Siddhartha Das, Thomas Thundat, Yang Liu, and Alope Kumar. "Bacterial floc mediated rapid streamer formation in creeping flows." *Scientific reports* 5 (2015). I was responsible for designing and performing the experiments (including chip fabrication, bacterial culture, and microfluidic experiments), results analysis, and Comsol simulations. Zahra Nikakhtari helped with bacterial culturing and preparing figures. Ranajay Ghosh helped with data analysis. Siddhartha Das, Thomas Thundat, and Yang Liu played an advisory role. Alope Kumar conceived and designed the

experiments and helped with data analysis. He also had an advisory role. All the authors contributed to the writing of manuscript.

Chapter 4 of this thesis has been published as Hassanpourfard, Mahtab, Ranajay Ghosh, Thomas Thundat, and Alope Kumar. "Dynamics of bacterial streamers induced clogging in microfluidic devices." *Lab on a Chip* (2016). I was responsible for designing and performing the experiments (including chip fabrication, bacterial culture, and microfluidic experiments), and results analysis. Ranajay Ghosh was involved in data analysis. Alope Kumar was involved in designing the experiments. He also played an advisory role. Thomas Thundat played an advisory role. All the authors contributed to the writing of the manuscript.

Chapter 5 of this thesis has been prepared as Hassanpourfard, Mahtab, Zahra Nikakhtari, Ravi Gaikwad, Alope Kumar, Orville Lee Maddan and Thomas Thundat. "Antibacterial effect of  $Mg(OH)_2$  nano-platelets on *Pseudomonas fluorescens* and its consequences on bacterial streamer formation in a microfluidic device." I was involved in conceiving, designing and performing the experiments. I also was responsible for data analysis and manuscript writing. Zahra Nikakhtari helped in performing the experiments and writing the manuscript. Ravi Gaikwad did the Atomic Force Microscopy (AFM) experiments and he helped in writing materials related to the AFM test. Alope Kumar played an advisory role. Orville Lee Madden prepared the  $Mg(OH)_2$  nano-platelets. Thomas Thundat conceived the experiments and played an advisory role.

*I would like to dedicate my thesis to my parents, Zari and Hossein, my uncle, Parviz, and my husband, Ali, for their love, supports, and encouragements.*

## **Acknowledgments**

I would like to express my deepest respect and gratitude to my supervisors, Professor Thomas Thundat and Dr. Alope Kumar, for all the inspiration and help, not only as research supervisors, but also as great life mentors. I would like to greatly acknowledge their patience, innovations, enthusiasm, and supports during the years of my Ph.D. They were always available for discussion and their comments were always insightful. It has been an honor to be their Ph.D. student.

I would like to thank Dr. Yang Liu for making her lab facilities available to me and also I would like to thank her graduate students and especially Xiaohui Sun who helped me.

I would like to thank Ni Yang for helping me using OSCIEF facilities. I would also like to thank all the personnel at Micro and Nanofabrication Facilities at university of Alberta for training me and providing their assistance in using various facilities.

I would like to acknowledge the financial support provided by Alberta Innovates Graduate Student Scholarship.

I would also like to thank all my group mates in our research group especially Parmiss Mojir Shaibani, Ghazaleh Haghghat, Amirreza Sohrabi, Amin Valiei, Zahra Nikhakhtari, Keren Jiang, Jun Liu, Inseok Chae, Faheem khan, and Priyesh Dhandharia for helping me during my research.

I am thankful to my parents and my husband who always support my decisions and encourage me to follow my dreams. Without their support, it was impossible to complete this journey.

## Table of Contents

1	Introduction.....	1
1.1	Bacterial communities & biofilms.....	1
1.2	Biofilms in porous media .....	4
1.3	Bacterial streamers- Filamentous biofilms.....	6
1.4	Objectives of this study .....	10
1.5	References .....	12
2	Protocol for biofilm streamer formation in a microfluidic device with micro-pillars .....	17
2.1	Introduction .....	17
2.2	Experimental .....	19
2.3	Results .....	23
2.4	Discussion .....	27
2.5	References .....	30
3	Bacterial floc mediated rapid streamer formation in creeping flows.....	32
3.1	Introduction .....	32
3.2	Experimental .....	36
3.2.1	Microchip fabrication:.....	36
3.2.2	Bacterial culture .....	36
3.2.3	Microscopy.....	37
3.2.4	Computational fluid mechanical (numerical) simulations .....	38

3.2.5	Velocity gradient calculation .....	38
3.3	Results .....	39
3.3.1	Initiation of floc-mediated streamers .....	39
3.3.2	Timescale and mechanism of floc-mediated streamer formation	45
3.3.3	Clogging action of the floc-mediated streamers .....	50
3.4	Discussion .....	52
3.5	References .....	56
4	Dynamics of bacterial streamers induced clogging in microfluidic devices	60
4.1	Introduction .....	60
4.2	Experimental .....	62
4.3	Results and discussion.....	65
4.4	Conclusion.....	76
4.5	References .....	77
5	Antibacterial effect of Mg(OH) <sub>2</sub> nano-platelets on <i>Pseudomonas fluorescens</i> and its consequences on bacterial streamer formation in a microfluidic device.....	81
5.1	Introduction: .....	81
5.2	Experimental .....	83
5.2.1	Bacterial culture .....	83
5.2.2	Agar plate experiment.....	84
5.2.3	Particle preparation for atomic force microscopy (AFM) studies	84

5.2.4	Bacterial solution preparation for AFM studies.....	85
5.2.5	Microchip fabrication.....	85
5.2.6	Nano-platelets characteristics and our experimental setup.....	85
5.3	Results and discussion.....	88
5.3.1	Antibacterial effect of Mg(OH) <sub>2</sub> nano-platelets on <i>P. fluorescens</i> 88	
5.3.2	Antibacterial effect of Mg(OH) <sub>2</sub> nano-platelets on <i>P. fluorescens</i> and its consequences on streamer formation.....	91
5.4	References .....	94
6	Concluding remarks .....	97
6.1	Conclusions .....	97
6.2	Future work .....	100
	References.....	102

## List of Tables

<b>Table 3.1:</b> Time scale of streamer formation from different experiments .....	34
<b>Table 4.1:</b> $t_0$ for different imposed flow speeds .....	68
<b>Table 4.2:</b> Repetitions per experiment .....	69
<b>Table 5.1:</b> Bacterial growth on agar plates according to visual observations ...	89

## List of Figures

<b>Figure 1.1:</b> 5 stages of biofilm development. 1) Transport and reversible attachment of bacteria cells to surface. 2) Irreversible attachment of bacteria and EPS production. 3) Microcolonies formation by replication, growth and EPS production of adsorbed cells. 4) Biofilm formation. 5) Detachment of some bacterial cells from biofilm [4, 8, 9]. .....	2
<b>Figure 1.2:</b> a) Biofilm in stagnant condition. b) Sustained fluid flow can lead to the deformation of a biofilm into a slender structure called streamer.....	7
<b>Figure 2.1:</b> Scanning electron microscope (SEM) images of the microfluidic channel (top-view). a) Inlet section, b) Region containing micro-pillars. ....	25
<b>Figure 2.2:</b> Sequential steps involved in bacterial culture. ....	25
<b>Figure 2.3:</b> Set up for microfluidic experiments. 1- Optical microscope (inverted), 2- Syringe pump, 3- Image and data acquisition, 4- Syringe containing dye (optional), 5- Syringe containing bacteria, 6- Waste reservoir. ....	26
<b>Figure 2.4:</b> Time-lapse confocal imaging of evolution of streamers. Image plane corresponds to $z= 25 \mu\text{m}$ i.e. middle of device. Dashed ellipses demonstrate biofilm streamers. ....	26
<b>Figure 2.5:</b> Computational fluid mechanical simulations showing streamlines and velocity contours of flow past micro-pillars. Fluid flow is from top to bottom and velocity scale is in m/s. ....	27
<b>Figure 3.1:</b> a) A schematic of experimental set-up under pressure driven flow with constant volume flow rate ( $Q$ ). b) Layout of staggered pattern porous media. Width ( $W$ ) of porous zone is $625 \mu\text{m}$ . The distance between the center of pillars ( $l$ ) and 2 rows of consecutive pillars is $75 \mu\text{m}$ . The diameter of the pillars and the height of the device ( $h_c$ ) both are $50 \mu\text{m}$ . c) Computational fluid mechanical simulations demonstrating the non-dimensionalized velocity (	

$\sqrt{v_x^2 + v_y^2} / U$ ) contour of the flow in the porous section of the microchannel.  $v_i$  depicts fluid velocity in  $i$ -th direction. In our device  $Q = 15 \mu\text{l/hr}$  corresponds to  $1.3 \times 10^{-4} \text{ m/s}$ . The scale bar is  $50 \mu\text{m}$ . (Inset) Streamlines for the same flow condition. ....40

**Figure 3.2:** a) Flocs of *P. fluorescens* bacteria after incubation at  $30^\circ\text{C}$  overnight. The scale bars are  $25 \mu\text{m}$ . b) Relative frequency histogram of the flocs. The  $x$ -axis is equivalent diameter of the flocs in the reservoir. The median and mode for this relative frequency histogram are  $21.28$  and  $22.23 \mu\text{m}$ , respectively. c) and d) Green and red fluorescent images, respectively, of the microchannel after injecting the bacteria with  $200 \text{ nm}$  fluorescent red polystyrene beads particles into it. The images were taken at the same time and place that was approximately at the middle of the channel height ( $z = 25 \mu\text{m}$ ). The red fluorescent particles clearly seed and enable visualization of the streamer. Note the regions demarcated by dashed ellipses where bacteria (green) are not significant, but the streamer itself is easy visualized due to red particles seeding the EPS network. The scale bars are  $50 \mu\text{m}$ . ....42

**Figure 3.3:** a) Relative frequency histogram of the flocs cultured in M9 media. The median and mode for this relative frequency histogram are  $6.78$  and  $5.85 \mu\text{m}$ , respectively b) and c) Comparison of streamer formation in LB and M9 media. Streamers did not form in M9 media at short-time scales ( $\sim$  few minutes) as compared to LB media. ....42

**Figure 3.4:** a) Rapid streamer formation in a short time scale (a few seconds). The scale bars are  $50 \mu\text{m}$ . See accompanying video. The images were taken approximately at the middle of the channel height ( $z = 25 \mu\text{m}$ ). In the top-left image, the arrows demarcate the advancing fluid meniscus. The ellipses demarcate two regions where streamers form. b) An arrow demarcates a floc,

which is first advected through the channel and then is attached to a micropillar wall at  $t=47$  s. Finally, at 95 s a streamer is formed. Scale-bars are 50  $\mu\text{m}$ ......44

**Figure 3.5:** Relative frequency of flocs sizes entering the microfluidic channel. ....45

**Figure 3.6:** a) Two points  $\alpha$  and  $\beta$  are tracked as the fluid velocity fluctuates in the channel. These two points would later form a streamer. The scale bar is 50  $\mu\text{m}$ . b) Stretch ratio of the two points as a function of time during the initial filling period of the channel. Streamer formation region (right) also co-incides with the onset of steady flow. Black dashed line depicts  $\lambda=1$  (Inset) Stretch ratio for a smaller time segment. The colored envelope represents estimated error. .47

**Figure 3.7:** a) Simulation results for the contour of the magnitude of the dimensionless shear stress  $\bar{\tau} = \frac{d}{U} \mu \frac{1}{2} (\nabla u + (\nabla u)^T)$ ,  $u$  being the velocity field b) Polar frequency histogram of where flocs attach on the pillars. Half of one pillar is considered.  $0^\circ$  represents upstream stagnation point and  $180^\circ$  represents downstream stagnation point. ....48

**Figure 3.8:** a) Temporal variation of the non-dimensional principal velocity gradient ( $L_1$ ) of a fully formed streamer. The experimentally obtained values (blue dots) show an approximately constant trend (dashed red line); two points demarcated through dashed green ellipses were neglected as outliers. (Inset) A point  $P$  was tracked on a fully formed streamer for calculation of the velocity gradient. Here  $U = 1.3 \times 10^{-4}$  m/s. b) Time-averaged principal velocity gradient ( $L_1$ ) of fully formed streamers as a function of non-dimensional flow speed ( $U$ ). ....50

**Figure 3.9:** Rapid and catastrophic clogging of the channel by streamers. a) Images of the channel at two time-points. The scale bars are 50  $\mu\text{m}$ . b) The

graph shows a gradual increase of surface coverage from 2% (3 min) to 5% (25 min). Then, it has a dramatic surge from 5% (25 min) to 37% (57 min). After that the graph plateaus. Solid curve represents a sigmoidal curve fit to the data.

.....51

**Figure 3.10:** a) Confocal sidebar shows the floc attachment through the height of the pillars. CLSM images of streamer formation at different heights in the chip. Such distribution of streamers across  $z$ -height is seen at other locations too. b) Numerical simulation of the non-dimensional  $z$ -component of the velocity at a downstream location ( $v_z^* = v_z/U$ ) (arrow shows the direction of the flow). Secondary flows, in a direction transverse to the main flow, converge at the middle plane in the chip. c) Histogram of streamer thickness as evaluated by CLSM after 30 mins of experimentation. ....54

**Figure 4.1:** a) Microfluidic experimental set-up. b) Top view of the porous section of the channel. The channel width ( $b$ ) is 625  $\mu\text{m}$  and the porous section of channel contains 400 ( $8 \times 50$ ) pillars. The micropillars' diameter ( $d$ ) and height ( $h$ ) are 50  $\mu\text{m}$  and they are set 75  $\mu\text{m}$  apart ( $l$ ). The fluid flow rate ( $Q$ ) was at a value that we had a creeping flow in the channel,  $Re$ , was  $O(10^{-3})$ . c) Time series of streamer development from slender body (high aspect ratio) to mature structures. ....64

**Figure 4.2:** SEM image of PDMS pillars in the micro-channel. Scale bar is 25  $\mu\text{m}$ . ....64

**Figure 4.3:** Relative frequency histogram of flocs of *P. fluorescens*. The mode and median for this relative frequency histogram are 21.48 and 20.68  $\mu\text{m}$  respectively. A total of 100 flocs were considered. See Hassanpourfard et al. [2] for details regarding image analysis. The inset shows two flocs of *P.*

*fluorescens* that were obtained after incubation at 30 °C for 2 days. Scale bar is 25  $\mu\text{m}$ . .....65

**Figure 4.4:** a) Time series image of streamer (*P. fluorescens*) that shows stick-slip behavior.  $t_0$  here is 83 min after beginning of experiment with the imposed flow velocity of  $1.33 \times 10^{-4} \text{ m/s}$ . Scale bar is 50  $\mu\text{m}$  and the white arrow shows the flow direction in the channel, which is from top to bottom. The green arrows delineate an advancing front undergoing stick-slip behavior. Note that the entire channel is liquid filled. b) Stick-slip behavior of *P. fluorescens* for different flow velocities. The particles in the front section were tracked and the cumulative length travelled was quantified. The inset shows the tracked front in the microfluidic device. The scale bar is 50  $\mu\text{m}$  and the arrow shows the flow direction in the channel. c) Stick-slip behavior of *P. fluorescens* in different time scales. Here  $t_0$  is 83 min after beginning of experiment with the imposed flow velocity of  $1.33 \times 10^{-4} \text{ m/s}$ . (inset) Stick-slip behavior also occur at much smaller time-scales. d) The stick-slip behavior of 2 different bacterial strains (*P. fluorescens* and *P. aeruginosa*) for flow velocity of  $1.33 \times 10^{-4} \text{ m/s}$ .  $\text{OD}_{600}$  for *P. aeruginosa* was about 0.6.....68

**Figure 4.5:** Stick-slip behavior of tracked particle in a mature streamer in a gravity-assisted pressure driven flow experiment due to the elevation of culture reservoir above the waste container. Here  $t_0$  is 11 min after the beginning of experiment.....69

**Figure 4.6:** Stick-slip behavior of *P. fluorescens* for imposed flow velocity of  $1.33 \times 10^{-4} \text{ m/s}$  from 3 different repetitions. Here  $t_0$  is between 30 to 90 min from beginning of the experiment.....70

**Figure 4.7:** a) Bacterial biomass detachment in the microfluidic device that leads to water channel formation imaged under green fluorescence.  $t_0$  is 108

min after the beginning of the experiment ( $U=1.33\times 10^{-4}$  m/s). Red arrows show movement of detached streamer. Scale bar represents 50  $\mu\text{m}$ . b) Green dash lines delineate a water channel formed in the device after 2 hours flow of *P. fluorescens* with flow speed of  $1.33\times 10^{-4}$  m/s. Images are top view of the porous section of the channel and were captured approximately at the middle height of the channel ( $z = 25$   $\mu\text{m}$ ). Scale bar represents 150  $\mu\text{m}$ . White arrows show the flow direction.....72

**Figure 4.8:** a) Water channel formation in the clogged part of the microfluidic device. Bacterial solutions (*P. fluorescens*) were injected for 3 hours into the channel and the experiments were performed for different imposed velocity scales of i)  $4.44\times 10^{-5}$  m/s, ii)  $1.33\times 10^{-4}$  m/s, iii)  $2.66\times 10^{-4}$  m/s and iv)  $5.33\times 10^{-4}$  m/s. Clogging didn't occur for  $U=4.44\times 10^{-5}$  m/s. Scale bar is 250  $\mu\text{m}$ . White arrow shows the flow direction that is from top to bottom in all the experiments. ....73

**Figure 4.9:** Water channel formation in the clogged part of the microfluidic device. 2 parallel dash lines demonstrate the location of water channel. Bacterial solution (*P. aeruginosa*) was injected for 3 hours into the channel with  $U=1.33\times 10^{-4}$  m/s. Scale bar is 150  $\mu\text{m}$ . White arrow shows the flow direction that is from top to bottom.....74

**Figure 4.10:** Various time scales related to our experiment. ....76

**Figure 5.1:** a) The AFM topography and b) The corresponding cross section of the  $\text{Mg}(\text{OH})_2$  nano-platelets deposited on  $\text{SiO}_2$  substrate. Scale bar is 0.5  $\mu\text{m}$ . ....86

**Figure 5.2:** a) Microfluidic experimental set-up. b) Porous section of the channel. Zoom in shows the pillars. The channel width ( $b$ ) is 625  $\mu\text{m}$ . and the porous section of channel contains 400 pillars. The micropillars' diameter ( $d$ )

and height are 50  $\mu\text{m}$  and they are set 75  $\mu\text{m}$  apart ( $l$ ). The fluid flow rate ( $Q$ ) was set 15  $\mu\text{l/h}$  (flow speed:  $1.3 \times 10^{-4}$  m/s) in our device. The reason for selecting this flow rate (15  $\mu\text{l/h}$ ) was having creeping flow regime in the microchip (Reynolds number,  $Re$ , was  $O(10^{-3})$ ). .....87

**Figure 5.3:** Bacterial growth on agar plates with different concentrations of  $\text{Mg(OH)}_2$  nano-platelets. ....89

**Figure 5.4:** AFM images of bacteria; a) Bacteria incubated in control solution, b) Bacteria incubated in 0.1X solution. c) and d) The corresponding cross-sections of the bacterial images for a) and b). Scales bars are 1  $\mu\text{m}$ . ....91

**Figure 5.5:** a) The effect of  $\text{Mg(OH)}_2$  nano-platelets in streamer formation in the microchannel. The first row shows supernatant of control bacterial solution injected into the channel. Second row demonstrates the inside of the channel after injecting supernatant of 1X solution. b) Streamer formation after 10 min of injecting supernatant of control bacterial solution into the microchannel. Scale bars are 50  $\mu\text{m}$ . ....93

# **1 Introduction**

## **1.1 Bacterial communities & biofilms**

Bacteria are prokaryotic microorganisms and are one of the ancient forms of life on earth [1, 2]. They are ubiquitous in the environment. Bacteria can live by themselves in a planktonic state or they can be part of community structures such as biofilm and floc [3, 4]. In biofilm mode, bacteria attach to surfaces and organize themselves into integrated and structured communities that contain the bacterial cells encased by extracellular polymeric substances (EPS) [5-7]. The complex nature of biofilm formation can be idealized as a multi-step process with defined stages (Fig. 1.1). For many bacterial species transport and attachment events are the first step of this process that can be facilitated by bacterial motility organelles such as flagella and pili [8]. Irreversible attachment to the surfaces is the second step of this process. Adhesion between cells and the surfaces is facilitated by secretion of EPS that contain proteins, polysaccharides, lipids, nucleic acids, and other biopolymers such as humic substances [4]. Then, microcolonies proliferate through cell division, including other planktonic cells and EPS production. In the next step, these microcolonies mature into three-dimensional structure of biofilm. Finally, some cells are detached from biofilm and then dispersed into the bulk to continue this cycle. [8, 9].

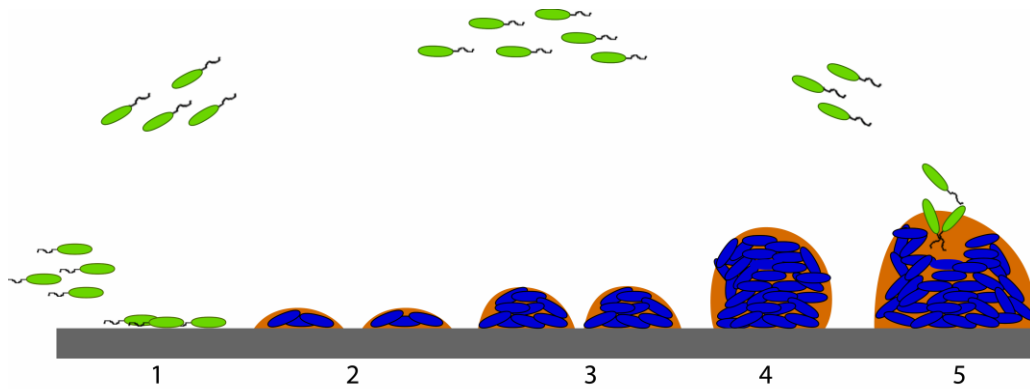


**Figure 1.1:** 5 stages of biofilm development. 1) Transport and reversible attachment of bacteria cells to surface. 2) Irreversible attachment of bacteria and EPS production. 3) Microcolonies formation by replication, growth and EPS production of adsorbed cells. 4) Biofilm formation. 5) Detachment of some bacterial cells from biofilm [4, 8, 9].

The multi-stage transition of planktonic bacteria to a biofilm stage has several advantages for bacteria. Previous studies suggested that bacterial resistance to antimicrobial agents increases in biofilm mode in comparison to the planktonic mode [5, 10]. This is due to the fact that biocidal agents can be diluted effectively to sublethal concentrations before reaching all bacteria cells in the biofilm when biocidal agents are bonded or neutralized by EPS [10]. Another mechanism of biofilm resistance to antimicrobial agents is the formation of starved and stationary phase in biofilm. To be effective, antibiotics need normal cellular activity in order to disrupt the microbial processes [5, 10]. Finally, the existence of resistant subpopulation phenotypes in biofilm known as ‘persister’ is another mechanism of protection in biofilm [5, 10]. The EPS matrix itself has several advantages for biofilms. For example, biofilm cells are immobilized and kept together in close proximity by EPS, which leads to intense interactions such as cell-cell communication [6]. The matrix turns into a recycle center by holding all the lysed cell components available [6]. The

matrix can also act as a nutrition source [6]. Furthermore, the matrix protects the bacteria cells from ultraviolet radiation, antibiotics, metal toxicity, etc. [6]. Therefore, the biofilm mode leads to protection of bacteria from a broad range of environmental challenges, increases their chance of survival in a hostile environment, and enhances their resistance to antibiotics by several orders of magnitude [5-7, 10].

Biofilm formation is a phenomenon that involves multiple spatial and temporal scales. [11]. For example, enzymes and molecular cues at the nanoscale facilitate communication and coordination among bacteria. Microcolonies develop at the microscale, but the dimensions of a typical biofilm belong to the mesoscale. In addition, a broad range of time scales are involved in biofilm processes from milliseconds in convective transport to several days of biomass development and detachment [11]. The significant implications of biofilm formation in industrial, clinical, and natural environments attract researchers' attention to better understand and control biofilm. However, understanding the biofilm's behavior is challenging due to a wide range of spatial and temporal scales related to biofilm developments in addition to extensive versatility in chemical composition, mechanical properties, and morphology of biofilms [11].

Studying the formation of biofilm on simple geometries such as tubes or flat surfaces has been the focus of researchers in recent years, and there has been significant progress in this area. However, the knowledge regarding biofilm growth in complex environments such as porous media is still in need of scientists' attention.

## 1.2 Biofilms in porous media<sup>1</sup>

An often-sought goal of biofilm research was using antimicrobial agents to eradicate biofilm. However, more recently, the potential advantages of biofilm in environmental and industrial applications have been recognized and become the focus of several ongoing studies [12]. Biofilms can form easily in porous media in which the intrinsic high surface to volume ratio provides them a suitable place to attach and develop [13]. Formation of biofilm in porous media is related to several environmental and industrial processes such as subsurface biofilm barriers [12], microbially enhanced oil recovery [12, 14], and water filtration systems [15].

Biofilm formation in porous media can change permeability, porosity, dispersion, and diffusion of the media. Depending on the application, this can be beneficial or detrimental [12]. For instance, soil is an example of porous media [16] and maximum reduction of permeability and porosity is required in the case of subsurface biofilm barriers [12]. Subsurface biofilm barriers that are engineered structures have been proposed in order to control and remediate contaminated soil and groundwater. Maximum reduction of permeability is the aim of these barriers by promoting thick biofilm growth. The growth of biofilm reduces the groundwater flow in certain subsurface areas. Moreover, it can direct groundwater flow into a certain direction in the case of treatment [12]. Microbially enhanced oil recovery (MEOR) is another example of biofilm applications in soil as a porous media. MEOR is applied in different ways, such as enhancement of oil mobility by production of biosurfactants, *in situ* biocracking of long alkane chains, and selective plugging of high-permeability

---

<sup>1</sup> Some part of this section is adopted from chapter 2.

sections of channels in reservoir rock [12]. On the other hand, in the case of wastewater treatment, e.g. biofilm reactors such as trickling filters, rotating biological contactors (RBC), submerged fixed bed biofilm reactors, membrane attached biofilm reactors, etc., an optimal biofilm thickness is required to provide an efficient substrate removal and simultaneously avoid clogging due to accumulation of excessive biofilms [12, 17].

Porous media can be mimicked by different methods. One way of simulating porous media is filling reactors and columns with different materials such as sand, rock, basalt, porous clay [12, 17-19], glass beads [18, 20], etc. However, observing biofilm formation in such complex habitats can often be challenging due to the opacity of porous media. In such situations, microfluidics based porous media platforms can prove extremely advantageous as they allow real-time and *in-situ* monitoring of biofilm [21].

Microfluidics is the science and technology to manipulate fluids at the micrometer scale [22]. The microfluidics field initially originated from microanalytical methods in the early 1990 [22, 23]. In the last decade, this field has flourished dramatically owing to the ease of micro-device fabrication based on the soft-lithography technique [23]. In this regard, polydimethylsiloxane (PDMS) is the most popular material for microfabrication to date due to its flexibility, transparency, gas permeability, biocompatibility, and chemical inertness [23, 24]. Microfluidic devices provide numerous advantages; ease of fabrication, minimal reagent use, rapid and low cost analysis, and, more importantly, a laminar fluid flow regime are just a few advantages of these devices [25, 26]. Furthermore, the small size of microfluidic devices makes it possible to be mounted on a microscope stage for real-time monitoring.

Another advantage of microfluidic devices is the ability to build multiple bioreactors on a single bio-microfluidic platform and simultaneously allow for online monitoring and/or incorporation of sensors. The flexibility to implement multiple laboratory experiments in one device and the ability to collect significant pertinent data for accurate statistical analysis is an important advantage of microfluidic systems [21, 27]. Due to these unique features of microfluidic devices, fundamental and applied research has been revolutionized in different fields such as biology, physical chemistry, material science, and biomedicine [23, 26].

The role of microfluidic devices in biological research is indispensable [23]. Biofilm can be studied in devices that mimic ecologically relevant spatiotemporal scales of biofilm habitat. In such a situation, the effect of different factors such as fluid dynamics, cell phenotype, and cellular communication that have direct influences on biofilm formation can be investigated [21].

### **1.3 Bacterial streamers- Filamentous biofilms<sup>2</sup>**

As discussed earlier, biofilm can form in soil. Further to biobarrier [12] and microbially enhanced oil recovery [12, 14], they also play a key role in maintaining soil ecology [28]. Biofilms can be used in water filtration systems [15]. Moreover, biofilm formation in medical devices is an important issue. In other words, biofilms can cause problems in medical devices, which make it an important area of research for scientists [7]. There are different factors that can affect growth of biofilm in porous media such as hydrodynamics,

---

<sup>2</sup> Some part of this section is adopted from chapter 3.

physicochemical conditions (e.g. pH, temperature), nutrient availability, and presence of inhibitory or stimulating compounds [12]. Biofilms are viscoelastic materials [29, 30] and they have a complex time-dependent response to external forces. One such phenomena that is usually observed due to the action of sustained hydrodynamic flow on biofilm is bacterial streamer. This is so named because of their filamentous, string like, morphology whose one (or both) end is attached to a surface and rest of the structure is suspended in the fluid (Fig. 1.2) [8, 31]. Bacterial streamers have been observed to form both in high ( $Re > 1000$ ) [30, 32-35], and in low Reynolds number conditions ( $Re \ll 1$ ) [36-40]. Streamer formation in low  $Re$  transport is of significant technological and biomedical interest due to relevance to a wide variety of critical operating scenarios, including clogging of biomedical devices such as heart stents, catheters, porous media, and water filtration systems [39, 41, 42]. Recent studies have shown that streamers can have a broad influence on natural or artificial media, because they can be precursors to the formation of mature structures in these media. Moreover, these structures accelerate the rapid and catastrophic disruption of flow; this issue emphasizes the necessity for more studies on the streamer dynamics [13, 43].

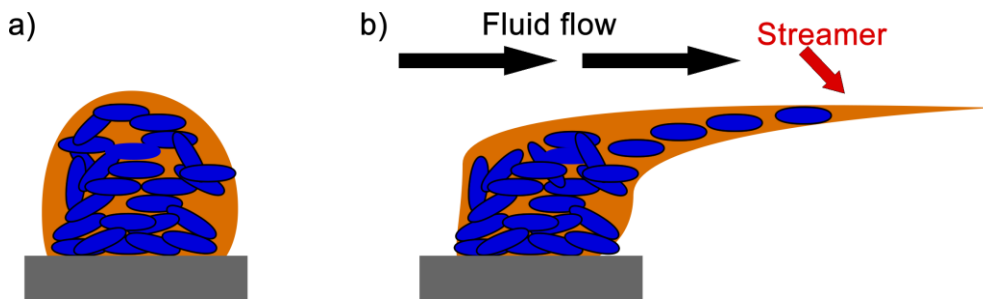


**Figure 1.2:** a) Biofilm in stagnant condition. b) Sustained fluid flow can lead to the deformation of a biofilm into a slender structure called streamer.

There are a few studies on dynamics of streamer formation in low  $Re$  regime of flow [13, 31, 37, 43-45]. For instance, Rusconi et al. [38], while studying the effect of curved channel geometries using a microfluidic device, found that *Pseudomonas aeruginosa* formed streamers in the curved sections of the microchannels with laminar flow condition. In their experiment, streamers were located in a plane positioned exactly at half of the channel height. They concluded that the probable mechanism for the streamer formation in their device is the accumulation of polymeric substances (secreted from bacteria) and the formation of precursor thread in the half height of the channel by secondary flow at the corner. The threads are then stretched and extended to the next corner by the primary flow. In another study, they [44] showed that the magnitude of secondary flow has an effect on streamer formation and the onset time for their formation. The sharper curvature angle of channel led to longer, thicker, and faster streamer formation [44]. In another study from the same group, Drescher et al. [41] showed that streamer formation in their device can lead to catastrophic clogging of the device. Furthermore, Valiei et al. [39] used a microfluidic device with micropillars and studied biofilm formation by *Pseudomonas fluorescens*. They found that, in certain flow rates, the bacteria formed extensive streamers resulting in a web-like network between the different pillars. Interestingly, secondary flows seem to have a little or no role in streamer's location in their device [39].

A commonality among the reports by Rusconi et al. [38], Drescher et al. [41] and Valiei et al. [39] is that the streamers appeared far later than the biofilms, and the corresponding streamer formation time-scale was of the order of hours from the beginning of the flow. Das and Kumar [46] have recently proposed that in such instances, where the streamer formation time-scale far

exceeded the relaxation time-scale of biofilms, streamers appeared from a highly viscous state of the intrinsically viscoelastic biofilms. In contrast to these studies, some other experiments conducted under apparently similar creeping flow conditions reported much smaller time-scale values ( $\sim$  minutes) [37, 45, 47]. For instance, Yazdi et al. [45] studied bacteria aggregation and biofilm formation in a vortical flow. In their studies, the oscillating bubble led to a pair of vortices in the flow adjacent to the bubble place. These vortices led to bacteria aggregation and consequently streamers formation. Marty et al. [37] looked at streamer formation in microfluidic devices, which mimicked water filtration membranes and found that streamers can grow rapidly and cover a large area of the device. Kim et al. [47] have reported even smaller streamer formation time-scales for the bacterium *Staphylococcus aureus*, though this was achieved by first coating the channel walls of the microfluidic device with human plasma. Such large variation in streamer formation time scale might indicate different physical mechanisms that govern the streamer formation process. Streamers forming at very large time scales ( $\sim$  hrs) have typically been reported in systems where formation of biofilm occurs prior to streamer formation, referred herein as biofilm-mediated streamer formation [38, 39, 41]. To the best of our knowledge, a proper quantitative evaluation of small time scale streamer formation is yet to be reported. Furthermore, much of the literature on streamer formation in low Reynolds number conditions is relatively recent in the context of literature on biofilms, and the physical basis of streamer formation remains an active area of research [48-50].

While the above-mentioned studies establish the acute relevance of the clogging phase, the clogging phenomena itself is yet to be fully explored and understood. In fact, fostering a deeper understanding of the relationship

between background flow and the streamers' short and intermediate time scales dynamics is critical in design, fabrication, and operation of different devices, such as medical devices. Furthermore, there is a growing need to control and inhibit streamers formation that requires more investigations.

## **1.4 Objectives of this study**

The main objective of this research is to develop a fundamental understanding of bacterial streamers growth in porous media. This understanding will help to control their behavior and their consequent related effects due to their formation and growth.

To achieve this goal, a pseudo porous microfluidic device was fabricated to establish a platform for our studies. In chapter 2, we explain in detail the fabrication process and bacterial culture method. Then, we investigate the biofilm-mediated streamer formation and its temporal development.

In chapter 3, we define a new type of streamers (floc-mediated streamers) and explain our discovery of floc mediated streamers. For the first time, we show the inception of streamers formation, their characteristics in initial and intermediate phases, and finally their consequential rapid clogging of device.

In chapter 4, we investigate the clogging phase of the floc-mediated streamers; we discover a nonlinear stick-slip type advance of the mature streamer front; we also show that the bulk of the clogging biomass demonstrates instability in the form of water channel formation in their structure.

In chapter 5, we investigate the antibacterial effect of  $\text{Mg}(\text{OH})_2$  nanoparticles on *P. fluorescens* in order to inhibit bacterial growth and floc formation; this leads to delay streamer formation and its consequences.

## 1.5 References

1. Jalasvuori, M. and E.V. Koonin, *Classification of prokaryotic genetic replicators: between selfishness and altruism*. Ann N Y Acad Sci, 2015. **1341**: p. 96-105.
2. Kasting, J.F. and J.L. Siefert, *Life and the evolution of Earth's atmosphere*. Science, 2002. **296**(5570): p. 1066-1068.
3. Costerton, J.W., et al., *Microbial Biofilms*. Annual Review of Microbiology, 1995. **49**(1): p. 711-745.
4. More, T.T., et al., *Extracellular polymeric substances of bacteria and their potential environmental applications*. J Environ Manage, 2014. **144C**: p. 1-25.
5. Costerton, J.W., *Bacterial Biofilms: A Common Cause of Persistent Infections*. Science, 1999. **284**(5418): p. 1318-1322.
6. Flemming, H.C. and J. Wingender, *The biofilm matrix*. Nat Rev Microbiol, 2010. **8**(9): p. 623-33.
7. Wong, G.C.L. and G.A. O'Toole, *All together now: Integrating biofilm research across disciplines*. MRS Bulletin, 2011. **36**(05): p. 339-342.
8. Stoodley, P., et al., *Biofilms as complex differentiated communities*. Annu Rev Microbiol, 2002. **56**: p. 187-209.
9. Renner, L.D. and D.B. Weibel, *Physicochemical regulation of biofilm formation*. MRS Bull, 2011. **36**(5): p. 347-355.
10. Hall-Stoodley, L., J.W. Costerton, and P. Stoodley, *Bacterial biofilms: from the natural environment to infectious diseases*. Nat Rev Microbiol, 2004. **2**(2): p. 95-108.
11. Karimi, A., et al., *Interplay of physical mechanisms and biofilm processes: review of microfluidic methods*. Lab Chip, 2015. **15**(1): p. 23-42.

12. Vafai, K., *Porous media: applications in biological systems and biotechnology*. 2010: CRC Press.
13. Valiei, A., et al., *A web of streamers: biofilm formation in a porous microfluidic device*. *Lab Chip*, 2012. **12**(24): p. 5133-7.
14. Sen, R., *Biotechnology in petroleum recovery: The microbial EOR*. *Progress in Energy and Combustion Science*, 2008. **34**(6): p. 714-724.
15. Vrouwenvelder, J.S., et al., *Impact of flow regime on pressure drop increase and biomass accumulation and morphology in membrane systems*. *Water Res*, 2010. **44**(3): p. 689-702.
16. Hassanpourfard, M., et al., *Dynamics of bacterial streamers induced clogging in microfluidic devices*. *Lab on a Chip*, 2016. **16**(21): p. 4091-4096.
17. *Biological wastewater treatment principles, modelling and design*, M. Henze, Editor. 2008, IWA Pub.: London :.
18. Cunningham, A.B., et al., *Influence of biofilm accumulation on porous media hydrodynamics*. *Environmental science & technology*, 1991. **25**(7): p. 1305-1311.
19. Brooks, R.H. and A.T. Corey, *Hydraulic properties of porous media and their relation to drainage design*. *Transactions of the ASAE*, 1964. **7**(1): p. 26-0028.
20. Lu, T.X., J.W. Biggar, and D.R. Nielsen, *Water movement in glass bead porous media: I. Experiments of capillary rise and hysteresis*. *Water Resources Research*, 1994. **30**(12): p. 3275-3281.
21. Neethirajan, S., et al., *Biofilms in Microfluidic Devices*, in *Encyclopedia of Nanotechnology*, B. Bhushan, Editor. 2012, Springer: New York.
22. Whitesides, G.M., *The origins and the future of microfluidics*. *Nature*, 2006. **442**(7101): p. 368-73.

23. Rusconi, R., M. Garren, and R. Stocker, *Microfluidics expanding the frontiers of microbial ecology*. *Annu Rev Biophys*, 2014. **43**: p. 65-91.
24. Weibel, D.B., W.R. Diluzio, and G.M. Whitesides, *Microfabrication meets microbiology*. *Nat Rev Microbiol*, 2007. **5**(3): p. 209-18.
25. Saleh-Lakha, S. and J.T. Trevors, *Perspective: microfluidic applications in microbiology*. *J Microbiol Methods*, 2010. **82**(1): p. 108-11.
26. Whitesides, G.M. and A.D. Stroock, *Flexible methods for microfluidics*. *Phys. Today*, 2001. **54**(6): p. 42-48.
27. Kumar, A., et al., *Microscale confinement features can affect biofilm formation*. *Microfluidics and Nanofluidics*, 2013. **14**(5): p. 895-902.
28. Barathi, S. and N. Vasudevan, *Utilization of petroleum hydrocarbons by Pseudomonas fluorescens isolated from a petroleum-contaminated soil*. *Environment International*, 2001. **26**(5-6): p. 413-416.
29. Shaw, T., et al., *Commonality of Elastic Relaxation Times in Biofilms*. *Physical Review Letters*, 2004. **93**(9).
30. Klapper, I., et al., *Viscoelastic fluid description of bacterial biofilm material properties*. *Biotechnology and Bioengineering*, 2002. **80**(3): p. 289-296.
31. Rusconi, R., et al., *Laminar flow around corners triggers the formation of biofilm streamers*. *J R Soc Interface*, 2010. **7**(50): p. 1293-9.
32. Stoodley, P., et al., *Biofilm material properties as related to shear-induced deformation and detachment phenomena*. *J. Ind. Microbiol. Biot.*, 2002. **29**(6): p. 361-367.

33. Stoodley, P., et al., *Oscillation characteristics of biofilm streamers in turbulent flowing water as related to drag and pressure drop*. Biotechnology and bioengineering, 1998. **57**(5): p. 536-544.
34. Stoodley, P., et al., *Evolving perspectives of biofilm structure*. Biofouling, 1999. **14**(1): p. 75-90.
35. Lewandowski, Z. and P. Stoodley, *Flow induced vibrations, drag force, and pressure drop in conduits covered with biofilm*. Water Science and Technology, 1995. **32**(8): p. 19.
36. Hassanpourfard, M., et al., *Protocol for Biofilm Streamer Formation in a Microfluidic Device with Micro-pillars*. JoVE (Journal of Visualized Experiments), 2014(90): p. e51732-e51732.
37. Marty, A., et al., *Formation of bacterial streamers during filtration in microfluidic systems*. Biofouling, 2012. **28**(6): p. 551-62.
38. Rusconi, R., et al., *Laminar flow around corners triggers the formation of biofilm streamers*. Journal of the Royal Society Interface, 2010. **7**(50): p. 1293-1299.
39. Valiei, A., et al., *A web of streamers: biofilm formation in a porous microfluidic device*. Lab on a Chip, 2012. **12**(24): p. 5133-5137.
40. Yazdi, S. and A.M. Ardekani, *Bacterial aggregation and biofilm formation in a vortical flow*. Biomicrofluidics, 2012. **6**(4).
41. Drescher, K., et al., *Biofilm streamers cause catastrophic disruption of flow with consequences for environmental and medical systems*. Proceedings of the National Academy of Sciences of the United States of America, 2013. **110**(11): p. 4345-4350.

42. Marty, A., et al., *Impact of tortuous flow on bacteria streamer development in microfluidic system during filtration*. *Biomicrofluidics*, 2014. **8**(1): p. 014105.
43. Drescher, K., et al., *Biofilm streamers cause catastrophic disruption of flow with consequences for environmental and medical systems*. *Proc Natl Acad Sci U S A*, 2013. **110**(11): p. 4345-50.
44. Rusconi, R., et al., *Secondary flow as a mechanism for the formation of biofilm streamers*. *Biophys J*, 2011. **100**(6): p. 1392-9.
45. Yazdi, S. and A.M. Ardekani, *Bacterial aggregation and biofilm formation in a vortical flow*. *Biomicrofluidics*, 2012. **6**(4): p. 044114.
46. Das, S. and A. Kumar, *Formation and post-formation dynamics of bacterial biofilm streamers as highly viscous liquid jets*. *Scientific Reports*, 2014. **4**: p. 7126.
47. Kim, M.K., et al., *Filaments in curved streamlines: rapid formation of Staphylococcus aureus biofilm streamers*. *New Journal of Physics*, 2014. **16**: p. 065024.
48. Hol, F.J.H. and C. Dekker, *Zooming in to see the bigger picture: Microfluidic and nanofabrication tools to study bacteria*. *Science*, 2014. **346**(6208): p. 438-+.
49. Karimi, A., et al., *Interplay of physical mechanisms and biofilm processes: review of microfluidic methods*. *Lab on a Chip*, 2015. **15**: p. 23-42.
50. Rusconi, R., M. Garren, and R. Stocker, *Microfluidics Expanding the Frontiers of Microbial Ecology*. *Annual Review of Biophysics*, 2014. **43**: p. 65-91.

## **2 Protocol for biofilm streamer formation in a microfluidic device with micro-pillars<sup>3</sup>**

Material in this chapter has been published in:

Hassanpourfard, Mahtab, Xiaohui Sun, Amin Valiei, Partha Mukherjee, Thomas Thundat, Yang Liu, and Alope Kumar. "Protocol for biofilm streamer formation in a microfluidic device with micro-pillars." *JoVE (Journal of Visualized Experiments)* 90 (2014): e51732-e51732.

### **2.1 Introduction**

Recently, we demonstrated bacterial biofilm formation dynamics in a porous microfluidic mimic device [1]. Bacterial biofilms are essentially colonies of surface aggregated bacteria that are encased by extracellular polymeric substances (EPS) [2-4]. These thin films of bacteria can form in almost every conceivable niche ranging from smooth surfaces to the much more complex habitat of porous media. Valiei et al. [1] used a microfluidic device with an array of micro-pillars to simulate a porous media structure and studied biofilm formation in this device as a function of fluid flow rate. They found that in a certain flow regime, filamentous biofilms known as streamers began to emerge between different pillars. Streamers can be tethered at one or both ends to solid surfaces, but the rest of the structure is suspended in liquid. Streamer formation typically starts after an initial layer of biofilm has formed and its formation can dictate the long term evolution of biofilm in such complex

---

<sup>3</sup> The video link for this chapter is: <https://www.jove.com/video/51732/protocol-for-biofilm-streamer-formation-microfluidic-device-with>

habitats. Recently, several researchers have investigated the dynamics of streamer formation. Yazdi et al. [5] showed that the streamers can form in vortical flows originating from an oscillating bubble. In another experiment, Rusconi et al. [6] investigated the effect of channel curvature and channel geometry on the formation of streamers. They found that the streamers can form in curved sections of microchannel, and streamer morphology is related to motility. Recent research has demonstrated that streamers can have wide repercussions in various natural and artificial scenarios as they can act as precursors to the formation of mature structures in porous interfaces, lead to rapid and catastrophic biofilm proliferation in a biomedical systems, and also cause substantial flow-structure interactions, etc. [1, 7-9].

Biofilm streamers often form in complex habitats such as porous media. Understanding biofilm growth in porous media environment is relevant to several environmental and industrial processes such as biological wastewater treatment [10], maintaining well-bore integrity in situations such as CO<sub>2</sub> capture [11] and plugging of pores in soil [12]. Observing biofilm formation in such complex habitats can often be challenging due to the opacity of porous media. In such situations, microfluidics based porous media platforms can prove extremely advantageous, as they allow real-time and *in-situ* monitoring. Another advantage of microfluidics is the ability to build multiple bioreactors on a single bio-microfluidic platform and simultaneously allow for online monitoring and/or incorporation of sensors. The flexibility to implement multiple laboratory experiments in one device and the ability to collect significant pertinent data for accurate statistical analysis is an important advantage of microfluidic systems [13, 14].

In the context of the above discussion, understanding streamer formation dynamics in a porous media environment would be beneficial to several applications. In this study, we develop the protocol for investigating streamer formation in a porous media mimic device. Fabrication of the microfluidic platform, necessary steps for cell culture, and experimentation are described. In our experiments, the wild type bacterial strain of *P. fluorescens* was employed. *P. fluorescens*, found naturally in soil, plays a key role in maintaining soil ecology [15]. The bacterial strain employed had been genetically engineered to express green fluorescent protein (GFP) constitutively.

## **2.2 Experimental**

Microfabrication protocols for creating the microfluidic platform are discussed in step 1. Step 2 describes the bacterial culture protocol (Figure 2.2), and step 3 pertains to assembly of the experimental setup (Figure 2.3). Finally, the actual experimental set-up is described in step 4.

### **Step 1. Chip fabrication procedure**

1. Design the mask with an appropriate software (e.g. L-Edit). The channel design consists of a main micro-channel of width 625  $\mu\text{m}$ . The central region of the channel contains an array of micro-posts 50  $\mu\text{m}$  in diameter, spaced 25  $\mu\text{m}$  apart.
2. Print this design on glass (5" x 5" soda lime glass) with thickness of 0.09" which is coated by approximately 70 nm Chromium using masking in order to prepare photo mask.
3. Photolithography:
  - 3.1. Clean a standard 4" silicon wafer chemically with piranha solution ( $\text{H}_2\text{SO}_4$  and  $\text{H}_2\text{O}_2$  with ratio of 3:1) for 20 minutes.

- 3.2. Rinse the wafer with DI water and dry it.
- 3.3. Heat the wafer on a hot plate (200°C for 15 minutes).
- 3.4. Coat the silicon wafer with photoresist. Here, the positive photoresist was spin-coated on a silicon wafer at 2000 rpm for 25 seconds to obtain a 12.5  $\mu\text{L}$  thick layer.
- 3.5. Remove all the solvent by soft baking of the wafer on a hot plate by floating the wafer for 90 seconds on nitrogen flow at 100°C. Then, keep it in vacuum at the same temperature for 60 seconds.
- 3.6. Place the wafer in a dark box for 24 hours for dehydration.
- 3.7. Expose the wafer to UV light in order to transfer the designed pattern to the photoresist.
- 3.8. Immerse the wafer in photoresist developer solution for 240 seconds. Then, rinse the wafer with isopropyl alcohol and dry it by placing in a stream of nitrogen gas.
4. ICP-DRIE (Plasma Induced- Deep Reactive Ion Etching) process:
  - 4.1. Apply DRIE etching. Choose the appropriate etch depth according to final depth required for device (50  $\mu\text{m}$  in this investigation). Photoresist acts as a masking layer during this process.
  - 4.2. Remove the remaining photoresist with acetone and clean the wafer.
5. PDMS (polydimethylsiloxane) casting:
  - 5.1. Use tri-chloro-methyl-silane (TCMS) for silanizing the silicon master mold. Pour 2 or 3 drops of tri-chloro-methyl-silane in a vial and place it in a desiccator beside the silicon master mold. Allow 2-3 hrs for the silanizing process to complete.
  - 5.2. In a separate container, mix the Sylgard 184 silicone base with curing agent by weight ratio of 10:1 to prepare PDMS. Degas the PDMS by subjecting it to vacuum conditions (about 2 hours).
  - 5.3. Put the silicon master mold in a holder. Then, pour the PDMS on the silicon master mold to form the PDMS stamp. Ensure that bubbles do not form in the PDMS during this process.

- 5.4. Cure the PDMS for 2 hours at 80°C.
- 5.5. Peel off the PDMS stamp from the master mold. Then, cut the PDMS stamp into separate microchips. Finally, drill holes for the inlet(s) and outlet(s).
6. Bonding of PDMS to glass:
  - 6.1. Expose the cover slip and PDMS stamp to oxygen plasma for 30 seconds. Bond PDMS stamp to the cover slip.
  - 6.2. Anneal the device by putting it in oven at 70°C for 10 minutes to attain a better sealing.

## **Step 2. Bacterial culture**

1. Prepare LB agar plates
  - 1.1. Add 20 g Luria-Bertani (LB) agar (Miller) powders and 500 mL of ultrapure water to a 1L flask. Stir to dissolve the powder.
  - 1.2. Sterilize by autoclaving at 15 psi, 121°C for 15 minutes.
  - 1.3. Allow flask to cool down to 50-55 °C on a bench or in a water bath in the biosafety hood.
  - 1.4. Add the antibiotic Tetracycline to achieve a final concentration of 50 µg/mL. Mix well by swirling.
  - 1.5. Pour the mixture into plates. Fill each plate till 1/2 - 2/3 full.
  - 1.6. Flame the air bubbles briefly to pop them if they form. Solidified air bubbles are difficult to spread bacterial culture over.
  - 1.7. Allow the plates to cool at room temperature overnight.
  - 1.8. When they are cool, put plates back into their sleeve, seal bag, label (antibiotic and date), and store at 4 °C. Please note: cover the stock of plates with tin foil, as light deactivates many antibiotics.
2. LB broth preparation
  - 2.1. Add 20 g Luria-Bertani (LB) broth (Miller) powders and 500 mL of ultrapure water to a 1L flask. Stir to dissolve the powder.
  - 2.2. Sterilize by autoclaving at 15 psi, 121°C for 15 minutes.

- 2.3. Allow flask to cool down to 50-55 °C on a bench or in a water bath in the biosafety hood.
- 2.4. Add the antibiotic Tetracycline to achieve a final concentration of 50 µg/mL. Mix well by swirling.
- 2.5. When cool, place the labeled bottle at 4 °C. Please note: cover the bottle with aluminum foil, as light deactivates many antibiotics.
3. Culture bacteria on an LB agar plate (This protocol uses *P. fluorescens*):
  - 3.1. Take the bacterial stock from the freezer (-80°C) and place it on ice.
  - 3.2. Place the -80°C bacterial stock and an LB agar plate inside a biosafety hood.
  - 3.3. Streak the bacterial strain onto an LB agar plate in a zigzag pattern. Cover the agar plate and incubate it at 30°C overnight. Finally, store the plate in the refrigerator at 4°C.
4. Prepare the bacterial solution (S1):
  - 4.1. Pour 50 ml LB broth media to an autoclaved flask. Perform this operation inside a biosafety hood.
  - 4.2. Transfer a single colony from the LB agar plate to the flask. This operation should also be performed inside a biosafety hood.
  - 4.3. Put the flask in a shaker incubator at 30°C and 150 rpm for adequate time (4 hours).
5. Prepare the dilute bacterial solution (S2):
  - 5.1. Pour some 5ml LB broth media into a sterilized plastic tube.
  - 5.2. Dilute S1 by mixing with LB broth media. The typical dilution is 1:100. Then, vortex the solution. Dilution can be repeated to obtain the desired optical density (OD measured at 600 nm =0.1).

### **Step 3. Prepare the experimental set-up**

1. Using tweezers connect flexible plastic tubes (0.20" ID) into the inlet(s) and outlet(s) of the microchip. The inlets and outlets were previously drilled

into the PDMS portion of the microchip. In this investigation, the microchip consists of two inlets and one outlet.

2. Fill syringe(s) with bacterial solution (S2 solution) and remove all the bubbles in the syringe(s).
3. Connect syringe tip(s) (30G 0.5' blunt needle) into inlet tube(s). Then, connect outlet tube(s) to waste container.

#### **Step 4. Run the experiment**

1. Place and fix syringe(s) onto the syringe pump. Then place the microchip under an optical microscope with objective lenses of desired magnification (e.g. 40X). Cover the microchip with a live cell chamber device to maintain a constant temperature environment for bacterial growth (30°C for *P. fluorescens*).
2. Set the pump to the desired flow rate level (say 10  $\mu\text{l/hr}$ ) and initiate fluid pumping.
3. Once bacteria are introduced into the chamber, biofilm formation is also initiated. Biofilm formation and maturation typically occurs over a period of several hours or even days. Observe and take images of biofilm growth through the microscope.

### **2.3 Results**

Using the above mentioned microfabrication protocol, a PDMS based microfluidic device was constructed. Figure 2.1 shows the scanning electron microscope (SEM) images of the PDMS device. Figure 2.1a shows the entrance section of the device. A fork-like entrance is created to equalize pressure head across the device. Further SEM imaging also showed that the pillar walls are almost vertical (Fig. 2.1b). The cultured bacterial solution (Fig. 2.2) was diluted

and its optical density was adjusted to a value of 0.1. We examined biofilm formation in the microfluidic device as a function of input flow rate. When *P. fluorescens* was injected into the device at a low flow-rate of 0.8  $\mu\text{l/hr}$ , bacterial attachment and biofilm formation occurred at the walls of the device. Even after a prolonged period of time ( $>20$  hrs), no other bacterial structures other than surface-hugging biofilms were observed. Next, the same experiment was repeated at a flow rate of 8  $\mu\text{l/hr}$ . In this case, biofilm formation again started after a few minutes of infusion of the diluted bacterial culture. However, after a few hours, appearance of filamentous structures extending between micro-pillars was observed near the mid-section of the device (Fig. 2.4). These filamentous structures could be visualized through the presence of immobile bacteria. These structures are known as streamers and they are filamentous biofilms that are only tethered at one or both ends to surfaces. The rest of the structure is often suspended in the liquid medium (as in this case). Figure 2.4 shows the time-evolution of biofilm streamer structure. Streamers usually form due to the effect of fluid shear on the viscoelastic biofilm. Figure 2.5 shows the streamlines and velocity contours for flow past a series of pillars. The simulation shows that the streamers that form in our microfluidic system are essentially aligned along the fluid flow streamlines. The correlation between the flow structures and formation of biofilm streamers is not yet well understood. However, Das and Kumar [16] have recently proposed that these streamers form as highly viscous liquid state of the intrinsically viscoelastic biofilms. They based their conjecture on the observation that the time-scale of biofilm streamer formation typically far exceeds the viscoelastic relaxation time scales of biofilms. Biofilms are known to behave as viscoelastic liquids and hence at time-scales much larger than the viscoelastic relaxation time scale, they

essentially behave as highly viscous liquids [17]. According to this formulation, streamers can be expected to originate at locations of high shear stresses. Figure 2.5 shows the locations of high velocity in the channel, and these locations coincide with locations of high shear stresses. In the initial phase of growth, streamers are observed to originate near these locations (Fig. 2.4).

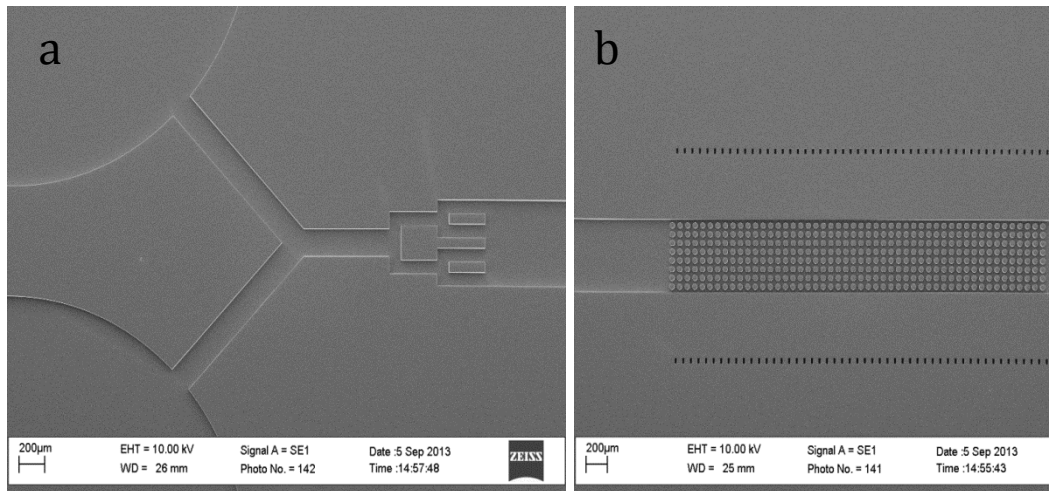


**Figure 2.1:** Scanning electron microscope (SEM) images of the microfluidic channel (top-view). a) Inlet section, b) Region containing micro-pillars.

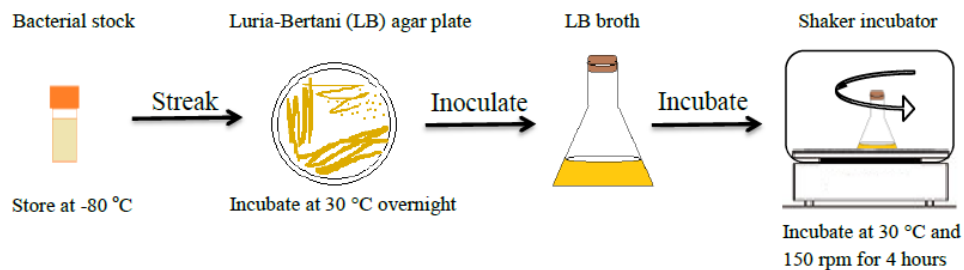


**Figure 2.2:** Sequential steps involved in bacterial culture.

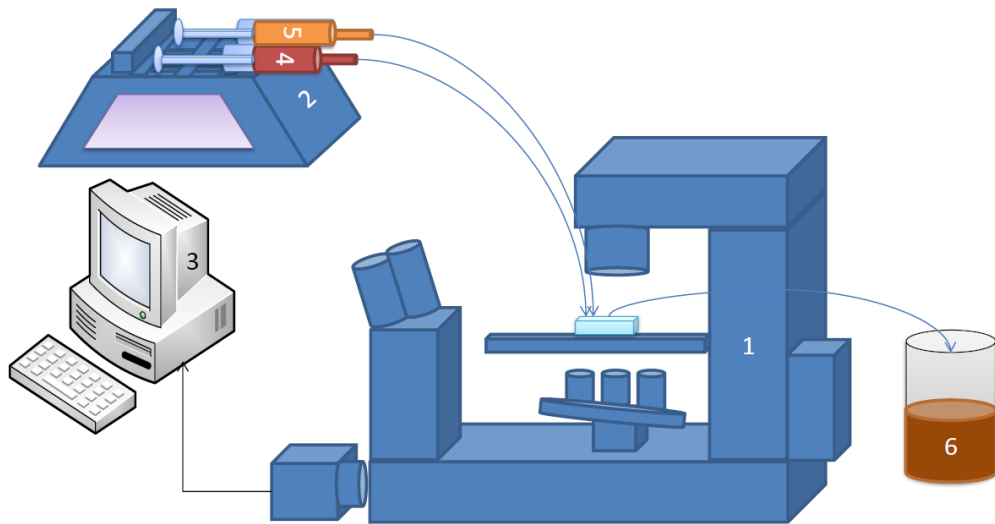


**Figure 2.3:** Set up for microfluidic experiments. 1- Optical microscope (inverted), 2- Syringe pump, 3- Image and data acquisition, 4- Syringe containing dye (optional), 5- Syringe containing bacteria, 6- Waste reservoir.

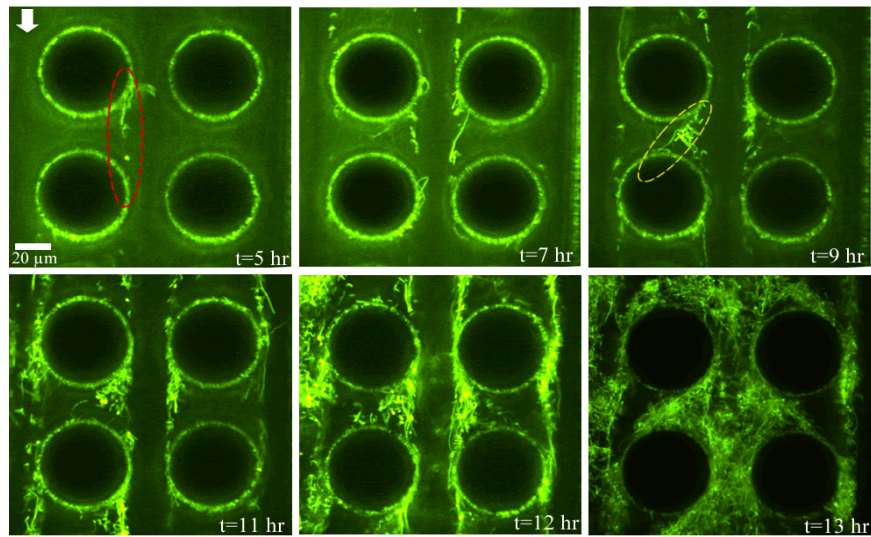


**Figure 2.4:** Time-lapse confocal imaging of evolution of streamers. Image plane corresponds to  $z = 25 \mu\text{m}$  i.e. middle of device. Dashed ellipses demonstrate biofilm streamers.

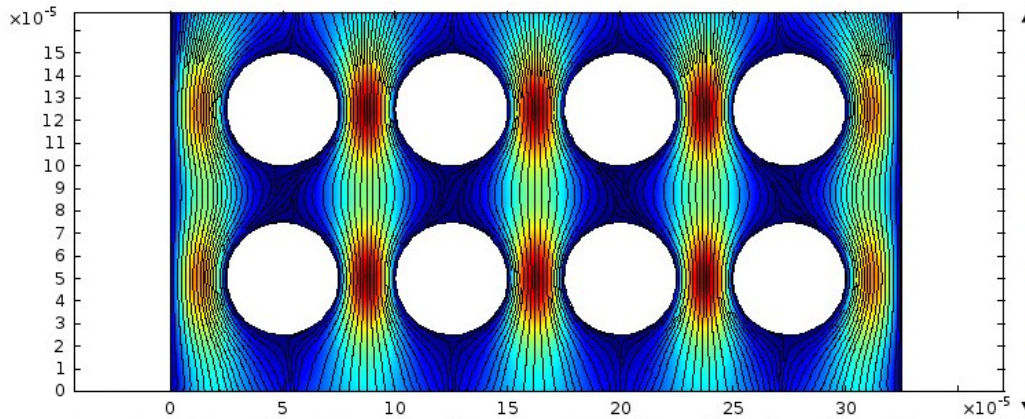


**Figure 2.5:** Computational fluid mechanical simulations showing streamlines and velocity contours of flow past micro-pillars. Fluid flow is from top to bottom and velocity scale is in m/s.

## 2.4 Discussion

We demonstrated a simple microfluidic device that mimics porous media for studying biofilm development in complex habitats. There are several critical steps that dictate the outcome of the experiments. They include device geometry. While the post geometry can vary, adequate pore-space for streamers to form is necessary. Moreover, Valiei *et al.* [1] have demonstrated that streamer formation occurs only in a certain flow rate range. At flow rates lower than a threshold value, deformation of biofilms into streamers may not be observed. Yet above a certain another threshold flow rate value, biofilm fracture can dominate and not allow formation of streamers. Another issue that can plague these experiments is gas bubbles that can become trapped in the

micro-pillar array. Usually these bubbles have to be removed by increasing the flow rate initially and then gradually decreasing it to the desired value.

Microfluidic platforms such as these offer several advantages and few limitations. The platform enables us to work with small culture volumes, and has the flexibility of incorporating user-defined features. For example, different porous structures can be simulated by altering the geometrical parameters of the micro-pillar array. Even structures which mimic the random structure of real porous media can be fabricated on microfluidic platforms [18]. Moreover, several such channels can be implemented on a single device allowing for collection of significant pertinent data for accurate statistical analysis. However, microfluidic systems typically mimic two-dimensional structure of porous media. Devices which can mimic the three-dimensional nature of porous media are usually quite challenging to fabricate.

Formation and evolution of streamers are not well understood yet, and further research is required in this direction. Understanding of how streamers form and lead to the formation of mature biofilm structures will be relevant to a wide variety of scenarios including clogging of biomedical devices such as heart stents, biofilms in soil, and filtration systems. Our microfluidic platform is a step in that direction.

**Acknowledgements:**

The authors would like to thank Professor Howard Ceri from the Biological Sciences Department of the University of Calgary for providing bacterial strains. A. Kumar acknowledges support from NSERC. T. Thundat acknowledges financial support from the Canada Excellence Research Chair

(CERC) program. The authors would also like to acknowledge help from Ms. Zahra Nikakhtari for help with videography.

## 2.5 References

1. Valiei, A., et al., *A web of streamers: biofilm formation in a porous microfluidic device*. Lab Chip, 2012. **12**(24): p. 5133-7.
2. Costerton, J.W., *Bacterial Biofilms: A Common Cause of Persistent Infections*. Science, 1999. **284**(5418): p. 1318-1322.
3. Flemming, H.C. and J. Wingender, *The biofilm matrix*. Nat Rev Microbiol, 2010. **8**(9): p. 623-33.
4. Wong, G.C.L. and G.A. O'Toole, *All together now: Integrating biofilm research across disciplines*. MRS Bulletin, 2011. **36**(05): p. 339-342.
5. Yazdi, S. and A.M. Ardekani, *Bacterial aggregation and biofilm formation in a vortical flow*. Biomicrofluidics, 2012. **6**(4): p. 044114.
6. Rusconi, R., et al., *Laminar flow around corners triggers the formation of biofilm streamers*. J R Soc Interface, 2010. **7**(50): p. 1293-9.
7. Drescher, K., et al., *Biofilm streamers cause catastrophic disruption of flow with consequences for environmental and medical systems*. Proceedings of the National Academy of Sciences of the United States of America, 2013. **110**(11): p. 4345-4350.
8. Marty, A., et al., *Formation of bacterial streamers during filtration in microfluidic systems*. Biofouling, 2012. **28**(6): p. 551-62.
9. Taherzadeh, D., et al., *Computational Study of the Drag and Oscillatory Movement of Biofilm Streamers in Fast Flows*. Biotechnology and Bioengineering, 2010. **105**(3): p. 600-610.

10. Vrouwenvelder, J.S., et al., *Impact of flow regime on pressure drop increase and biomass accumulation and morphology in membrane systems*. Water Research, 2010. **44**(3): p. 689-702.
11. Mitchell, A.C., et al., *Biofilm enhanced geologic sequestration of supercritical CO<sub>2</sub>*. International Journal of Greenhouse Gas Control, 2009. **3**(1): p. 90-99.
12. Soleimani, S., et al., *Modeling of biological clogging in unsaturated porous media*. J Contam Hydrol, 2009. **106**(1-2): p. 39-50.
13. Kumar, A., et al., *Microscale confinement features can affect biofilm formation*. Microfluidics and Nanofluidics, 2013. **14**(5): p. 895-902.
14. Neethirajan, S., et al., *Biofilms in Microfluidic Devices*, in *Encyclopedia of Nanotechnology*, B. Bhushan, Editor. 2012, Springer: New York.
15. Barathi, S. and N. Vasudevan, *Utilization of petroleum hydrocarbons by Pseudomonas fluorescens isolated from a petroleum-contaminated soil*. Environment International, 2001. **26**(5-6): p. 413-416.
16. Das, S. and A. Kumar, *Formation and post-formation dynamics of bacterial biofilm streamers as highly viscous liquid jets*. arXiv preprint arXiv:1312.6056, 2013.
17. Shaw, T., et al., *Commonality of Elastic Relaxation Times in Biofilms*. Physical Review Letters, 2004. **93**(9).
18. Berejnov, V., N. Djilali, and D. Sinton, *Lab-on-chip methodologies for the study of transport in porous media: energy applications*. Lab on a Chip, 2008. **8**(5): p. 689-693.

### **3 Bacterial floc mediated rapid streamer formation in creeping flows**

Material in this chapter has been published in:

Hassanpourfard, Mahtab, Zahra Nikakhtari, Ranajay Ghosh, Siddhartha Das, Thomas Thundat, Yang Liu, and Alope Kumar. "Bacterial floc mediated rapid streamer formation in creeping flows." *Scientific reports* 5 (2015).

#### **3.1 Introduction**

In their natural state bacteria can be found in either disparate planktonic forms or living in tight knit communities such as flocs, mats, pellicles or biofilms [1-3]. The latter, aggregative modes of bacterial growth are characterized by cells embedded in a matrix, usually of self-produced extracellular polymeric substances (EPS) composed of long-chain biomolecules such as polysaccharides, nucleic acids and lipids [1, 4-7]. This composite soft matter, consisting of bacteria and EPS, has been attracting intense scrutiny due to a complex interplay between material behavior and the underlying life processes brought about by large deformation even at very low Reynold's number ( $Re$ ); for example, in the case of filamentous bacterial streamers generated from bacterial biofilms [8-11].

Streamers are so named due to their distinguishing filamentous morphology. They have been reported in systems with sustained hydrodynamic flows [9]. These slender bacterial aggregates are typically tethered at one or both ends to solid surfaces, while the rest of the structure is suspended in a

liquid environment. Bacterial streamers have been observed to form both in high [12, 13], and in low Reynolds number conditions ( $Re \ll 1$ ) [10, 11, 14-16]. Streamer formation in low  $Re$  transport is of significant technological and biomedical interest due to relevance to a wide variety of critical operating scenarios including clogging of biomedical devices such as heart stents, catheters, porous media, and water filtration systems [8, 11, 17]. Rusconi et al. [10], while studying the effect of curved channel geometries using a microfluidic device, found that *P. aeruginosa* formed streamers in the curved sections of the microchannels. Drescher et al. [8] later showed that streamer formation in microfluidic devices with curved sections can lead to catastrophic clogging. Valiei et al. [11] used a microfluidic device with micropillars, and studied biofilm formation by *P. fluorescens*. They found that, in a certain flow regime, the bacteria formed extensive streamers resulting in a web-like network between the different pillars. A commonality between the reports by Valiei et al. [11], Rusconi et al. [10] and Drescher et al. [8] is that the streamers appeared far later than the biofilms, and the corresponding streamer formation time-scale,  $t_s$ , was of the order of hours from the beginning of the flow. Das and Kumar [18] have recently proposed that in such instances, where the streamer formation time-scale far exceeded the relaxation time-scale of biofilms, streamers appeared from a highly viscous state of the intrinsically viscoelastic biofilms. In contrast to these studies, some other experiments conducted under apparently similar creeping flow conditions reported much smaller  $t_s$  values ( $t_s \sim$  minutes) [15, 16] (see Table 3.1). Kim et al. [19] have reported even smaller streamer formation time scales for the bacterium *Staphylococcus aureus*, though this was achieved by first coating the channel walls of the microfluidic device with human plasma. Such large variation in streamer formation time

scale might indicate different physical mechanisms that govern the streamer formation process. Streamers forming at very large time scales ( $t_s \sim hrs$ ) have typically been reported in systems where formation of a biofilm occurs prior to streamer formation; referred herein as biofilm-mediated streamer formation [8, 10, 11]. To the best of our knowledge, a proper quantitative evaluation of small time scale streamer formation is yet to be reported. Furthermore, much of the literature on streamer formation in low Reynolds number conditions is relatively recent in the context of literature on biofilms and the physical basis of streamer formation remains an active area of research [9, 20, 21].

**Table 3.1:** Time scale of streamer formation from different experiments

<b>Bacteria</b>	<b>Streamer formation time scale (hr)</b>	<b>Comment</b>	<b>Ref.</b>
<i>Pseudomonas aeruginosa</i>	6-7		Rusconi et al. [10]
<i>Pseudomonas aeruginosa</i>	18		Rusconi et al.[22]
<i>Pseudomonas fluorescens</i>	few hours	for certain flow rates (8-12-20 ul/h)	Valiei et al. [11]
<i>Pseudomonas aeruginosa</i>	50		Drescher et al. [8]
<i>Staphylococcus epidermis</i>	6		Weaver et al.[23]
<i>Escherichia coli</i>	0.5		Yazdi and Ardekani [16]

<i>Pseudomonas fluorescens</i>	$\sim 10^{-4}$ (i.e. a few seconds)		<b>Present work</b>
--------------------------------	-------------------------------------	--	---------------------

In this study, we report our discovery of a new kind of bacterial streamer formation – these streamers do not appear from biofilms, rather they appear due to flow-induced deformation of the pre-formed bacterial flocs. We conduct our experiments in a microfluidic device composed of micropillars and containing solution laden with flocs of the bacterium *P. fluorescens*. We are able to optically probe the inception process of the streamers by embedding the bacterial flocs with 200 nm red fluorescent polystyrene beads that serve as tracers. We discover that fluid flow first advects the flocs some of which then get attached to the micropillars; subsequently, the hydrodynamic shear forces deform them into filamentous streamers. Interestingly, the formation timescale of this floc-mediated streamer formation is less than a second, which is in sharp contrast to the much larger timescale witnessed for biofilm-mediated streamers. Next, we find that the streamers are not purely elastic structures since we observed perceptible viscous behavior at time scales larger than its formation time scale but still far from clogging regime. Our methodology of using nanoscale fluorescent tracers, allows for the first time a direct quantification of the evolution of the streamer morphology. This gives us valuable clues about the fundamental mechanism of floc-mediated streamer formation in contrast to the much more extensively studied biofilm-mediated streamer formation, which still remains a highly contentious problem.

## **3.2 Experimental**

### **3.2.1 Microchip fabrication:**

A 4" silicon master mold was prepared by following the conventional photolithography process from the designed pattern. Then, by applying soft lithography processes and using the prepared master mold, the final device was fabricated from polydimethylsiloxane (PDMS, Sylgard 184, Dow Corning, NY, USA). Next, by exposing the cover slip and the PDMS stamp to oxygen plasma for 30 seconds, the PDMS stamp and the cover slip were bonded together to prepare the microchip. At the end, the microchip was annealed at 70 °C for 10 min to attain better sealing. The protocol is described in detail by Hassanpourfard et al. [14].

### **3.2.2 Bacterial culture**

In this experiment, colonies of *P. fluorescens* CHA0 (wild type) were grown on Luria-Bertani (LB) agar plate at 30 °C overnight. Next, one colony from an agar plate was inoculated into LB broth medium. One colony was also inoculated in M9 broth medium. To prepare the M9 broth, first, a 5X concentrated stock solution was prepared by stirring 56.4g of powder (containing the salt components 33.9g/L Na<sub>2</sub>HPO<sub>4</sub>, 15g/L KH<sub>2</sub>PO<sub>4</sub>, 5g/L NH<sub>4</sub>Cl, and 2.5g/L NaCl) in 1L of water. This solution was autoclaved for 15 minutes at 121°C in order to sterilize it. After cooling the 5X concentrated M9 stock, it was diluted to a 1X working solution by adding 200ml of the 5X M9 stock to 700ml sterile water. Afterwards, 2ml of sterile 1M MgSO<sub>4</sub>, 0.1 ml of sterile 1 M CaCl<sub>2</sub> and 20 ml of 20% glucose were added. Then, the solution was adjusted to have a final volume of 1L by adding sterilized distilled water (the final glucose

concentration was 0.4%). The strain of bacteria here is green fluorescent as they express green fluorescent protein (GFP) constitutively. To stimulate floc formation in the bacterial solution, the bacterial solution was kept in a shaker incubator (New Brunswick Scientific Co., NJ) at 30 °C and 150 rpm for about 48 h. Longer incubation duration leads to nutrient depletion and subsequent floc formation [24]. Here in the LB medium, the OD<sub>600</sub> for the bacterial culture was approximately 1.7 after 48 hours and for the M9 medium under the same conditions the OD<sub>600</sub> was approximately 0.7.

### **3.2.3 Microscopy**

The microfluidic chip was placed on the stage of an inverted optical microscope (Nikon Eclipse Ti). The bacteria solution was injected continuously into the microchip by using a syringe pump (Harvard Apparatus, MA, USA). The temperature of microchip was set at 30 °C by the aid of an on-stage microscope incubator (Pathologic Devices, Inc., MD, USA). Particle tracking was performed using the object tracking module in Nikon NIS-Element AR software interface. Effective surface area calculations were also performed using the same software. Error for stretch ratio calculation was estimated to be approximately 8%. Surface coverage percentage was calculated by defining a threshold value for green color intensity. If the green color intensity of a pixel was above the threshold value, then corresponding pixel was counted. Next, we calculated the surface coverage percentage by dividing the counted pixels to the total number of pixels in the image (except area covered by the pillars) and multiplying by 100. This procedure is the same as that outlined in a previous publication by Kumar et al. [25]. Furthermore, the streamer's location in

different  $z$  directions was investigated by capturing  $z$ -stack images using a confocal laser scanning microscope (CLSM) (Carl Zeiss, Inc., NY, USA).

### 3.2.4 Computational fluid mechanical (numerical) simulations

We performed 2-D fluid mechanical simulations using the commercial package Comsol Multiphysics® to simulate the device flow. In this simulation, we assumed that the fluid going through the channel has the same properties as water at 30°C and pressure. To describe the fluid flow in the channel the incompressible Navier-Stokes and continuity equations were used. The inlet velocity was calculated according to the flow rate (here 15  $\mu\text{l/h}$ ). The no-slip and the no penetration boundary condition were imposed on the walls and a constant atmospheric pressure was imposed at the channel outlet, respectively. Mesh density was increased until no mesh dependency was observed in the solution. Velocity is non-dimensionalized with respect to the velocity scale,  $U = Q / (W \times h_c)$ , where  $Q$  is the volume flow rate (imposed by the syringe pump).

### 3.2.5 Velocity gradient calculation

We tracked a particle  $\mathbf{P}$  which moves in a fixed Eulerian grid from  $P_0(x_0, y_0)$  to  $P_1(x_1, y_1)$  in time  $\delta t_1$  and then further moves to  $P_2(x_2, y_2)$  in another time  $\delta t_2$ .

The normalized velocity gradient at  $P_0$  is then given by forward-difference discretization:

$$[L] \approx \frac{l}{U \delta t_1 \delta t_2} \begin{pmatrix} \frac{x_2 \delta t_1 - x_1 (\delta t_1 + \delta t_2) + x_0 \delta t_2}{x_1 - x_0} & \frac{x_2 \delta t_1 - x_1 (\delta t_1 + \delta t_2) + x_0 \delta t_2}{y_1 - y_0} \\ \frac{y_2 \delta t_1 - y_1 (\delta t_1 + \delta t_2) + y_0 \delta t_2}{x_1 - x_0} & \frac{y_2 \delta t_1 - y_1 (\delta t_1 + \delta t_2) + y_0 \delta t_2}{y_1 - y_0} \end{pmatrix} \quad (1)$$

Two eigenvalues of  $[L]$  corresponding to two principal eigenvectors were found. One of the eigenvectors was found to be nearly aligned with the orientation of the streamer and the eigenvalue corresponding to the other eigenvector was vanishingly small as expected. Thus for the purpose of this work, we denote the larger eigenvalue (which is aligned with the streamer orientation) of the velocity gradient tensor as the principal velocity gradient,  $L_1$ . Note that this principal velocity gradient component is assumed to be mostly inelastic in the time frame considered with elastic and rotational components assumed negligible.

### 3.3 Results

#### 3.3.1 Initiation of floc-mediated streamers

Our microfluidic device (Fig. 3.1a, b) consisted of a sequence of polydimethylsiloxane (PDMS) micropillars in a periodic staggered grid pattern. The micropillars had a diameter ( $d$ ) of 50  $\mu\text{m}$  and spaced 75  $\mu\text{m}$  apart ( $l$ ). The fluid flow rate ( $Q$ ) was maintained at levels such that the resultant flow in our device was in the creeping flow regime (Reynolds number,  $Re$ , was  $O(10^{-3})$ ). Numerical simulations provide the velocity profile inside the channel under these conditions. Fig 3.1c depicts the non-dimensionalized (with respect to  $U = Q/(W \times h_c)$  where  $W$  &  $h_c$  are channel width and height respectively) contour plot of magnitude of velocity and also streamlines (inset) in the device.

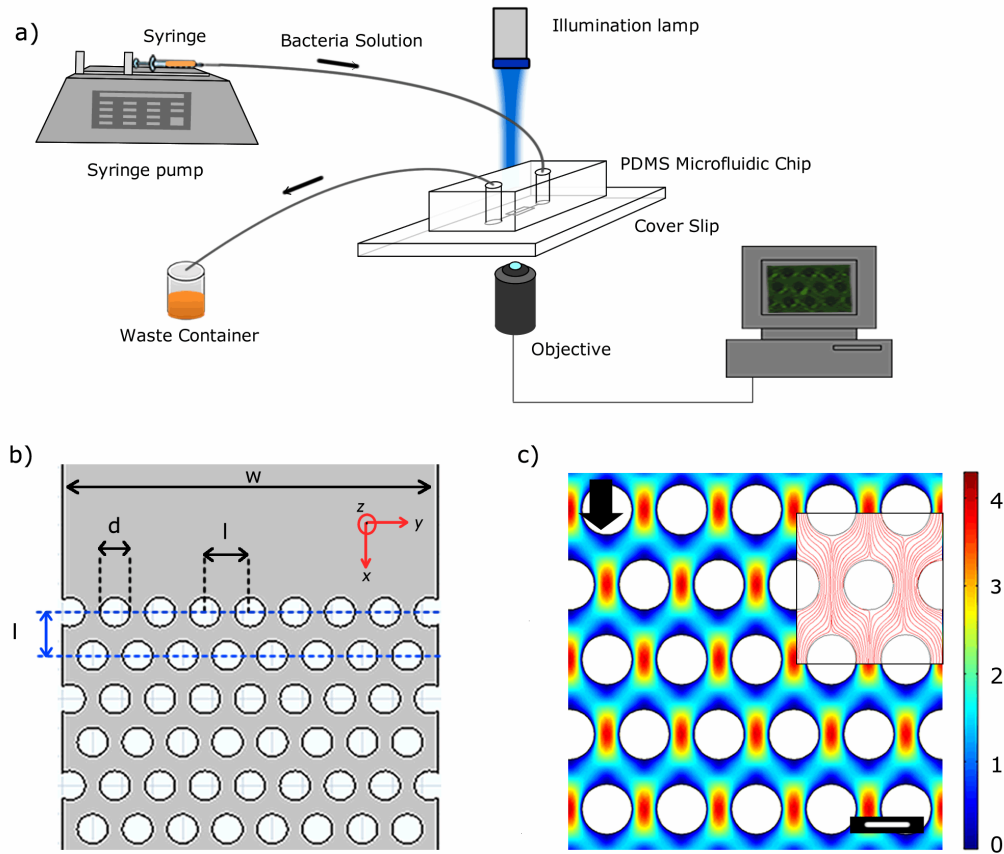
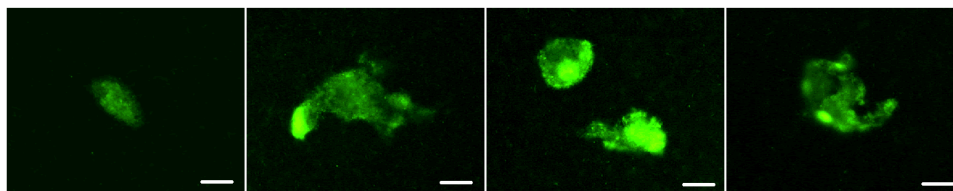


**Figure 3.1:** a) A schematic of experimental set-up under pressure driven flow with constant volume flow rate ( $Q$ ). b) Layout of staggered pattern porous media. Width ( $W$ ) of porous zone is  $625 \mu\text{m}$ . The distance between the center of pillars ( $l$ ) and 2 rows of consecutive pillars is  $75 \mu\text{m}$ . The diameter of the pillars and the height of the device ( $h_c$ ) both are  $50 \mu\text{m}$ . c) Computational fluid mechanical simulations demonstrating the non-dimensionalized velocity ( $\sqrt{v_x^2 + v_y^2} / U$ ) contour of the flow in the porous section of the microchannel.  $v_i$  depicts fluid velocity in  $i$ -th direction. In our device  $Q = 15 \mu\text{l/hr}$  corresponds to  $1.3 \times 10^{-4} \text{ m/s}$ . The scale bar is  $50 \mu\text{m}$ . (Inset) Streamlines for the same flow condition.

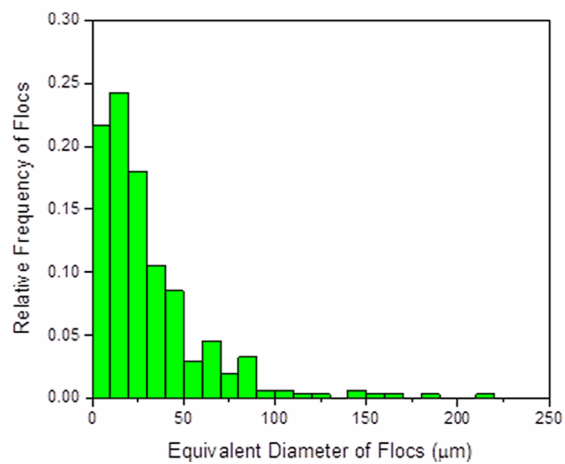
We studied the behavior of the wild type (WT) strain of *P. fluorescens*, a bacteria that plays a vital role in maintaining plant physiology [26]. The genetically modified WT expressed green fluorescent protein (GFP)

constitutively and hence was green fluorescent. Pre-formed biomass of *P. fluorescens* in the form of bacterial flocs was utilized in our study (Fig 3.2a). The bacterium was cultured in LB and M9 media (see Materials and Methods). While biomass/floc formation occurred in both media, flocs formed in M9 media were significantly smaller than the flocs produced in LB and they did not form streamers (see Fig. 3.3). This shows that growth conditions are also relevant factors; here we focus on flocs produced in LB media and defer investigation of growth conditions to a subsequent manuscript.

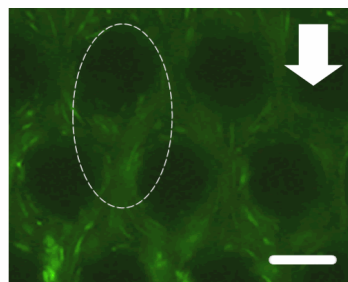
a)



b)



c)



d)

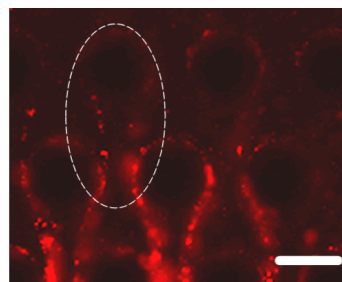


**Figure 3.2:** a) Flocs of *P. fluorescens* bacteria after incubation at 30 °C overnight. The scale bars are 25  $\mu\text{m}$ . b) Relative frequency histogram of the flocs. The  $x$ -axis is equivalent diameter of the flocs in the reservoir. The median and mode for this relative frequency histogram are 21.28 and 22.23  $\mu\text{m}$ , respectively. c) and d) Green and red fluorescent images, respectively, of the microchannel after injecting the bacteria with 200 nm fluorescent red polystyrene beads particles into it. The images were taken at the same time and place that was approximately at the middle of the channel height ( $z = 25 \mu\text{m}$ ). The red fluorescent particles clearly seed and enable visualization of the streamer. Note the regions demarcated by dashed ellipses where bacteria (green) are not significant, but the streamer itself is easy visualized due to red particles seeding the EPS network. The scale bars are 50  $\mu\text{m}$ .

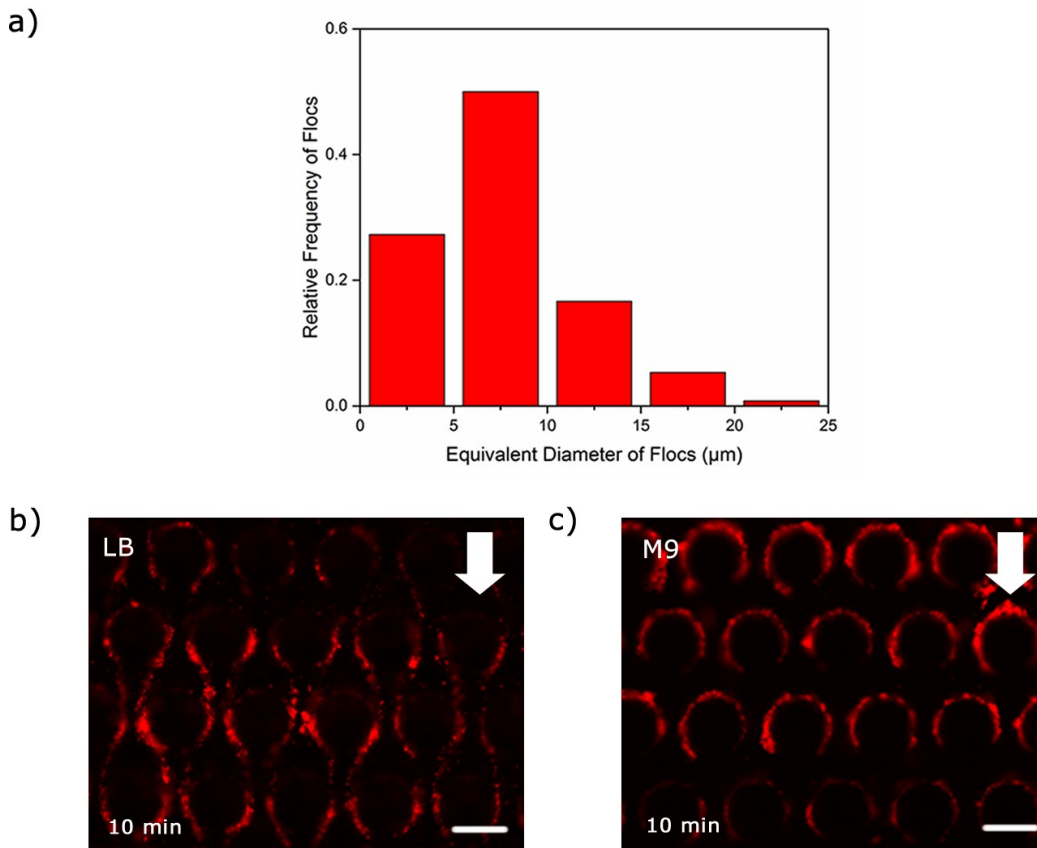


**Figure 3.3:** a) Relative frequency histogram of the flocs cultured in M9 media. The median and mode for this relative frequency histogram are 6.78 and 5.85  $\mu\text{m}$ , respectively b) and c) Comparison of streamer formation in LB and M9 media. Streamers did not form in M9 media at short-time scales ( $\sim$  few minutes) as compared

to LB media.

Bacterial flocs are EPS encapsulated aggregates of the bacteria that are dispersed in a liquid phase. These flocs were imaged first in quiescent media and their equivalent diameter was measured. For our system we observed a wide variation in the equivalent diameter. Their quantification was done through a relative frequency histogram, which shows that the mode for these flocs occurred at approximately 22  $\mu\text{m}$  (Fig. 3.2b). These flocs were further mixed with 200 nm red fluorescent amine coated polystyrene (PS) particles and the mixture was allowed to flow through the microfluidic device. Two color imaging was performed for the system as the bacteria were green fluorescent and PS particles were red fluorescent. The red fluorescent beads were embedded in the EPS matrix of the flocs and thus provided clear visualization of the dynamics of these flocs (Fig. 3.2c and d). Such two-color visualization helps us overcome the difficulty in visualizing EPS, which is almost transparent under brightfield illumination.

The solution containing planktonic bacteria and bacterial flocs was flown through the device for several minutes and it was observed that streamer like structures formed within a few minutes of the initiation of the experiment (Fig. 3.4 and Video 1<sup>4</sup>). The bacterial flocs could be seen to attach to the micro-pillar posts and then deformed by fluid shear. A dashed ellipse marks the location of this event. Similarly, in the right hand side, another floc undergoes a similar process. It is interesting to note that the size distribution of flocs measured in quiescent media (Fig. 3.2a) is not reflected in the size of flocs that were observed to flow past the pillars (see Fig 3.5). For instance, although the mode

---

<sup>4</sup> The link for video 1 is: <http://www.nature.com/articles/srep13070>

of floc sizes was similar to the pillar diameter, such flocs were not observed in the flow past these pillars (Fig. 3.5).

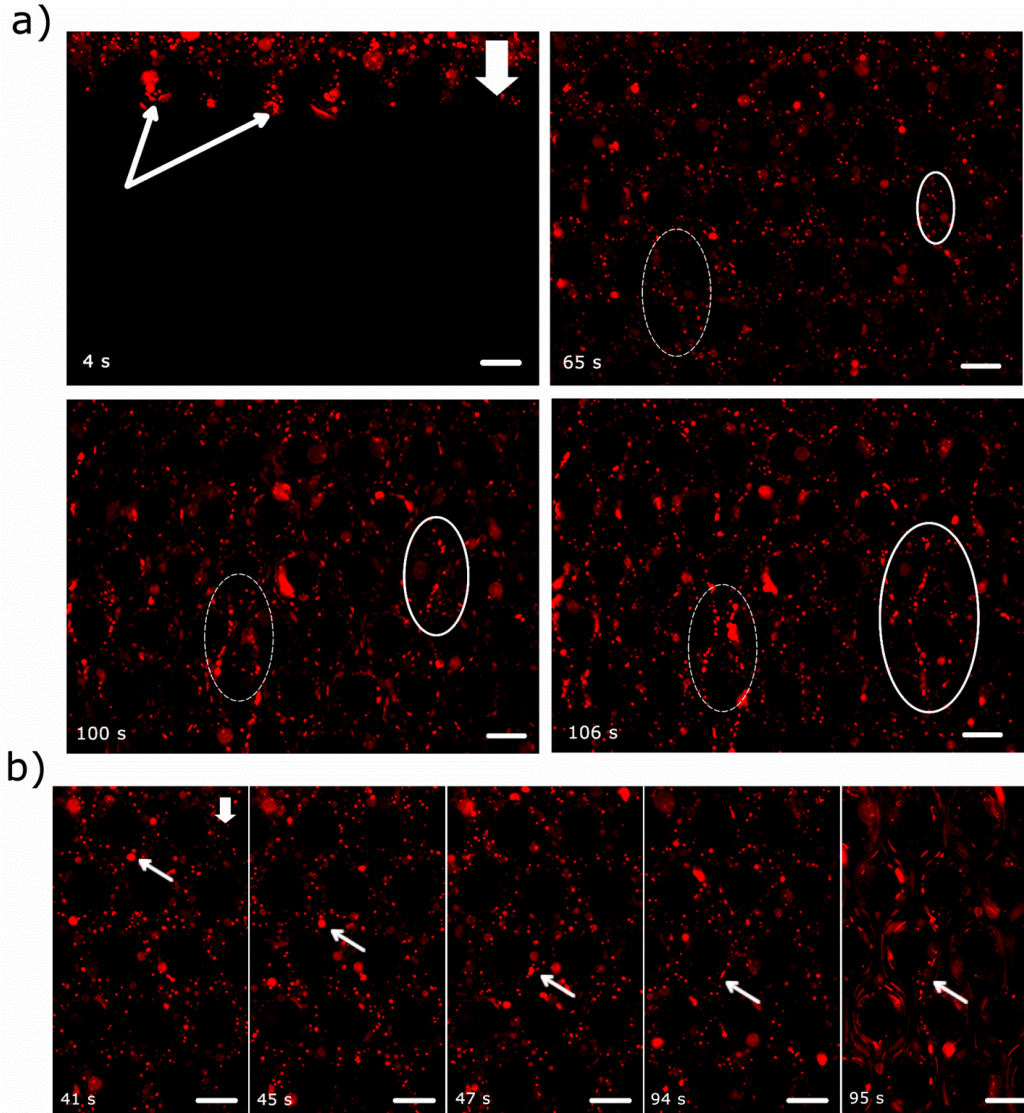


**Figure 3.4:** a) Rapid streamer formation in a short time scale (a few seconds). The scale bars are 50  $\mu\text{m}$ . See accompanying video. The images were taken approximately at the middle of the channel height ( $z=25 \mu\text{m}$ ). In the top-left image, the arrows demarcate the advancing fluid meniscus. The ellipses demarcate two regions where streamers form. b) An arrow demarcates a floc, which is first advected through the channel and then is attached to a micropillar wall at  $t=47 \text{ s}$ . Finally, at 95 s a streamer is formed. Scale-bars are 50  $\mu\text{m}$ .

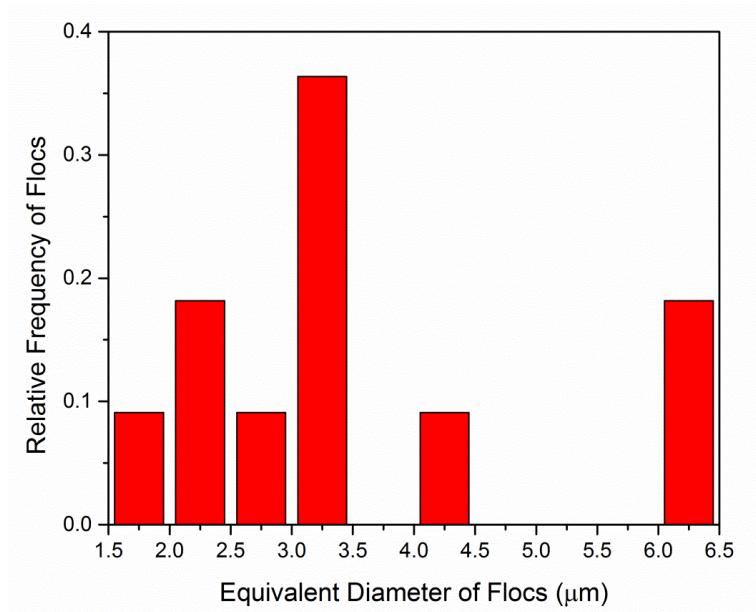


**Figure 3.5:** Relative frequency of flocs sizes entering the microfluidic channel.

### 3.3.2 Timescale and mechanism of floc-mediated streamer formation

The central result of our study is that the time-scale of formation of these floc-mediated streamers ( $t_s$ ) is very small (Fig. 3.4 and Video 1). A close examination of video 1 reveals that the floc in the right hand side of Fig 3.4 undergoes large deformation at  $t_s < 1$  sec. For instance, in the left hand side of Fig. 3.4, a floc approximately 3-3.5  $\mu\text{m}$  in diameter undergoes very large deformation to form a streamer like structure. In video 1, a constant volume flow rate (or a constant  $U$ ) is enforced by the syringe pump; however in the initial period when all pillars have not been wetted,  $U$  can have considerable oscillatory component in time [27]. Let us denote the time for this initial

wetting as  $t_{\text{wetting}}$ , which is observed to be about ( $\sim 95$  s) and taken to be the time when  $U$  becomes constant indicating the onset of completion of wetting. Thus at  $t > t_{\text{wetting}}$ , we assume that wetting of all pillars is complete, and  $U$  becomes constant. For  $t < t_{\text{wetting}}$ , i.e. when  $U$  has an oscillatory component in time, the response of the flocs to a temporally varying fluid shear at a spatial location can be seen clearly (Fig 3.6 and Video 1). Probing further, we track a set of closely placed particle couplets and measure the ratio of their separation along the streamer to their initial separation. This stretch ratio ( $\lambda$ ) contains useful information regarding the material behavior of the streamer. To this end, a floc is chosen where embedded PS beads act as tracers and allow us to identify two closely situated points,  $\alpha$  and  $\beta$ , and then these are tracked as a function of time (Fig. 3.6a). The point  $\alpha$  is largely immobile due to its adhesion to the cylinder wall, while  $\beta$  is displaced by the fluid shear forces. As the fluid shear force scales with velocity  $\tau \sim \mu \frac{U}{L}$ , a time-periodic  $U$  results in a time-periodic  $\tau$ . The distance between the two points in their initial (reference state) is denoted by  $d\mathbf{X}$  and in the current state by  $d\mathbf{x}$ . The axial stretch ratio defined as  $\lambda(t) = \frac{|d\mathbf{x}|}{|d\mathbf{X}|}$  is plotted with respect to time in Figure 3.6b. As expected, Figure 3.6b indicates that, at  $t < t_{\text{wetting}}$ ,  $\lambda(t)$  oscillates between unity and a maximum value of approximately 3 (i.e. 200% engineering strain). This initial recoverable strain clearly indicates an elastic component of the streamer material. As the flow velocity increases, the streamer stretching begins to increase until, at the advent of steady flow, the floc is stretched into the slender geometry characteristic of streamer. After the initial wetting period ( $t > 95$  s),

the streamer becomes attached between two successive pillar walls indicating stretch of the order of seven (Fig 3.6b). If a complete loss of material strength is assumed at this deformation, a lower limit of streamer formation time can be estimated from the background fluid velocity profile obtained from the simulations (Fig 3.1c). Assuming an average transport speed of approximately  $U = 13 \times 10^{-5}$  m/s, and transport distance as the inter-pillar separation length, of  $l = 75 \times 10^{-6}$  m, we get  $t_s \sim \frac{l}{U}$  which comes to be approximately of the order of  $t_s$  is  $O(10^{-1})$  s. This time scale agrees well with our experiments. Furthermore, from the numerical simulations, the role of shear deformation in streamer formation is strongly suggested as well (see Fig. 3.7), since most of the streamers originate from regions corresponding to maximum shear stress.

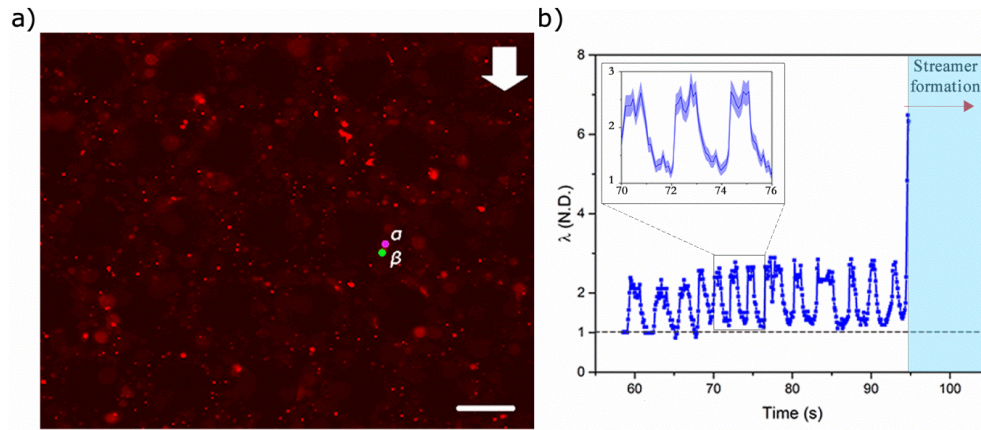


**Figure 3.6:** a) Two points  $\alpha$  and  $\beta$  are tracked as the fluid velocity fluctuates in the channel. These two points would later form a streamer. The scale bar is 50  $\mu\text{m}$ . b) Stretch ratio of the two points as a function of time during the initial filling period of the channel. Streamer formation region (right) also co-incides with the onset of steady flow. Black dashed line depicts  $\lambda=1$  (Inset) Stretch ratio for a smaller time segment. The colored envelope represents estimated error.

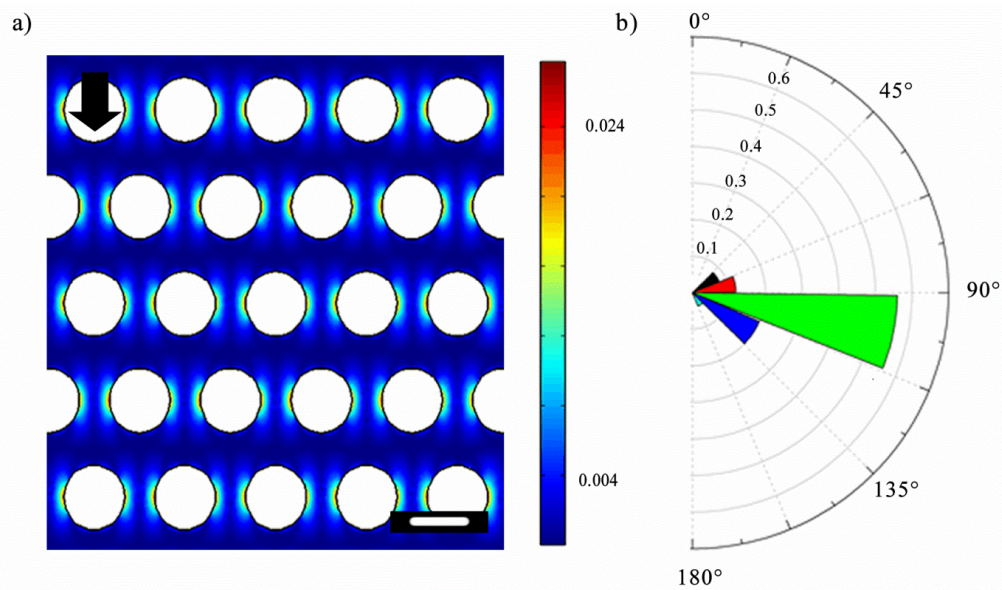


**Figure 3.7:** a) Simulation results for the contour of the magnitude of the dimensionless shear stress  $\bar{\tau} = \frac{d}{U} \mu \frac{1}{2} (\nabla u + (\nabla u)^T)$ ,  $u$  being the velocity field b) Polar frequency histogram of where flocs attach on the pillars. Half of one pillar is considered.  $0^\circ$  represents upstream stagnation point and  $180^\circ$  represents downstream stagnation point.

Streamers eventually lead to catastrophic clogging of the device, such as that observed by Drescher et al. [8]. Interestingly however, the time period spanning the advent of streamer formation to final clogging is not marked by a sudden transition if closer look at the streamer behavior is taken. In this context, on an experimental time scale greater than the streamer formation time-scale ( $t > t_s$ ), but still far from clogging related change of overall velocity profile and streamer shape, there is a perceptible viscous component indicated by a creeping response of a material point of the streamer material (Video 2<sup>5</sup>). Quantification of this response is made possible by evaluation of the temporal

<sup>5</sup> The link for video 2 is: <http://www.nature.com/articles/srep13070>

response of the principal velocity gradient (strain rate) at a constant background velocity, which itself scales as the shear stress. This creeping response is well demonstrated by a temporal change in velocity gradients at the middle of the streamer. Although the velocity gradient variation for all streamers were found to be approximately constant in the time scale of scrutiny, for brevity we report the explicit temporal variation for a streamer only at velocity scale  $U$  of  $1.3 \times 10^{-4}$  m/s, Fig. 3.8a (see Materials and Methods). This indicates a steady creep regime under the flow conditions during the time scale of measurement. We further probe this behavior by plotting an averaged velocity gradient at a point for various flow rates, Fig. 3.8b. The figure clearly shows a nonlinear relationship between shear stress and strain rate and the slope, which is a rough estimation of the inverse of viscosity, shows a decreasing trend with stress. This suggests significant shear thickening component. Although the precise physical origin of this effect and the determination of the exact constitutive relationship to describe the inelasticity would need further experiments, this behavior is consistent with the structure of a typical biofilm and the relatively short period of observation. The film, which is itself a composite made up of suspended bacteria, flocs and aggregates in the EPS interact weakly with one another. However, as shear stress increases, these constituents come closer thereby increasing viscosity. Note that in time scales longer than the ones observed, several other complex phenomena such as mass aggregation and transition of inelasticity regimes would likely occur.

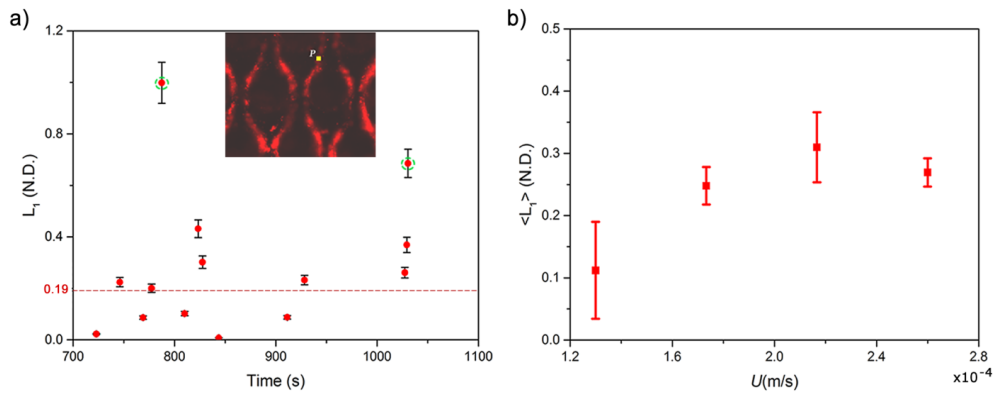


**Figure 3.8:** a) Temporal variation of the non-dimensional principal velocity gradient ( $L_1$ ) of a fully formed streamer. The experimentally obtained values (blue dots) show an approximately constant trend (dashed red line); two points demarcated through dashed green ellipses were neglected as outliers. (Inset) A point  $P$  was tracked on a fully formed streamer for calculation of the velocity gradient. Here  $U = 1.3 \times 10^{-4}$  m/s. b) Time-averaged principal velocity gradient ( $\langle L_1 \rangle$ ) of fully formed streamers as a function of non-dimensional flow speed ( $U$ ).

### 3.3.3 Clogging action of the floc-mediated streamers

At a time-scale much greater than the streamer formation time-scale ( $t \gg t_s$ ), a very different picture emerges. Streamer formation is a dynamic phenomenon where the streamer grows in width as it accrues additional mass from its surrounding fluid. Figure 3.9a shows that in approximately one hour after the beginning of the experiment a large part of the device is covered in biomass. This can be quantified by measuring the surface coverage by the biofilm as a function of time. Figure 3.9b shows that very quickly about 50% of the device is covered by the bacterial film. Thus clogging in this device can not only be catastrophic [8] but also take place at a rapid clogging rate. The exponential increase in surface coverage can be explained by previously

developed models for streamer growth as explained by Dreshcer et al. [8] and later corrected by Das and Kumar [18].

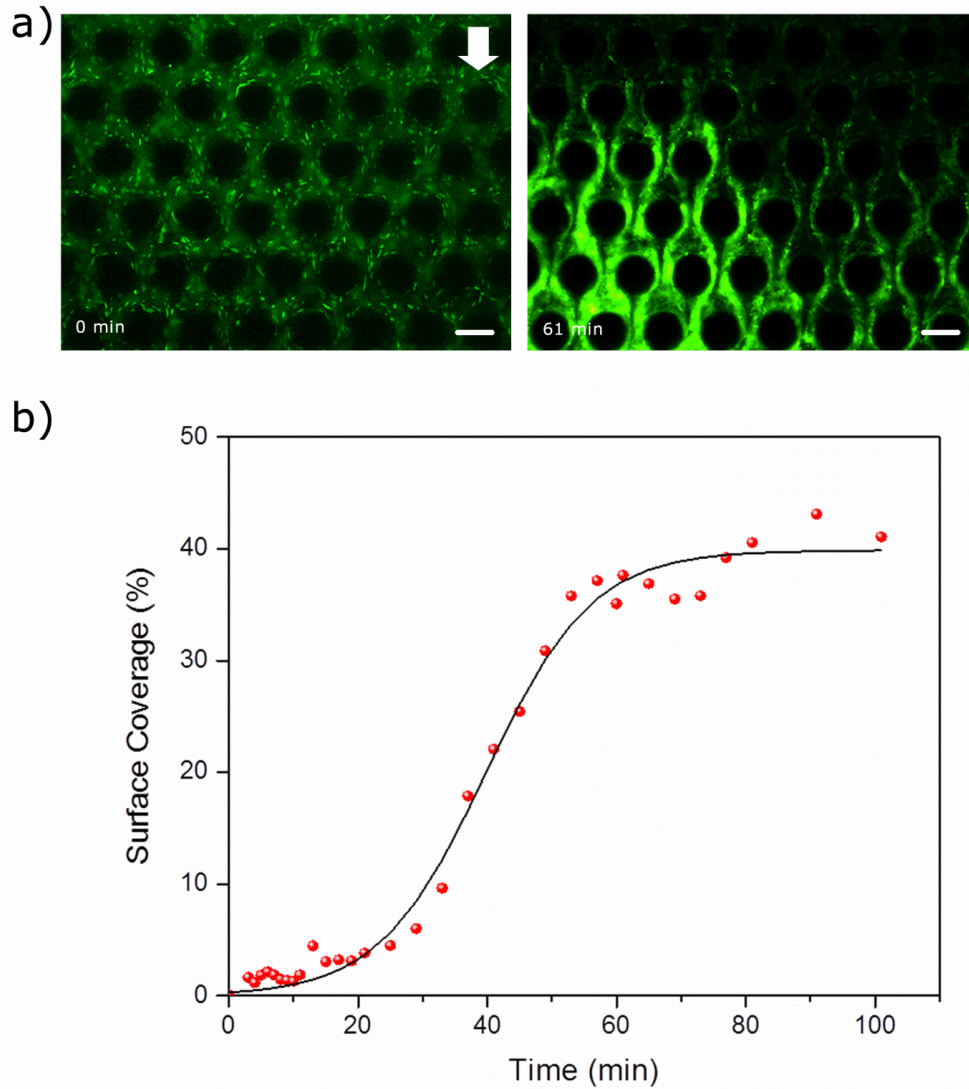


**Figure 3.9:** Rapid and catastrophic clogging of the channel by streamers. a) Images of the channel at two time-points. The scale bars are 50  $\mu\text{m}$ . b) The graph shows a gradual increase of surface coverage from 2% (3 min) to 5% (25 min). Then, it has a dramatic surge from 5% (25 min) to 37% (57 min). After that the graph plateaus. Solid curve represents a sigmoidal curve fit to the data.

### 3.4 Discussion

Here, using seeded particles, which allowed very precise quantification of the deformation of the biomass structures, we clearly demonstrate that pre-formed biomass, in the form of bacterial flocs, can lead to streamer formation through the process of large deformations, even when fluid flow in a system lies in the creeping flow regime. This is the first experimental observation, where the formation of a streamer has been demonstrated and we have shown that pre-formed biomass can lead to very rapid streamer formation time scales. Furthermore, particle tracking enabled us to conclude that the material behavior of the streamer can have both significant elastic as well as viscous component making them highly dynamic mechanical structures even in creeping flows. Finally, streamers cause not only catastrophic, but very rapid clogging of devices.

The exact material constitution of the bacterial communities is of great interest for a range of applications [9]. However, traditional material characterization techniques are impractical for *in situ* applications thus making the characterization of this system far more challenging. However, important material information is obtained by scrutinizing the response of the streamer due to fluidic loading by the background flow. The temporal behavior of the axial strain as quantified by  $\lambda(t)$ , offers important insights into the mechanics of streamer formation. An interesting aspect of the streamer formation is the ability of the biomass to remain elastic under relatively large stretch ratios (engineering strain  $\sim 200\%$ ). This is typical of elastomeric materials. Such large strain elasticity is typically attributed to a molecular level ‘chain stretching’ [28]. However, for the current material, it may also include straining of a more

complex intermediate hierarchical microstructure well known in biofilm morphological literature [1, 29]. This study would thus serve as an important motivation for such future extensions. As the flow develops fully, the shear stress on the incipient streamer increases significantly. This results in a significant increment of the shear stress causing the incipient structure to undergo even larger deformation after which the streamer extends between adjacent pillars and streamers are formed, see Fig 3.4. The strain regime corresponding to this highly extended state ( $\lambda \sim 7$ ), typically indicate substantial inelastic behavior. This is confirmed by observing a material point couple which move slowly through the streamer even when the background flow is constant (Fig.3.8 a,b). We assume that the measured velocity gradient at these deformations is almost entirely inelastic in nature.

It is also important to note that the time-scale of streamer formation, as observed in the current investigation, is much smaller than both biological growth time-scales and viscoelastic relaxation time scales of biofilms [30]. This indicates that floc-driven streamer formation is physically distinct from biofilm-driven streamer formation [18]. In practical terms, the long time-lag observed in biofilm-driven streamer formation [8, 10, 11] is not observed here, thus leading to very rapid streamer growth and clogging. We would also like to note that secondary flows seem to have little or no role in streamer location in our device. Rusconi et al. [10] had credited secondary flows for the formation of a single streamer at the mid-height of their device. We investigated streamer distribution in the device along the  $z$ -axis using confocal laser scanning microscopy (CLSM) (Fig. 3.10a). In our device transverse secondary flows converging at the mid-plane of the device (similar to those seen by Rusconi et al. [10]) are also seen (Fig. 3.10b), but localization of streamers at  $z = h_c/2$  is

not seen. In fact, we found that streamers were distributed at different heights in the device (Fig. 3.10a). The non-dimensional streamer thickness,  $h^* = h_s/h_c$ , where  $h_s$  is the dimensional streamer thickness, at time 30 min is plotted in Fig 3.10c.

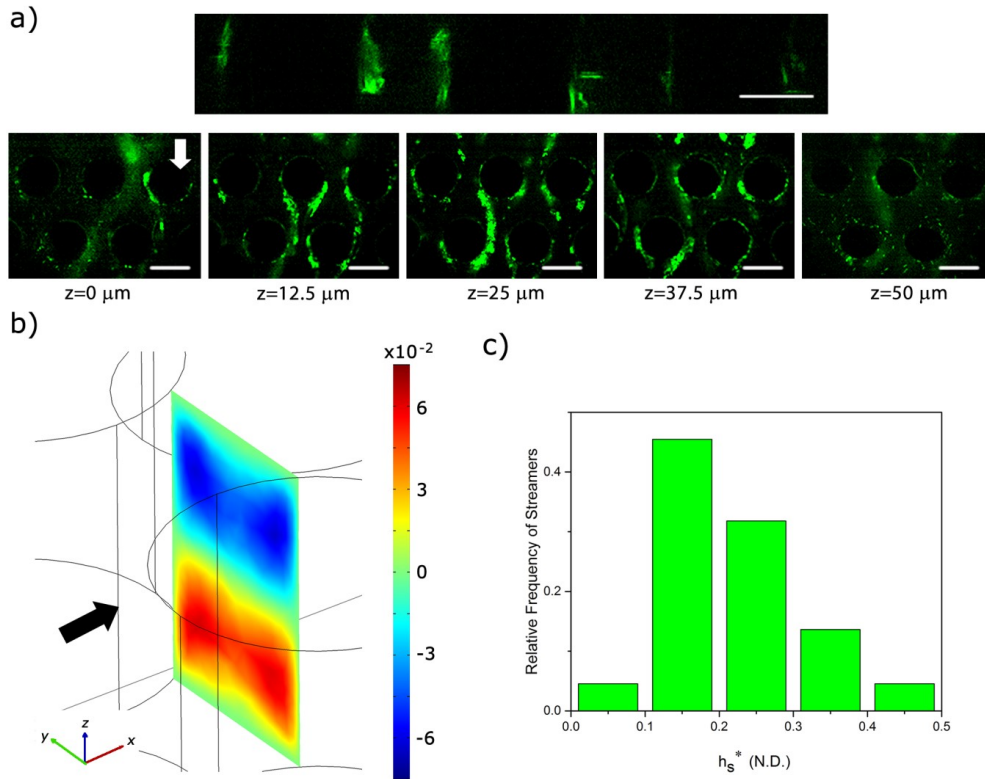


**Figure 3.10:** a) Confocal sidebar shows the floc attachment through the height of the pillars. CLSM images of streamer formation at different heights in the chip. Such distribution of streamers across  $z$ -height is seen at other locations too. b) Numerical simulation of the non-dimensional  $z$ -component of the velocity at a downstream location ( $v_z^* = v_z/U$ ) (arrow shows the direction of the flow). Secondary flows, in a direction transverse to the main flow, converge at the middle plane in the chip. c) Histogram of streamer thickness as evaluated by CLSM after 30 mins of experimentation.

Biofilm streamer formation remains an exciting frontier with several open ended unanswered questions. Here, we clearly demonstrate that pre-formed biomass, in the form of bacterial flocs, can lead to streamer formation through large deformations, even when fluid flow in a system lies in the creeping flow regime. This is the first direct experimental observation, where the formation of a streamer and their behavior in the intermediate time scale with respect to clogging has been demonstrated by using seeding particles for very precise quantification of the biomass structures. The key results of this work include demonstration of very rapid streamer formation and subsequent creep response of fully formed streamers. Finally, we show that streamer formation lead to rapid clogging of the device.

### **Acknowledgments**

MH acknowledges support of Alberta Innovates Technology Futures. TT acknowledges support from the Canada Excellence Research Chair program. YL acknowledges support from the NSERC. AK acknowledges support from the NSERC Discovery Program.

### 3.5 References

1. Flemming, H.C. and J. Wingender, *The biofilm matrix*. Nature Reviews Microbiology, 2010. **8**(9): p. 623-633.
2. Wingender, J., T.R. Neu, and H.-C. Flemming, *What are bacterial extracellular polymeric substances?*, in *Microbial extracellular polymeric substances*. 1999, Springer. p. 1-19.
3. Wu, C., et al., *Quantitative Analysis of Amyloid-Integrated Biofilms Formed by Uropathogenic Escherichia coli at the Air-Liquid Interface*. Biophys. J., 2012. **103**(3): p. 464-471.
4. Whitfield, C., *Bacterial extracellular polysaccharides*. Can J Microbiol, 1988. **34**(4): p. 415-420.
5. Flemming, H.C., T.R. Neu, and D.J. Wozniak, *The EPS matrix: The "House of Biofilm cells"*. Journal of Bacteriology, 2007. **189**(22): p. 7945-7947.
6. More, T.T., et al., *Extracellular polymeric substances of bacteria and their potential environmental applications*. Journal of Environmental Management, 2014. **144**: p. 1-25.
7. Friedman, B.A., et al., *Structure of Exocellular Polymers and Their Relationship to Bacterial Flocculation*. Journal of Bacteriology, 1969. **98**(3): p. 1328-&.
8. Drescher, K., et al., *Biofilm streamers cause catastrophic disruption of flow with consequences for environmental and medical systems*. Proceedings of the National Academy of Sciences of the United States of America, 2013. **110**(11): p. 4345-4350.
9. Karimi, A., et al., *Interplay of physical mechanisms and biofilm processes: review of microfluidic methods*. Lab on a Chip, 2015. **15**: p. 23-42.

10. Rusconi, R., et al., *Laminar flow around corners triggers the formation of biofilm streamers*. Journal of the Royal Society Interface, 2010. **7**(50): p. 1293-1299.
11. Valiei, A., et al., *A web of streamers: biofilm formation in a porous microfluidic device*. Lab on a Chip, 2012. **12**(24): p. 5133-5137.
12. Stoodley, P., et al., *Biofilm material properties as related to shear-induced deformation and detachment phenomena*. J. Ind. Microbiol. Biot., 2002. **29**(6): p. 361-367.
13. Stoodley, P., et al., *Oscillation characteristics of biofilm streamers in turbulent flowing water as related to drag and pressure drop*. Biotechnology and bioengineering, 1998. **57**(5): p. 536-544.
14. Hassanpourfard, M., et al., *Protocol for Biofilm Streamer Formation in a Microfluidic Device with Micro-pillars*. JoVE (Journal of Visualized Experiments), 2014(90): p. e51732-e51732.
15. Marty, A., et al., *Formation of bacterial streamers during filtration in microfluidic systems*. Biofouling, 2012. **28**(6): p. 551-62.
16. Yazdi, S. and A.M. Ardekani, *Bacterial aggregation and biofilm formation in a vortical flow*. Biomicrofluidics, 2012. **6**(4).
17. Marty, A., et al., *Impact of tortuous flow on bacteria streamer development in microfluidic system during filtration*. Biomicrofluidics, 2014. **8**(1): p. 014105.
18. Das, S. and A. Kumar, *Formation and post-formation dynamics of bacterial biofilm streamers as highly viscous liquid jets*. Scientific Reports, 2014. **4**: p. 7126.
19. Kim, M.K., et al., *Filaments in curved streamlines: rapid formation of Staphylococcus aureus biofilm streamers*. New Journal of Physics, 2014. **16**: p. 065024.

20. Hol, F.J.H. and C. Dekker, *Zooming in to see the bigger picture: Microfluidic and nanofabrication tools to study bacteria*. Science, 2014. **346**(6208): p. 438-+.
21. Rusconi, R., M. Garren, and R. Stocker, *Microfluidics Expanding the Frontiers of Microbial Ecology*. Annual Review of Biophysics, 2014. **43**: p. 65-91.
22. Rusconi, R., et al., *Secondary flow as a mechanism for the formation of biofilm streamers*. Biophys J, 2011. **100**(6): p. 1392-9.
23. Weaver, W.M., et al., *Fluid flow induces biofilm formation in Staphylococcus epidermidis polysaccharide intracellular adhesin-positive clinical isolates*. Appl Environ Microbiol, 2012. **78**(16): p. 5890-6.
24. De Schryver, P., et al., *The basics of bio-flocs technology: The added value for aquaculture*. Aquaculture, 2008. **277**(3-4): p. 125-137.
25. Kumar, A., et al., *Microscale confinement features can affect biofilm formation*. Microfluidics and Nanofluidics, 2013. **14**(5): p. 895-902.
26. Mercado-Blanco, J. and P.A. Bakker, *Interactions between plants and beneficial Pseudomonas spp.: exploiting bacterial traits for crop protection*. Antonie Van Leeuwenhoek, 2007. **92**(4): p. 367-89.
27. Chen, H.-H., J. Shi, and C.-L. Chen, *Wetting dynamics of multiscaled structures*. Appl. Phys. Lett., 2013. **103**(17): p. 171601.
28. Arruda, E.M. and M.C. Boyce, *A three-dimensional constitutive model for the large stretch behavior of rubber elastic materials*. J Mech Phys Solids, 1993. **41**(2): p. 389-412.

29. De Beer, D., et al., *Effects of biofilm structures on oxygen distribution and mass transport*. Biotechnology and bioengineering, 1994. **43**(11): p. 1131-1138.
30. Shaw, T., et al., *Commonality of Elastic Relaxation Times in Biofilms*. Physical Review Letters, 2004. **93**(9).

## 4 Dynamics of bacterial streamers induced clogging in microfluidic devices

Material in this chapter has been published in:

Hassanpourfard, Mahtab, Ranajay Ghosh, Thomas Thundat, and Alope Kumar. "Dynamics of bacterial streamers induced clogging in microfluidic devices." *Lab on a Chip* (2016).

### 4.1 Introduction

Bacterial streamers, which are microscopically slender filamentous aggregates primarily comprising of bacterial cells encased in a matrix of self-secreted extra-cellular polymeric substances (EPS) are typically formed due to the action of sustained hydrodynamic flows on bacterial soft matter [1-4]. Although, streamers are known to form under a wide range of hydrodynamic conditions, including turbulent flow conditions ( $Re > 1000$ ) and creeping/Stokes flow ( $Re \ll 1$ ) conditions [3-9], their formation and implications are issues that are yet to be fully resolved. Recent investigations, especially those using porous microfluidic devices [2, 3, 7, 8] indicated that streamers development has two mutually distinct phases. The initial phase, which is soon after formation, is characterized by streamers which appear morphologically similar to slender strings with a high length ( $l_s$ ) to diameter ( $d_s$ ) ratio ( $l_s/d_s \sim O(10)$ ). Once formed, the streamers continue to accrue mass from the background flow thereby thickening (decreasing aspect ratio), finally maturing into a biomass that covers the entire pore-space of the device [2, 3] thereby transitioning into

the later ‘clogging’ phase. In the context of the present work, the latter phase is characterized by the streamer diameter becoming of the same order as the pore-scale ( $l$ ) i.e. ( $d_s \sim l$ ) (Fig. 4.1). These thickened streamers which make their appearance at a later stage of the flow experiment are termed ‘mature streamer’ to distinguish them from the initial slender streamers.

Recent research indicates that an important impact of streamer formation in creeping flow regime ( $Re \ll 1$ ) is the rapid mass accrual and catastrophic clogging of porous media [2, 3], biomedical devices [2, 10], and filtration units [8]. In this context, this clogging phase can disrupt the performance of numerous medical devices such as catheters, heart stents, and filtration membranes that can be vital for patients [10]. Moreover, their ability to detach, and then form aggregates elsewhere pose the potential risk for severe infections [11, 12]. In contrast to these biomedical concerns, recent investigations of streamer formation in microfluidic porous media mimics have also been motivated by the need to understand microbial growth and proliferation in natural porous media such as soils and rocks [3, 13].

While the above-mentioned studies establish the acute relevance of the clogging phase, the clogging phenomena itself is yet to be fully explored and understood. In fact, fostering a deeper understanding of the relationship between background flow and the streamers’ short and intermediate time-scale dynamics is critical in the design, fabrication and operation of such medical devices. In this context, the understanding of biological macromolecular interfaces in such systems, which affect the relative motion of mature streamer vis-à-vis device walls, needs to be advanced.

Here we investigate clogging dynamics of bacterial streamers using a microfabricated pseudo-porous platform. Our device employs pore sizes that are  $O(10^{-5})$  m, a range that is often found in artificial and natural porous structures such as membranes [1] and soil [13, 14]. We observed that mature structures formed from bacterial streamers have three-phase interface (bacterial biomass, media and solid interface) that show a ‘stick-slip’ behavior in their movement in the channel. These mature structures eventually undergo failure if the volume flow rate in the device is kept constant and this can lead to the formation of distinct water channels. Two bacterial strains viz. *P. fluorescens*, a soil-dwelling bacterium [15-17], and *P. aeruginosa*, an opportunistic pathogen [10], were employed and they exhibited similar dynamical response.

## 4.2 Experimental

In our experiments, a microfluidic device fabricated from polydimethylsiloxane (PDMS, Sylgard 184, Dow Corning, NY, USA) was used as a platform to mimic porous media. To fabricate this device, we followed the steps of conventional photolithography process and soft lithography process to create PDMS stamps. The microfluidic devices themselves were created by finally bonding a glass coverslip and PDMS stamp by oxygen plasma process. The fabrication details are standard practice in nanofabrication and interested readers can refer to Hassanpourfard et al. [7] for process details. Figure 4.1a demonstrates our microfluidic set up. The microfluidic device contains a channel with arrays of PDMS micro-pillars. Figure 4.1b shows a porous section of the device which contains 400 micropillars. The arrangement of micropillars allows the device to function as rough two-dimensional analog of a porous media. SEM image of pillars shows that the pillars are very regular and

perpendicular structures (Fig. 4.2). Using the syringe pump (Harvard Apparatus, MA, USA), fluid laden with bacterial flocs of wild type (WT) strain of *P. fluorescens* was introduced into the device with a constant volume flow rate of the fluid ( $Q$ ) for each experiment. The genetically modified WT strain expressed green fluorescent protein (GFP) constitutively and hence was green fluorescent. The velocity scale ( $U$ ) corresponding to an imposed flow rate is given by  $U = Q/(b \times h)$ , where  $b$  and  $h$  are channel width and height respectively. To prepare bacterial flocs, the bacterial solutions were prepared by firstly streaking the -80 °C bacterial stocks of *P. fluorescens* onto the LB agar plate. The agar plate was incubated in the incubator overnight at 30 °C. One colony from agar plate was transferred into the LB broth and it was placed into shaker incubator at 30 °C for about 2 days, until the optical density at 600 nm ( $OD_{600}$ ) reached a value of approximately 0.7. The longer incubation period was adopted so that nutritional stress condition results in the formation of bacterial flocs [2]. Bacterial flocs are an aggregative mode of bacterial growth, where bacterial cells are embedded in EPS. Unlike biofilms, flocs do not necessarily form at a liquid-solid interface and instead can be found suspended in a liquid environment [18]. In our experiment, the equivalent diameter of flocs was measured in the quiescent media and their quantification was shown as a relative frequency histogram. The result shows that the mode for these flocs is approximately 21.5  $\mu\text{m}$  (Fig. 4.3).

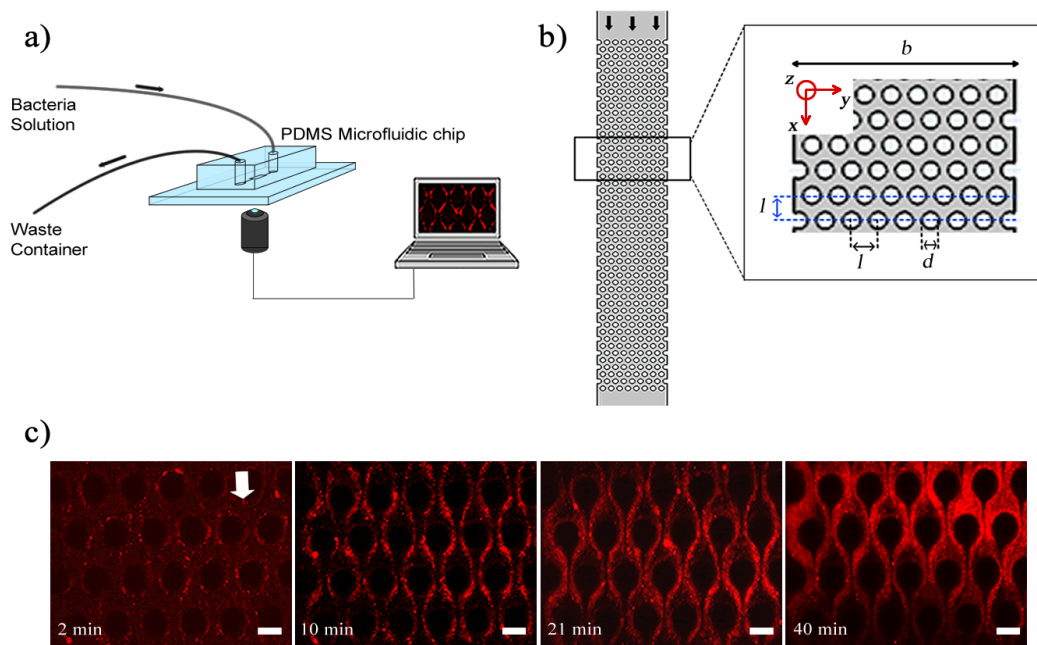


**Figure 4.1:** a) Microfluidic experimental set-up. b) Top view of the porous section of the channel. The channel width ( $b$ ) is  $625\ \mu\text{m}$  and the porous section of channel contains 400 ( $8 \times 50$ ) pillars. The micropillars' diameter ( $d$ ) and height ( $h$ ) are  $50\ \mu\text{m}$  and they are set  $75\ \mu\text{m}$  apart ( $l$ ). The fluid flow rate ( $Q$ ) was at a value that we had a creeping flow in the channel,  $Re$ , was  $O(10^{-3})$ . c) Time series of streamer development from slender body (high aspect ratio) to mature structures.

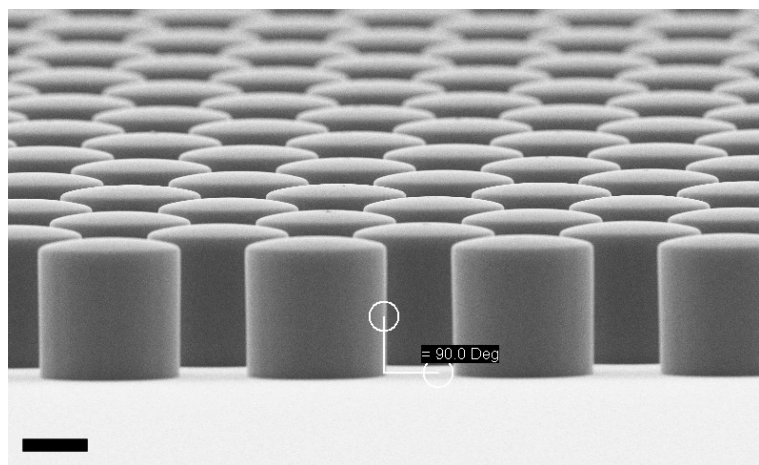


**Figure 4.2:** SEM image of PDMS pillars in the micro-channel. Scale bar is  $25\ \mu\text{m}$ .

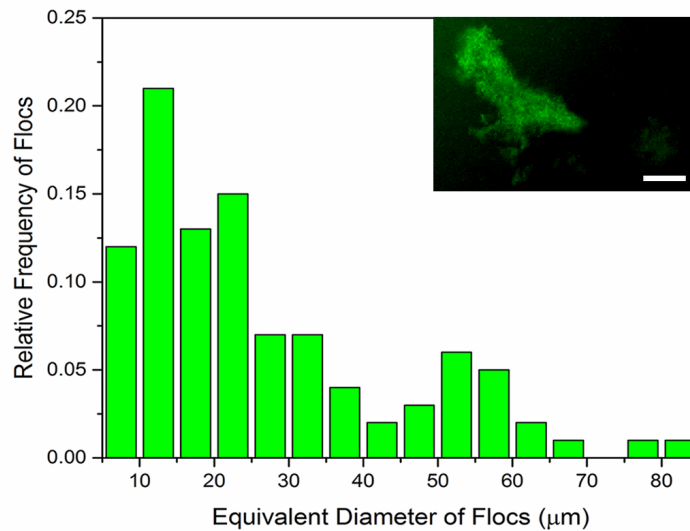


**Figure 4.3:** Relative frequency histogram of flocs of *P. fluorescens*. The mode and median for this relative frequency histogram are 21.48 and 20.68  $\mu\text{m}$  respectively. A total of 100 flocs were considered. See Hassanpourfard et al. [2] for details regarding image analysis. The inset shows two flocs of *P. fluorescens* that were obtained after incubation at 30  $^{\circ}\text{C}$  for 2 days. Scale bar is 25  $\mu\text{m}$ .

### 4.3 Results and discussion

Once bacterial flocs were introduced into the microfluidic device, some of them adhered to the micro-pillar walls and were stretched by hydrodynamic shear forces into streamers. The time-scale of such streamer formation ( $t_s$ ) was only a few seconds. The initial formation phase which was characterized earlier by Hassanpourfard et al. [2] was once again clearly visible. These slender structures then thickened into ‘mature streamers’ increasingly occupying the pore space thereby causing clogging of the device. The clogging time-scale

( $t_{clogging}$ ) was reported to be of the order of  $10^3$  seconds. In order to image the dynamics of the biomass, the original bacteria solution was seeded with red fluorescent amine coated polystyrene (PS) particles with 200 nm diameter. We should note at this point that typically only the cells (length scale  $\sim$  few microns) are visible under fluorescence illumination, and the EPS itself is invisible, thus posing a challenge for tracking the movement of the entire streamer biomass. PS particles, which easily seed the EPS, were added to overcome the challenge of tracking the biomass. Thus, the 200 nm PS beads aid in streamer visualization. The temporal change in the morphology of streamers is shown in Figure 4.1c.

The mature streamers which clog the pore-space, also show the formation of a three-phase front (biomass, pillar walls and fluidic media). These streamers start to flow with different velocity from the background flow, as shown previously [2] aiding their movement downstream. In this study, we observed that this movement is not smooth, but rather proceeds through a ‘stick-slip’ mechanism (see Fig. 4.4a for time series data and Video 3<sup>6</sup>). To further quantify this stick-slip phenomena, we tracked the movement of a Lagrangian point (i.e a trapped PS particle) in the mature streamer close to the three-phase contact line (Fig. 4.4b inset). Then we calculated the cumulative arc length ( $s$ ) that travelled by the Lagrangian point as function of time ( $s = \sum_{t_0}^t s_t$  where  $s_t = \sqrt{(x_t - x_{t-1})^2 + (y_t - y_{t-1})^2}$ ). Figure 4.4b depicts the temporal variation of  $s$  for various flow speeds. The  $x$ -axis for Figure 4.4b is translated by a time ( $t_0$ ), which indicates the time elapsed since the beginning of the stick-slip behavior. This was different for different flow rates (Table 4.1). Figure 4.4b, clearly

---

<sup>6</sup> The link for video 3 is:  
<http://pubs.rsc.org/en/content/articlelanding/2016/lc/c6lc01055e#!divAbstract>

shows that  $s$  increased in steps, indicating a stick-slip behavior. In order to ensure that the stick-slip behavior was not a result of intermittency caused by the pump, a separate experiment was also conducted where gravity assisted pressure driven flow was used. Even in this case, the results demonstrate a stick-slip movement of the mature streamer (Fig. 4.5). A further matter of interest would be the deformation of the pillars themselves under the flow loading. To this end, we found that the PDMS micropillars demonstrated no noticeable deformation (within imaging uncertainty) during any of our experiments as confirmed through time-resolved microscopy. Figure 4.4b reveals a gross stick-slip behavior, although regions with linear behaviors can also be discerned. Even for these regions, we find that when the time-scales for particle tracking are refined, the stick-slip behavior occurs at smaller time-scales (Fig. 4.4c). This stick-slip motion was also observed for *P. aeruginosa*. This shows that this behavior may be a more general mechanical phenomena and independent of the bio-physical issues associated with bacterial strains (Fig. 4.4d). Another interesting aspect of these experiments is that despite the inherent heterogeneity of biological samples, the overall phenomena are quite repeatable. We found this to be a general aspect of this types of experiments reported both in our previous reported works [2, 3, 7, 19] as well as many similar experiments as part of our ongoing research effort. All our experiments were repeated at least 3 times (Table 4.2) and similar behavior was observed for different replications (Fig. 4.6).

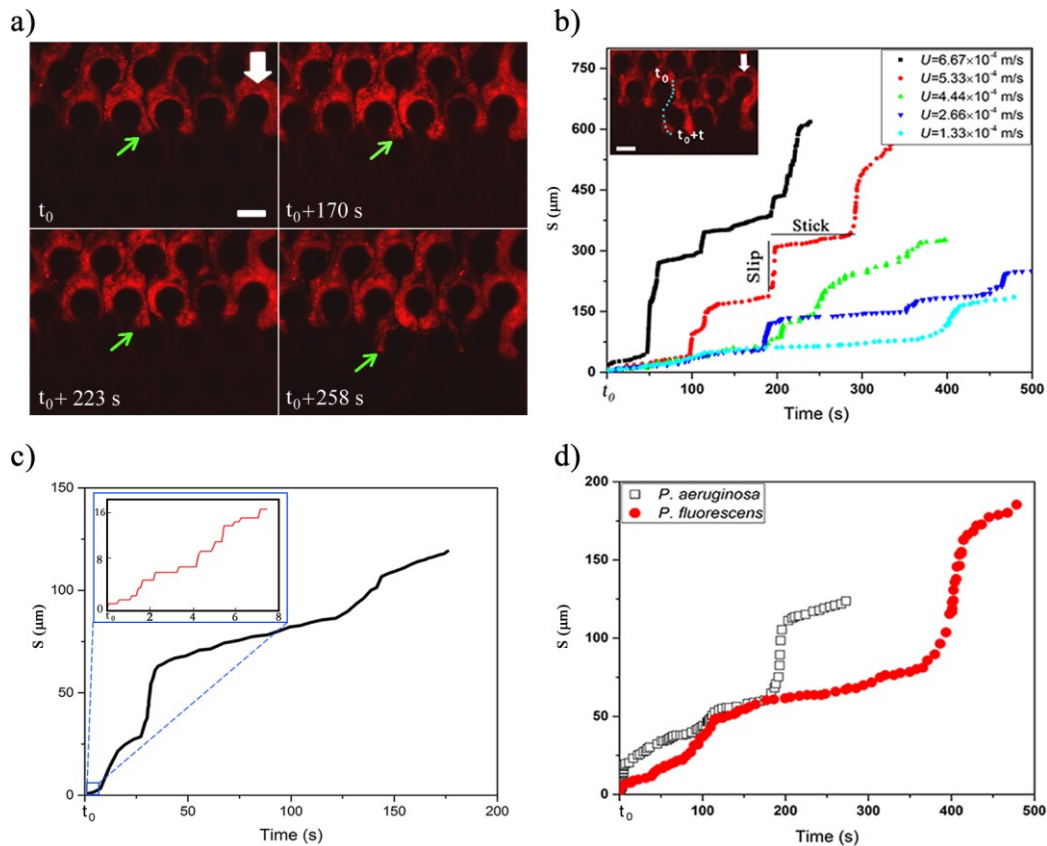


**Figure 4.4:** a) Time series image of streamer (*P. fluorescens*) that shows stick-slip behavior.  $t_0$  here is 83 min after beginning of experiment with the imposed flow velocity of  $1.33 \times 10^{-4} \text{ m/s}$ . Scale bar is  $50 \mu\text{m}$  and the white arrow shows the flow direction in the channel, which is from top to bottom. The green arrows delineate an advancing front undergoing stick-slip behavior. Note that the entire channel is liquid filled. b) Stick-slip behavior of *P. fluorescens* for different flow velocities. The particles in the front section were tracked and the cumulative length travelled was quantified. The inset shows the tracked front in the microfluidic device. The scale bar is  $50 \mu\text{m}$  and the arrow shows the flow direction in the channel. c) Stick-slip behavior of *P. fluorescens* in different time scales. Here  $t_0$  is 83 min after beginning of experiment with the imposed flow velocity of  $1.33 \times 10^{-4} \text{ m/s}$ . (inset) Stick-slip behavior also occur at much smaller time-scales. d) The stick-slip behavior of 2 different bacterial strains (*P. fluorescens* and *P. aeruginosa*) for flow velocity of  $1.33 \times 10^{-4} \text{ m/s}$ .  $\text{OD}_{600}$  for *P. aeruginosa* was about 0.6.

**Table 4.1:**  $t_0$  for different imposed flow speeds

U (m/s)	t <sub>0</sub> (min)
$1.33 \times 10^{-4}$	80
$2.66 \times 10^{-4}$	48
$4.44 \times 10^{-4}$	23
$5.33 \times 10^{-4}$	20
$6.67 \times 10^{-4}$	11

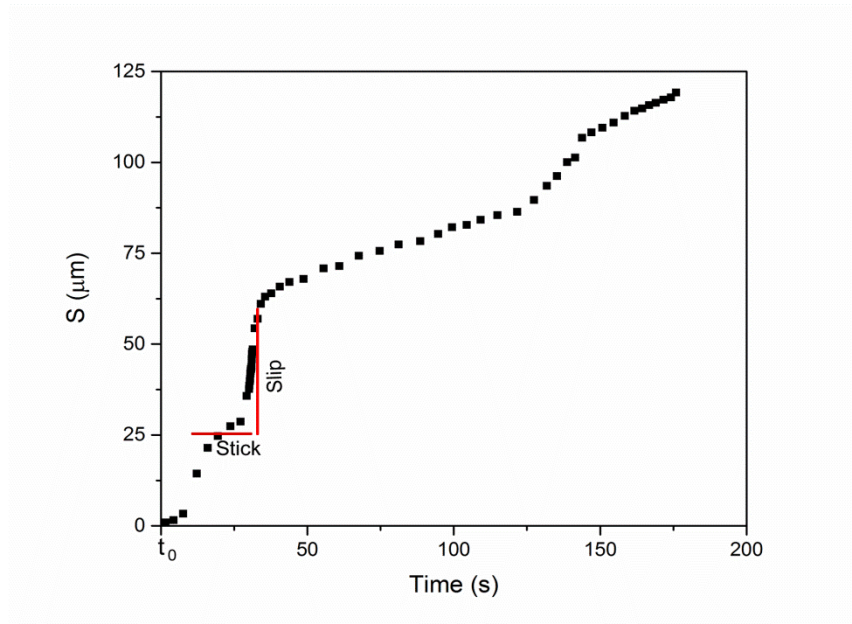


**Figure 4.5:** Stick-slip behavior of tracked particle in a mature streamer in a gravity-assisted pressure driven flow experiment due to the elevation of culture reservoir above the waste container. Here  $t_0$  is 11 min after the beginning of experiment.

**Table 4.2:** Repetitions per experiment

U (m/s)	Number of experiments
<i>P. fluorescens</i>	

$4.44 \times 10^{-5}$	3
$1.33 \times 10^{-4}$	4
$2.66 \times 10^{-4}$	3
$4.44 \times 10^{-4}$	3
$5.33 \times 10^{-4}$	3
$6.67 \times 10^{-4}$	3
<b><i>P. aeruginosa</i></b>	
$1.33 \times 10^{-4}$	3

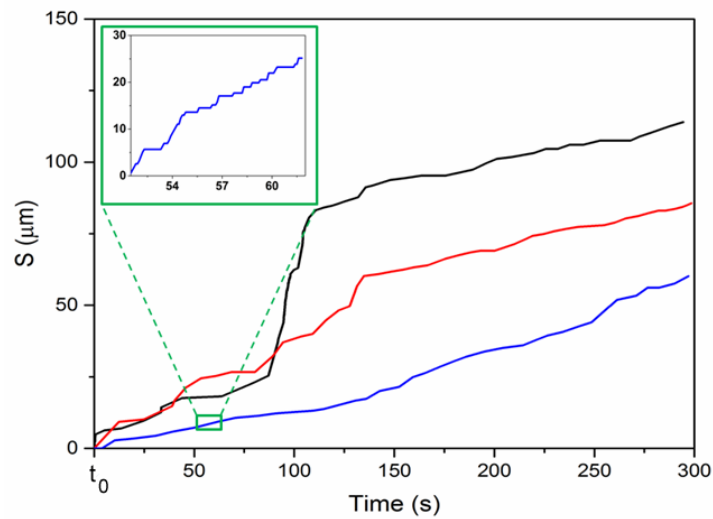


**Figure 4.6:** Stick-slip behavior of *P. fluorescens* for imposed flow velocity of  $1.33 \times 10^{-4}$  m/s from 3 different repetitions. Here  $t_0$  is between 30 to 90 min from beginning of the experiment.

Stick-slip behavior is fairly common between sliding surfaces and often attributed to multiple causes [20-26]. Moreover, viscoelastic materials can experience stick-slip or spurt flows due to instabilities [21, 27-29]. Recently,

Gashti et al. [30] also noticed that biofilms subject to continuous shear can show a non-monotonic velocity, which they attributed to possible non-Newtonian behavior of the biofilm [30]. However, in the current case, this behavior may have far more complex origins due to both the multiphasic nature of the interface and material nonlinearities typical of *in-situ* bacterial streamers. Therefore, a more detailed characterization has been left for a future work.

While figure 4.4 depicts the behavior of the advancing front of the clogging biomass, interestingly, the bulk of the clogging biomass also shows interesting behavior. Since, the syringe pump enforces a constant volumetric flow rate ( $Q$ ), clogging led to increased flow velocities in the clogged portion leading to a non-uniform flow field within the clogged device. This resulted in failure and breakage of mature streamers (Fig. 4.7a) at critical locations, leading to the formation of water-channels in the biomass, whose length scale was found to be several times that of the pore-length scale ( $l$ ) (Fig. 4.7b) (also see video 4<sup>7</sup>). Water channel formation depends on the imposed flow speeds. Water channels were observed for velocity scales of  $1.33 \times 10^{-4}$ ,  $2.66 \times 10^{-4}$  and  $5.33 \times 10^{-4}$  m/s after 3h injection of *P. fluorescens* bacterial solution while no visible water channel was observed for  $U = 4.44 \times 10^{-5}$  m/s (Fig. 4.8). Furthermore, water channels also formed in a microchip clogged with *P. aeruginosa* strongly indicating a mechanical origin of these phenomena (Fig. 4.9). The origin of this mode of failure is not yet fully understood.

---

<sup>7</sup> The link for video 4 is:  
<http://pubs.rsc.org/en/content/articlelanding/2016/lc/c6lc01055e#!divAbstract>

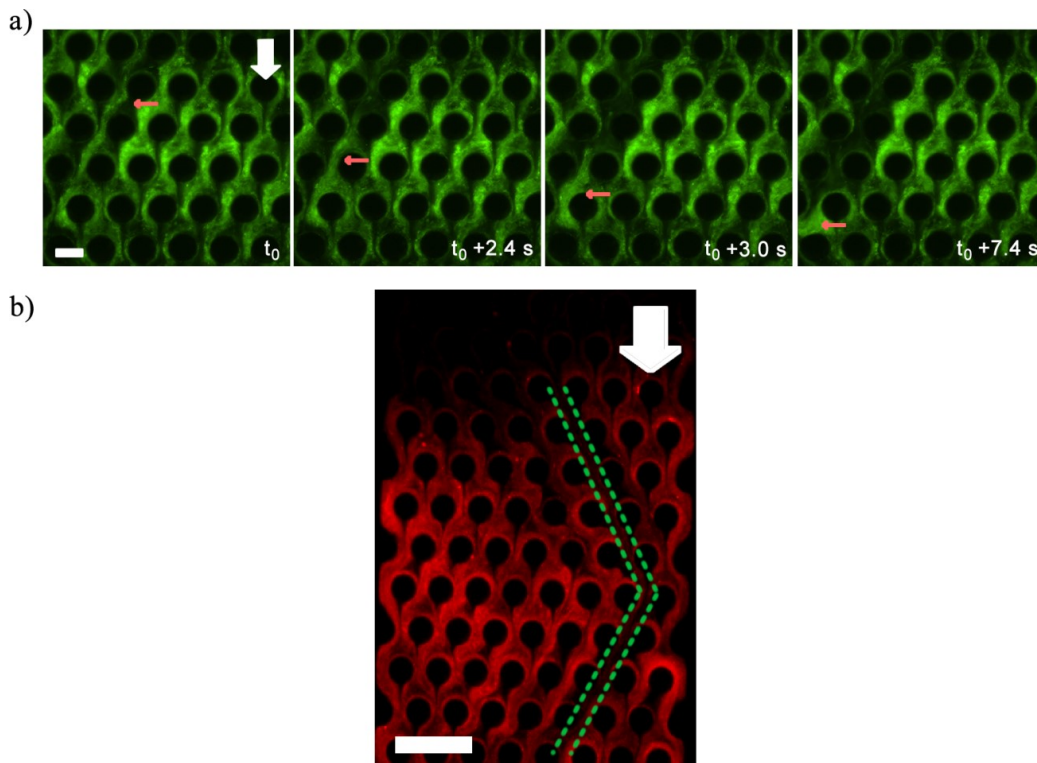


**Figure 4.7:** a) Bacterial biomass detachment in the microfluidic device that leads to water channel formation imaged under green fluorescence.  $t_0$  is 108 min after the beginning of the experiment ( $U=1.33 \times 10^{-4}$  m/s). Red arrows show movement of detached streamer. Scale bar represents 50  $\mu\text{m}$ . b) Green dash lines delineate a water channel formed in the device after 2 hours flow of *P. fluorescens* with flow speed of  $1.33 \times 10^{-4}$  m/s. Images are top view of the porous section of the channel and were captured approximately at the middle height of the channel ( $z = 25$   $\mu\text{m}$ ). Scale bar represents 150  $\mu\text{m}$ . White arrows show the flow direction.

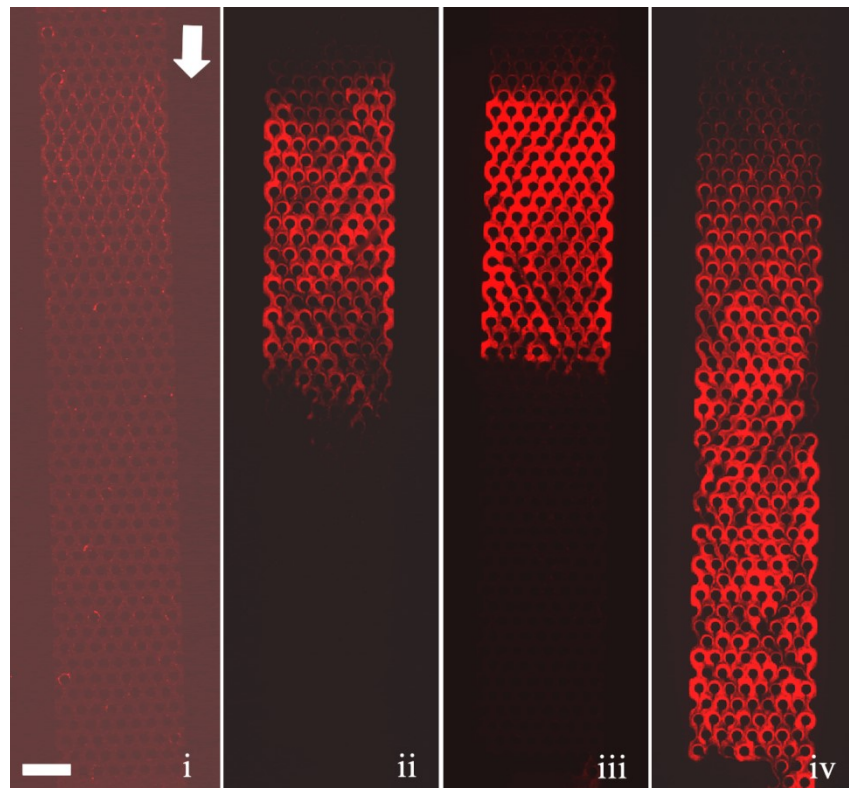


**Figure 4.8:** a) Water channel formation in the clogged part of the microfluidic device. Bacterial solutions (*P. fluorescens*) were injected for 3 hours into the channel and the experiments were performed for different imposed velocity scales of i)  $4.44 \times 10^{-5} \text{ m/s}$ , ii)  $1.33 \times 10^{-4} \text{ m/s}$ , iii)  $2.66 \times 10^{-4} \text{ m/s}$  and iv)  $5.33 \times 10^{-4} \text{ m/s}$ . Clogging didn't occur for  $U=4.44 \times 10^{-5} \text{ m/s}$ . Scale bar is  $250 \mu\text{m}$ . White arrow shows the flow direction that is from top to bottom in all the experiments.

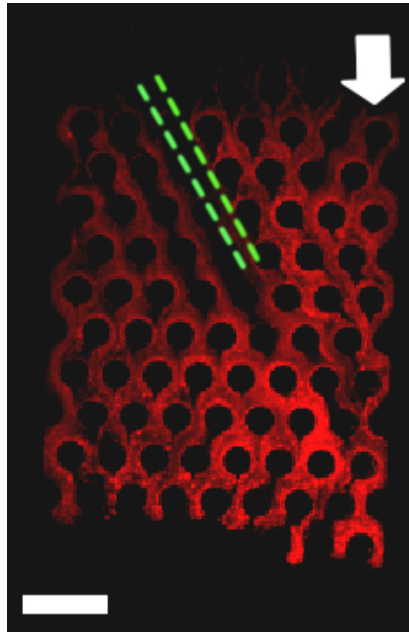


**Figure 4.9:** Water channel formation in the clogged part of the microfluidic device. 2 parallel dash lines demonstrate the location of water channel. Bacterial solution (*P. aeruginosa*) was injected for 3 hours into the channel with  $U=1.33\times 10^{-4}$  m/s. Scale bar is 150  $\mu\text{m}$ . White arrow shows the flow direction that is from top to bottom

Figure 4.10 summarizes the characteristic time-scales of various phenomena observed in our experiments. It is important to note that various events such as clogging of the device, failure and breakage of biomass have the same time-scale as the biological cell doubling time-scale. This suggests that mechanical effects are the dominant contributors to the observed phenomena. Interestingly, no direct correlation between the cross sectional area and the character of the stick-slip behavior was revealed from the experiments. In ‘stick-slip’ motion, during the stick stage, there is no relative motion between two surfaces and during the slip stage motion occurs; this pattern usually repeats itself [31]. In this context, note that in spite of the topical similarity of certain regions of the deformation time plot (Fig. 4.4c-d) with a viscous or

viscoelastic material, when taken in totality they do not support a purely material origin of this behavior. This is confirmed through visual data which indicates pronounced sliding at interfaces as well as looking into the myriad jumps in the plots at different time resolutions of the stick-slip plots (Fig. 4.4c-d). This is because such sudden changes in deformation characteristics are typically associated with instabilities and phase changes whose consequences are often prominently visible in the structure such as necking failure [19]. Similarly, the formation of water channels in the current paper also point to a substantial material source of instability. However, in the case of stick-slip, we observe no substantial changes in material constitution near the tracking points with the same regularity as the jumps (which appeared at even finer time scales). Thus, we conclude that the sudden changes in deformations (the spurting ‘slip’ and the sudden arrest of it through ‘stick’) primarily reflect a more global motion aided by the onset and arrest of sliding at the interfaces, further confirmed through microscopy data. Therefore, in this paper the nomenclature of stick-slip as used by Zhang & Li [31], where stick-slip processes are defined for two sliding surfaces has been adopted. A more detailed investigation of the observed phenomena would require substantial bulk and interfacial characterization and is left as an exercise for the future.

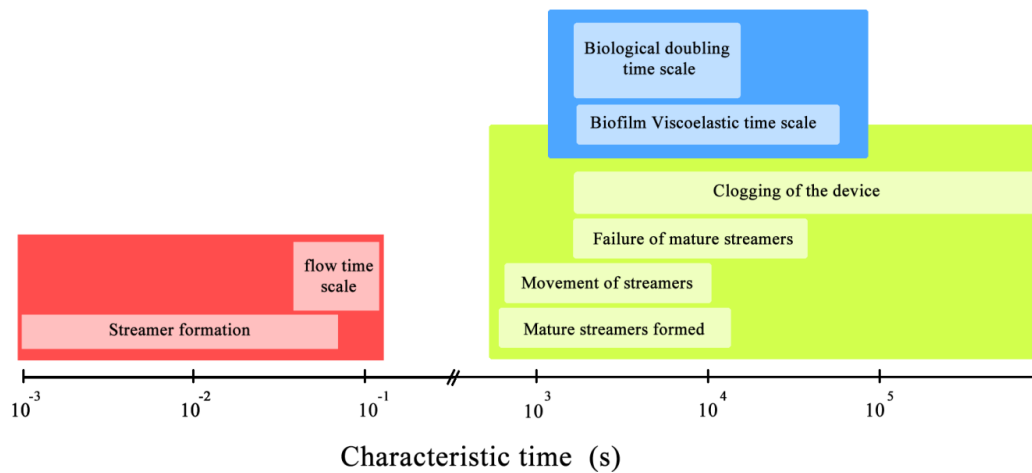


**Figure 4.10:** Various time scales related to our experiment.

#### 4.4 Conclusion

In conclusion, in this work we revealed important yet unreported aspects of the dynamics of bacterial streamer induced clogging in a microfluidic device. Particularly, we discovered a highly nonlinear stick-slip type advance of the mature streamer structure which causes the clogging front to move in spurts rather than following a continuous advance. In addition, we also find that even after the onset of substantial clogging in the device, the biomass retains a highly complex dynamic state characterized by marked instabilities and failures which result in extended distinct water channels in the device.

## 4.5 References

1. Karimi, A., et al., *Interplay of physical mechanisms and biofilm processes: review of microfluidic methods*. Lab Chip, 2015. **15**(1): p. 23-42.
2. Hassanpourfard, M., et al., *Bacterial floc mediated rapid streamer formation in creeping flows*. Scientific Reports, 2015. **5**: p. 13070.
3. Valiei, A., et al., *A web of streamers: biofilm formation in a porous microfluidic device*. Lab Chip, 2012. **12**(24): p. 5133-7.
4. Rusconi, R., et al., *Laminar flow around corners triggers the formation of biofilm streamers*. J R Soc Interface, 2010. **7**(50): p. 1293-9.
5. Stoodley, P., et al., *Biofilm material properties as related to shear-induced deformation and detachment phenomena*. J Ind Microbiol Biotechnol, 2002. **29**(6): p. 361-7.
6. Stoodley, P., et al., *Oscillation characteristics of biofilm streamers in turbulent flowing water as related to drag and pressure drop*. Biotechnology and bioengineering, 1998. **57**(5): p. 536-544.
7. Hassanpourfard, M., et al., *Protocol for Biofilm Streamer Formation in a Microfluidic Device with Micro-pillars*. JoVE (Journal of Visualized Experiments), 2014(90): p. e51732-e51732.
8. Marty, A., et al., *Formation of bacterial streamers during filtration in microfluidic systems*. Biofouling, 2012. **28**(6): p. 551-62.
9. Yazdi, S. and A.M. Ardekani, *Bacterial aggregation and biofilm formation in a vortical flow*. Biomicrofluidics, 2012. **6**(4): p. 044114.

10. Drescher, K., et al., *Biofilm streamers cause catastrophic disruption of flow with consequences for environmental and medical systems*. Proc Natl Acad Sci U S A, 2013. **110**(11): p. 4345-50.
11. Okuda, K., T. Kato, and K. Ishihara, *Involvement of periodontopathic biofilm in vascular diseases*. Oral Diseases, 2004. **10**(1): p. 5-12.
12. Fux, C.A., S. Wilson, and P. Stoodley, *Detachment characteristics and oxacillin resistance of Staphylococcus aureus biofilm emboli in an in vitro catheter infection model*. J Bacteriol, 2004. **186**(14): p. 4486-91.
13. Stanley, C.E., et al., *Soil-on-a-Chip: microfluidic platforms for environmental organismal studies*. Lab on a Chip, 2016. **16**(2): p. 228-241.
14. Hajnos, M., et al., *Complete characterization of pore size distribution of tilled and orchard soil using water retention curve, mercury porosimetry, nitrogen adsorption, and water desorption methods*. Geoderma, 2006. **135**: p. 307-314.
15. Hardoim, P.R., L.S. van Overbeek, and J.D.v. Elsas, *Properties of bacterial endophytes and their proposed role in plant growth*. Trends in Microbiology, 2008. **16**(10): p. 463-471.
16. Zuber, S., et al., *GacS sensor domains pertinent to the regulation of exoproduct formation and to the biocontrol potential of Pseudomonas fluorescens CHA0*. Molecular plant-microbe interactions, 2003. **16**(7): p. 634-644.
17. Vidhyasekaran, P. and M. Muthamilan, *Development of formulations of Pseudomonas fluorescens for control of chickpea wilt*. Plant disease, 1995. **79**(8): p. 782-786.

18. Salehizadeh, H. and S.A. Shojaosadati, *Extracellular biopolymeric flocculants: Recent trends and biotechnological importance*. Biotechnology Advances, 2001. **19**(5): p. 371-385.
19. Biswas, I., et al., *Nonlinear deformation and localized failure of bacterial streamers in creeping flows*. Scientific Reports, 2016. **6**: p. 32204.
20. Ben-David, O., S.M. Rubinstein, and J. Fineberg, *Slip-stick and the evolution of frictional strength*. Nature, 2010. **463**(7277): p. 76-79.
21. Denn, M.M., *Extrusion instabilities and wall slip*. Annual Review of Fluid Mechanics, 2001. **33**(1): p. 265-287.
22. Mate, C.M., et al., *Atomic-Scale Friction of a Tungsten Tip on a Graphite Surface*. Physical Review Letters, 1987. **59**(17): p. 1942-1945.
23. Orejon, D., K. Sefiane, and M.E.R. Shanahan, *Stick-Slip of Evaporating Droplets: Substrate Hydrophobicity and Nanoparticle Concentration*. Langmuir, 2011. **27**(21): p. 12834-12843.
24. Socoliuc, A., et al., *Transition from stick-slip to continuous sliding in atomic friction: entering a new regime of ultralow friction*. Phys Rev Lett, 2004. **92**(13): p. 134301.
25. Tomanek, D., W. Zhong, and H. Thomas, *Calculation of an atomically modulated friction force in atomic-force microscopy*. EPL (Europhysics Letters), 1991. **15**(8): p. 887.
26. Yoshizawa, H. and J. Israelachvili, *Fundamental Mechanisms of Interfacial Friction .2. Stick-Slip Friction of Spherical and Chain*

- Molecules*. Journal of Physical Chemistry, 1993. **97**(43): p. 11300-11313.
27. Denn, M.M., *Issues in Viscoelastic Fluid-Mechanics*. Annual Review of Fluid Mechanics, 1990. **22**: p. 13-34.
  28. Denn, M.M., *Wall Slip and Extrusion Instabilities*. Polymer Melt Processing: Foundations in Fluid Mechanics and Heat Transfer, 2008: p. 199-216.
  29. Wang, S.Q. and P.A. Drda, *Superfluid-like stick-slip transition in capillary flow of linear polyethylene melts .1. General features*. Macromolecules, 1996. **29**(7): p. 2627-2632.
  30. Gashti, M.P., et al., *Live-streaming: Time-lapse video evidence of novel streamer formation mechanism and varying viscosity*. Biomicrofluidics, 2015. **9**(4): p. 041101.
  31. Zhang, S.L. and J.C.M. Li, *Slip process of stick–slip motion in the scratching of a polymer*. Materials Science and Engineering: A, 2003. **344**(1–2): p. 182-189.

## **5 Antibacterial effect of Mg(OH)<sub>2</sub> nano-platelets on *Pseudomonas fluorescens* and its consequences on bacterial streamer formation in a microfluidic device**

### **5.1 Introduction:**

Bacteria are ubiquitous in the environment [1]. They can form a protected mode of life known as biofilm [1-3], where bacteria are attached to a surface and enclosed in a matrix of extracellular polymeric substances (EPS) produced by themselves, which acts as a support system holding the cells together [4]. Due to the effect of fluid flow, biofilm can deform into a filamentous structure called a streamer [5-10]. More specifically, these filamentous structures are attached to a surface from one or both ends while the rest of their structures are suspended in the liquid. Their formation, especially in low Reynolds number fluid transport, which is similar to some medical devices such as catheters and heart stents, water filtration systems, and porous media, have attracted a lot of attention lately [6, 7, 11]. Recently, Hassanpourfard et al. [12] showed that bacterial streamers not only can form as a result of highly viscous behavior of attached viscoelastic biofilm, but also they can form from flow-induced preformed bacterial flocs deformation [12]. Once they form, they rapidly accelerate the clogging process [7, 12] by forming a spider web like structure which is able to accrue more biomass from the solution [6]. Moreover, biofilms are resistant to antimicrobial agents by 3 orders of magnitude and therefore, they are a universal concern [13]. For example, in the health field, researchers have determined that biofilms growth on surfaces, whether on medical devices

or oral surfaces such as teeth, have the ability to detach, form aggregates and pose potential risks for severe infections [14, 15]. In water filtration systems, typical consequences of resistant biofilm formation include a decrease in membranes' performance, pollution of previously purified water, and higher power and pressure requirements due to the flux decline [16].

As such, there is a growing need to prevent biofilms and streamers formation. Controlling or inhibiting their growth by utilizing antibacterial agents can achieve this aim. Currently, there is continued emphasis on finding new antibacterial agents, especially because of the increasing microbial resistance to multiple antibiotics [17, 18]. Thus, many are interested in focusing on developing novel antimicrobial agents to combat the emergence of antibiotic resistant microbial organisms, and their consequences [2, 3]. In particular, nanoparticles have received much attention due to their nano-scale size and structures, which enables them to demonstrate new and enhanced biological, physical and chemical properties, and functionalities [17]. Silver, copper, metal oxides including  $\text{TiO}_2$ ,  $\text{MgO}$  and  $\text{ZnO}$  and metal hydroxide material such as  $\text{Ca(OH)}_2$ , and  $\text{Mg(OH)}_2$  have been acknowledged as antibacterial nanoparticles [13]. Among the metal hydroxide material,  $\text{Mg(OH)}_2$  is the preferable choice due to its low cost and non-toxicity [19]. It is currently being used as an environmentally friendly flame retardant, paper conservation agent [13, 20-22], acid neutralizer [13, 19], and most importantly as an antibacterial agent [19].

In this study, to inhibit the formation of streamers, we used  $\text{Mg(OH)}_2$  nano-platelets to constrain the growth of planktonic bacteria due to the fact that the complex process of biofilms and bacterial flocs formation are initiated by

planktonic bacteria themselves [23]. Herein,  $\text{Mg}(\text{OH})_2$  nano-platelets were studied for their antibacterial effects. More specifically, the antibacterial effects on *P. fluorescens* in LB media were investigated. As previously stated, bacteria cells in EPS matrix are much more resistant to antibiotics than their less commonly found planktonic counterparts [24], and therefore, are of interest to research. In our experiment, solutions of varying  $\text{Mg}(\text{OH})_2$  nano-platelet concentrations in LB media were prepared and cultured on agar plates to visualize the effects qualitatively. The effects of  $\text{Mg}(\text{OH})_2$  nano-platelets on *P. fluorescens* bacterial floc mediated streamer formation and its consequences including biofouling and clogging mechanisms were investigated using a microfluidic device designed to resemble porous media. Using microfluidic devices gives us more insight regarding the properties, nature, and evolution of microbial biofilms and streamers [23].

## **5.2 Experimental**

### **5.2.1 Bacterial culture**

In the initial step of the experiment, by streaking  $-80^\circ\text{C}$  *P. fluorescens* CHA0 (wild type) bacterial stock onto a LB agar plate, the bacterial sample was prepared. This particular strain of bacteria expresses GFP (green fluorescent protein) constitutively. The agar plate was incubated at  $30^\circ\text{C}$  overnight. Next, a colony from the agar plate was transferred into LB broth medium, which was then incubated in a shaker incubator (New Brunswick Scientific Co., NJ) at  $30^\circ\text{C}$ , 150 rpm overnight. For the experimental solutions, we mixed LB broth medium with different concentrations of  $\text{Mg}(\text{OH})_2$  nano-platelets (1X, 0.75X, 0.5X, 0.25X, 0.1X, 0.01X and 0X (Control); X= 50 g/l). To disperse the nano-

platelets in the LB media, each solution was sonicated for 10 min and then autoclaved for 20 min at 121°C and 151 psi. The control flask only contained LB medium. Afterwards, bacterial solution with the ratio of 1 (bacteria) to 100 (media) was added to each flask. Then the solutions were placed in shaker incubator at 30 °C and 150 rpm.

### **5.2.2 Agar plate experiment**

3 drops of each experimental solution of about 25 µl each were poured onto 3 sections of LB agar plates. The plates were incubated at 30 °C. Images of the plates were taken after 24 hours of incubation.

### **5.2.3 Particle preparation for atomic force microscopy (AFM) studies**

The Mg(OH)<sub>2</sub> nano-platelets (10 mg) were suspended in 1-butanol dry organic solvent (20 mL) in a covered glass flask and immersed in an ultrasonic bath under ambient conditions of temperature and pressure. The SiO<sub>2</sub> substrates were cleaned with ethanol, treated in oxygen plasma and dipped in the colloidal suspension of the Mg(OH)<sub>2</sub> nano-platelets under continuous ultrasonic treatment for 90 s. Mg(OH)<sub>2</sub> nano-platelets crystals were attached to the cleaned Si wafer and the additional loosely bound Mg(OH)<sub>2</sub> nano-platelets were removed by further sonication in pure 1-butanol for additional 1 min. The sample was then left to dry in an evaporating chamber overnight for complete evaporation of the solvent and used for characterization using AFM [19].

#### **5.2.4 Bacterial solution preparation for AFM studies**

To prepare the bacterial solution for AFM test, bacteria was cultured in solution and incubated for 8 hours. Afterwards, the bacterial solution was centrifuged at 800 rpm at 4 °C for 10 minutes. The supernatant was discarded after complete centrifugation and a 10X diluted solution of phosphate-buffered saline (PBS) was added. This process was repeated three times to wash the bacteria cells.

#### **5.2.5 Microchip fabrication**

Three steps were followed to fabricate the polydimethylsiloxane (PDMS, Sylgard 184, Dow Corning, NY, USA) microchip. The three steps included standard photolithography, soft lithography, and bonding coverslip and PDMS stamp by oxygen plasma processes. The particulars of this procedure can be found in Hassanpourfard et al. [9].

#### **5.2.6 Nano-platelets characteristics and our experimental setup**

In order to characterize the  $\text{Mg}(\text{OH})_2$  nano-platelets, we used atomic force microscopy (AFM). The detailed process for the  $\text{Mg}(\text{OH})_2$  nano-platelets' fabrication is in Ref. [25]. The AFM topography and the corresponding cross section of the  $\text{Mg}(\text{OH})_2$  nano-platelets deposited on  $\text{SiO}_2$  substrate is shown in Figure 5.1a and 1b respectively. As seen from the topography, the platelets range from 100 nm to 300 nm in width while the height of them is around 6-7 nm. The platelets can be stacked on top of each other in some cases and the step heights can be easily seen in the corresponding cross section graph (Fig. 5.1b). Furthermore, in order to quantify the effect of  $\text{Mg}(\text{OH})_2$  nano-platelets on  $P$ .

*fluorescens* in real scenarios, we used a microfluidic device as a platform to mimic porous media. Figure 5.2 shows our microfluidic setup and the porous section of the channel. A periodic staggered grid pattern was designed by a sequence of micropillars in the microchip to mimic porous media.

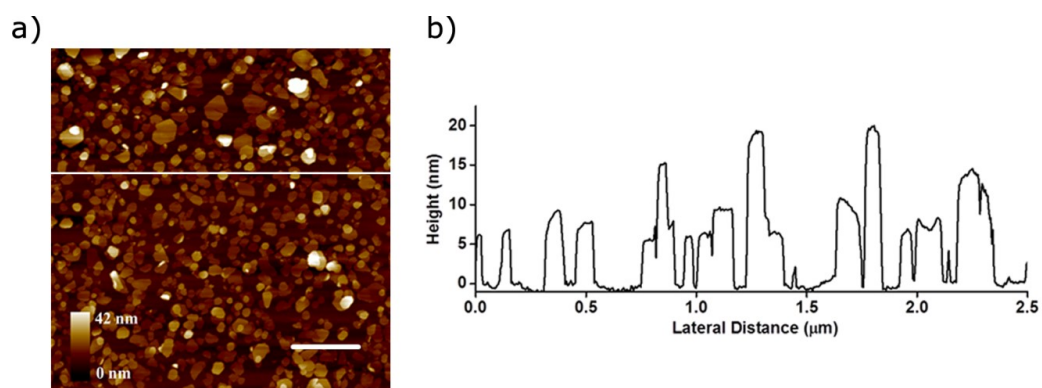


**Figure 5.1:** a) The AFM topography and b) The corresponding cross section of the Mg(OH)<sub>2</sub> nano-platelets deposited on SiO<sub>2</sub> substrate. Scale bar is 0.5 μm.

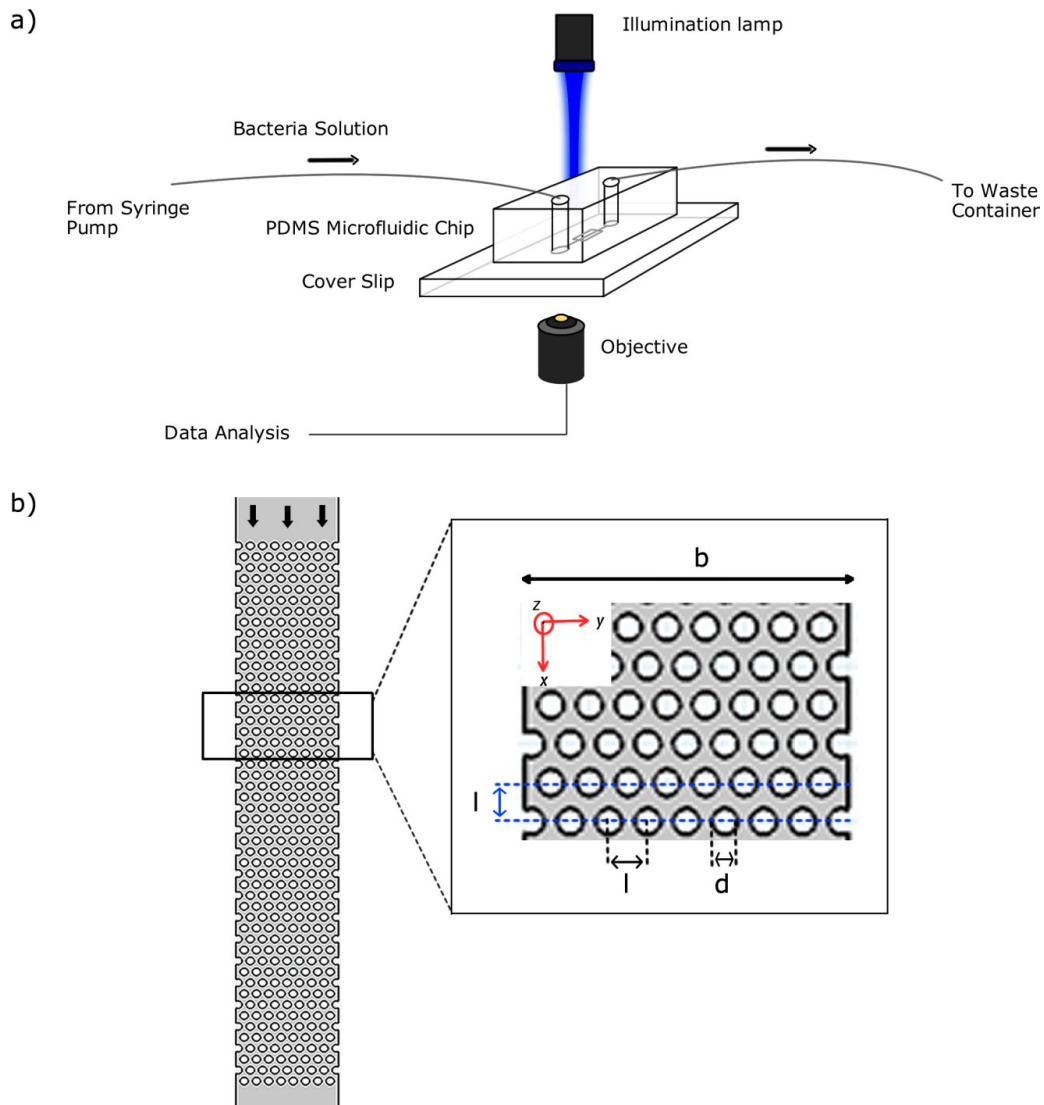


**Figure 5.2:** a) Microfluidic experimental set-up. b) Porous section of the channel. Zoom in shows the pillars. The channel width ( $b$ ) is  $625\ \mu\text{m}$ . and the porous section of channel contains 400 pillars. The micropillars' diameter ( $d$ ) and height are  $50\ \mu\text{m}$  and they are set  $75\ \mu\text{m}$  apart ( $l$ ). The fluid flow rate ( $Q$ ) was set  $15\ \mu\text{l/h}$  (flow speed:  $1.3 \times 10^{-4}\ \text{m/s}$ ) in our device. The reason for selecting this flow rate ( $15\ \mu\text{l/h}$ ) was having creeping flow regime in the microchip (Reynolds number,  $Re$ , was  $O(10^{-3})$ ).

## 5.3 Results and discussion

### 5.3.1 Antibacterial effect of Mg(OH)<sub>2</sub> nano-platelets on *P. fluorescens*

A series of experiments were performed to investigate the antibacterial efficiency of Mg(OH)<sub>2</sub> nano-platelets on *P. fluorescens*. *P. fluorescens* is a widespread bacterium commonly presents in the soil and rivers [26], which is capable of producing EPS and forming a robust, surface attaching biofilm [24]. We chose *P. fluorescens* as a model for biofilm forming bacteria. The results of agar plates from 0 hour samples demonstrate the growth of bacterial colonies on the agar plates indicating the presence of bacteria in all the solutions at the beginning of the experiment (Fig. 5.3). We repeated this procedure after 2, 4 and 8 h of incubation of the solutions. Interestingly, we did not observe any bacterial colonies on the agar plates for the solution that contained 1X concentration of Mg(OH)<sub>2</sub> nano-platelets even after 2 h of incubation which indicates the antibacterial effect of Mg(OH)<sub>2</sub> nano-platelets on *P. fluorescens* (Fig. 5.3 and table 5.1). Table 5.1 summarizes the bacterial growth results on the agar plates that were visually measured. Antibacterial behavior of Mg(OH)<sub>2</sub> nano-platelets on *E. coli* was reported in previous studies [13, 27]. In those studies, they used 10 g/l (0.2X) of Mg(OH)<sub>2</sub> nano-platelets and reported that after 40 h [13] and 24 h [27] incubation no live bacteria were observed. In this study, for low concentrations of Mg(OH)<sub>2</sub> nano-platelets (0.1X and 0.01X) confluent growth of bacteria on the agar plate was observed even after 24 h of incubation with Mg(OH)<sub>2</sub> nano-platelets demonstrating that for these concentrations, the time of incubation is not important for observing antibacterial behavior (Fig. 5.3). However, when we tried different

concentrations of Mg(OH)<sub>2</sub> nano-platelets (0.25X, 0.5X, 0.75X) the time of incubation was important to observe the antibacterial behavior of Mg(OH)<sub>2</sub> nano-platelets (Table 5.1).

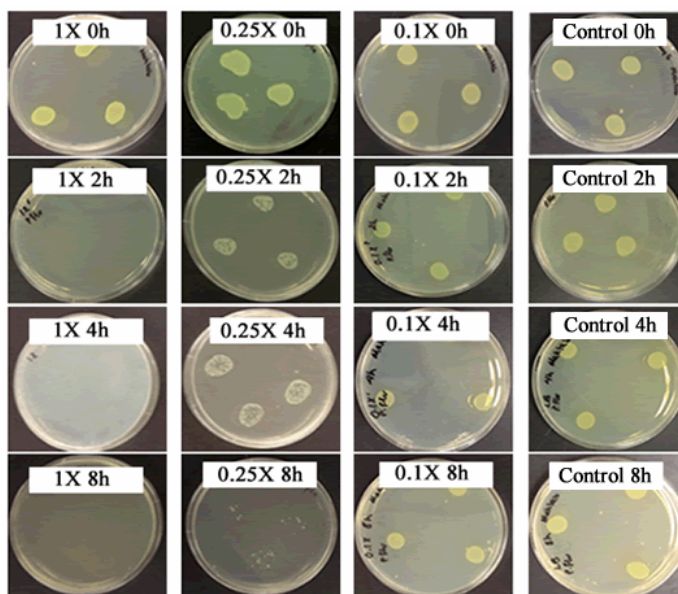


**Figure 5.3:** Bacterial growth on agar plates with different concentrations of Mg(OH)<sub>2</sub> nano-platelets.

**Table 5.1:** Bacterial growth on agar plates according to visual observations

	<b>1X</b>	<b>0.75X</b>	<b>0.5X</b>	<b>0.25X</b>	<b>0.1X</b>	<b>0.01X</b>	<b>Control</b>
<b>0h</b>	G	G	G	G	G	G	G
<b>2h</b>	NG	PG	PG	G	G	G	G
<b>4h</b>	NG	PG	PG	PG	G	G	G
<b>6h</b>	NG	NG	PG	PG	G	G	G
<b>8h</b>	NG	NG	NG	PG	G	G	G
<b>12h</b>	NG	NG	NG	PG	G	G	G
<b>24h</b>	NG	NG	NG	PG	G	G	G

G: Growth; PG: Partial Growth; NG: No Growth

Now the question is: what is the mechanism for such behavior? Due to the low solubility of  $\text{Mg}(\text{OH})_2$  nano-platelets in water, almost in all the solutions there are the same amounts of  $\text{Mg}^{2+}$  and  $\text{OH}^-$ ; here, the solubility product constant ( $K_{sp}$ ) is  $5.61 \times 10^{-12}$  [13]. Furthermore, Dong et al. [13] investigated the effect of  $\text{OH}^-$  and  $\text{Mg}^{2+}$  on *E. coli* and they found that these ions have no effect on *E. coli* viability and bacterial growth, respectively [13]. Therefore, particles have to attach to the cells to interact with them. Due to the high surface energy that the nano-platelets have in comparison with the bacteria cells (2 orders of magnitude higher) [28, 29], they interact with bacteria cells. Attached particles to bacteria cells were observed by AFM (Fig. 5.4b). Figure 5.4 shows a collection of *P. fluorescens* in control solution (Fig. 5.4a) and 0.1X (Fig. 5.4b) solutions. The *P. fluorescens* bacteria samples are prepared by depositing them on cleaned  $\text{SiO}_2$  substrate and imaged with peak-force tapping mode AFM. Figure 5.4a represents the topography of normal bacterium surface that shows the cell membrane is relatively smooth, having no visible deformations. On the other hand, Figure 5.4b clearly shows the attachments of  $\text{Mg}(\text{OH})_2$  nano-platelets on the bacterium cell surface. The corresponding cross-sections of the bacterial images are shown in Figure 5.4c and d. The cross-section of the normal bacteria shows no significant membrane deterioration or any attachment to the normal bacterial cell membrane (Fig. 5.4c).

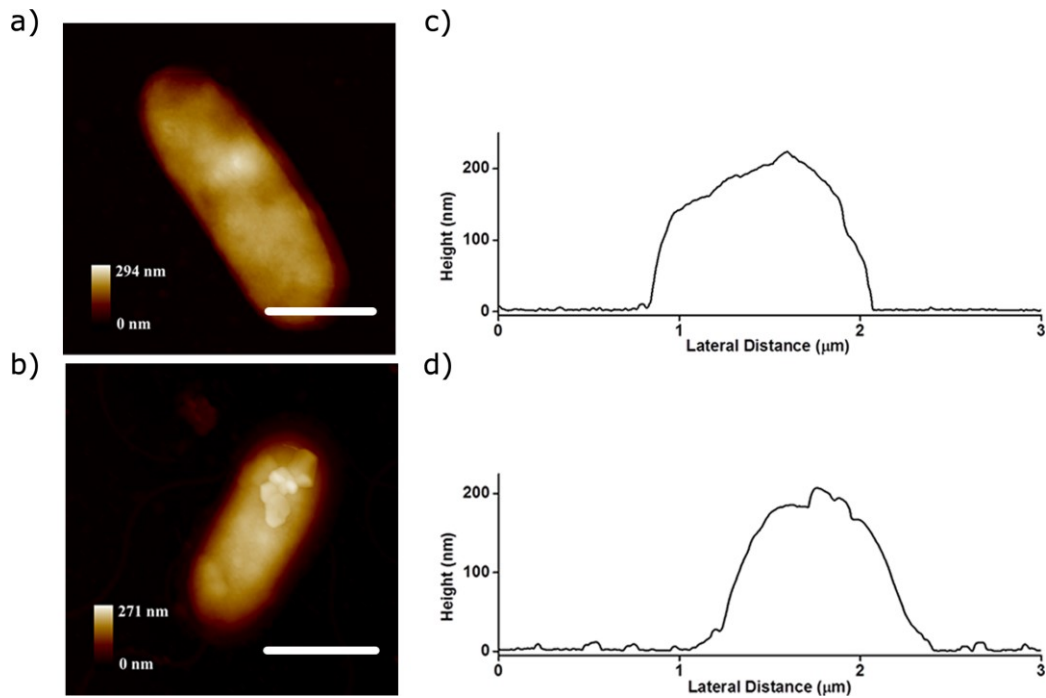


**Figure 5.4:** AFM images of bacteria; a) Bacteria incubated in control solution, b) Bacteria incubated in 0.1X solution. c) and d) The corresponding cross-sections of the bacterial images for a) and b). Scales bars are 1  $\mu\text{m}$ .

### 5.3.2 Antibacterial effect of $\text{Mg}(\text{OH})_2$ nano-platelets on *P. fluorescens* and its consequences on streamer formation

The effect of incubating *P. fluorescens* with  $\text{Mg}(\text{OH})_2$  nano-platelets for 48 h on the clogging dynamics of porous media was investigated by using a microfluidic device (Fig. 5.2). To see the clogging dynamics due to the biomass in the channel, the dispersed  $\text{Mg}(\text{OH})_2$  nano-platelets in the solution (1X) were allowed to precipitate (4 h), and then the supernatant of this solution was injected into the channel. We repeated the same procedure for the control bacterial solution. Figure 5.5a shows the middle height of the channel. The images are taken at the middle height of the channel since this location has the

maximum effect on the clogging of the device [7]. The results of this experiment indicate that the supernatant of control solution had the ability to clog the channel after 1 h. Interestingly, the supernatant of 1X solution did not have this ability; we did not observe any biomass accumulation in the channel for this solution (Fig. 5.5a). This considerably different behavior originates from the amount of biomass that enter the channel due to the effect of  $\text{Mg}(\text{OH})_2$  nano-platelets. Moreover, to investigate the clogging dynamics by control solution we took the images before the clogging occurred (10 min after injecting the solution into the microchip) and we found that the clogging is occurring because of the streamer formation in the channel (Fig. 5.5b). As a result, the antibacterial effect of  $\text{Mg}(\text{OH})_2$  nano-platelets inhibits streamer formation and clogging of the channel.

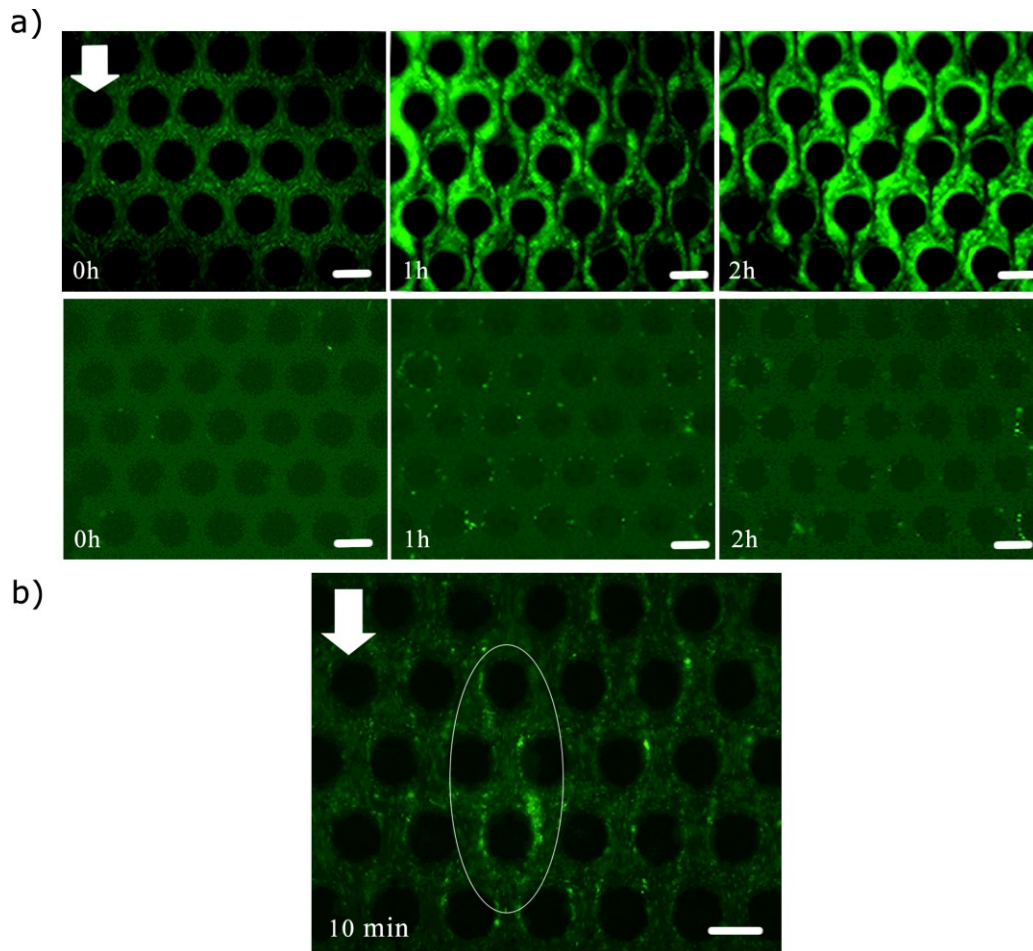


**Figure 5.5:** a) The effect of  $\text{Mg}(\text{OH})_2$  nano-platelets in streamer formation in the microchannel. The first row shows supernatant of control bacterial solution injected into the channel. Second row demonstrates the inside of the channel after injecting supernatant of 1X solution. b) Streamer formation after 10 min of injecting supernatant of control bacterial solution into the microchannel. Scale bars are 50  $\mu\text{m}$ .

### **Acknowledgments:**

M. Hassanpourfard acknowledges support from Alberta Innovates Technology Futures. The authors would also like to thank Inseok Chae and Priyesh Dhandharia for their helps with the experiments.

## 5.4 References

1. Costerton, J.W., *Bacterial Biofilms: A Common Cause of Persistent Infections*. Science, 1999. **284**(5418): p. 1318-1322.
2. More, T.T., et al., *Extracellular polymeric substances of bacteria and their potential environmental applications*. J Environ Manage, 2014. **144C**: p. 1-25.
3. Costerton, J.W., et al., *Microbial Biofilms*. Annual Review of Microbiology, 1995. **49**(1): p. 711-745.
4. Wong, G.C.L. and G.A. O'Toole, *All together now: Integrating biofilm research across disciplines*. MRS Bulletin, 2011. **36**(05): p. 339-342.
5. Rusconi, R., et al., *Laminar flow around corners triggers the formation of biofilm streamers*. J R Soc Interface, 2010. **7**(50): p. 1293-9.
6. Valiei, A., et al., *A web of streamers: biofilm formation in a porous microfluidic device*. Lab Chip, 2012. **12**(24): p. 5133-7.
7. Drescher, K., et al., *Biofilm streamers cause catastrophic disruption of flow with consequences for environmental and medical systems*. Proc Natl Acad Sci U S A, 2013. **110**(11): p. 4345-50.
8. Rusconi, R., et al., *Secondary flow as a mechanism for the formation of biofilm streamers*. Biophys J, 2011. **100**(6): p. 1392-9.
9. Hassanpourfard, M., et al., *Protocol for Biofilm Streamer Formation in a Microfluidic Device with Micro-pillars*. JoVE (Journal of Visualized Experiments), 2014(90): p. e51732-e51732.
10. Hassanpourfard, M., et al. *Biofilm Streamer Formation in a Microfluidic Porous Media Mimic*. in *ASME 2014 International*

- Mechanical Engineering Congress and Exposition*. 2014. American Society of Mechanical Engineers.
11. Marty, A., et al., *Formation of bacterial streamers during filtration in microfluidic systems*. *Biofouling*, 2012. **28**(6): p. 551-62.
  12. Hassanpourfard, M., et al., *Bacterial floc mediated rapid streamer formation in creeping flows*. *Scientific Reports*, 2015. **5**: p. 13070.
  13. Dong, C., et al., *Investigation of Mg(OH)<sub>2</sub> nanoparticles as an antibacterial agent*. *Journal of Nanoparticle Research*, 2009. **12**(6): p. 2101-2109.
  14. Okuda, K., T. Kato, and K. Ishihara, *Involvement of periodontopathic biofilm in vascular diseases*. *Oral Diseases*, 2004. **10**(1): p. 5-12.
  15. Fux, C.A., S. Wilson, and P. Stoodley, *Detachment characteristics and oxacillin resistance of Staphylococcus aureus biofilm emboli in an in vitro catheter infection model*. *J Bacteriol*, 2004. **186**(14): p. 4486-91.
  16. Kochkodan, V., et al., *Adhesion of microorganisms to polymer membranes: a photobactericidal effect of surface treatment with TiO<sub>2</sub>*. *Desalination*, 2008. **220**(1-3): p. 380-385.
  17. Dong, C., et al., *Antibacterial study of Mg(OH)<sub>2</sub> nanoplatelets*. *Materials Research Bulletin*, 2011. **46**(4): p. 576-582.
  18. Stewart, P.S. and J. William Costerton, *Antibiotic resistance of bacteria in biofilms*. *The Lancet*, 2001. **358**(9276): p. 135-138.
  19. Pan, X., et al., *Investigation of antibacterial activity and related mechanism of a series of nano-Mg(OH)<sub>2</sub>*. *ACS Appl Mater Interfaces*, 2013. **5**(3): p. 1137-42.
  20. Chen, Y., et al., *A Novel Preparation of Nano-sized Hexagonal Mg(OH)<sub>2</sub>*. *Procedia Engineering*, 2015. **102**: p. 388-394.

21. Jiao, C.M., *Flame Retardation of Ethylene-Vinyl Acetate Copolymer Using Nano Magnesium Hydroxide and Nano Hydrotalcite*. Journal of Fire Sciences, 2006. **24**(1): p. 47-64.
22. Giorgi, R., et al., *Nanoparticles of Mg (OH) 2: synthesis and application to paper conservation*. Langmuir, 2005. **21**(18): p. 8495-8501.
23. Neethirajan, S., et al., *Biofilms in Microfluidic Devices*, in *Encyclopedia of Nanotechnology*, B. Bhushan, Editor. 2012, Springer Netherlands. p. 213-219.
24. O'Toole, G.A. and R. Kolter, *Initiation of biofilm formation in Pseudomonas fluorescens WCS365 proceeds via multiple, convergent signalling pathways: a genetic analysis*. Molecular Microbiology, 1998. **28**(3): p. 449-461.
25. Maddan, O.L., *Nanoplatelet metal hydroxides and methods of preparing same*. 2014, Google Patents.
26. Ude, S., et al., *Biofilm formation and cellulose expression among diverse environmental Pseudomonas isolates*. Environ Microbiol, 2006. **8**(11): p. 1997-2011.
27. Dong, C., et al., *Study on antibacterial mechanism of Mg(OH)<sub>2</sub> nanoparticles*. Materials Letters, 2014. **134**: p. 286-289.
28. Nanda, K.K., et al., *Higher Surface Energy of Free Nanoparticles*. Physical Review Letters, 2003. **91**(10).
29. Busscher, H.J., et al., *Measurement of the surface free energy of bacterial cell surfaces and its relevance for adhesion*. Applied and environmental microbiology, 1984. **48**(5): p. 980-983.

## 6 Concluding remarks

### 6.1 Conclusions

This thesis provides comprehensive studies of bacterial streamers in pseudo porous devices in order to predict and control their behavior. We used a microfluidic device as a pseudo porous platform for our studies. Observing bacterial streamer formation in actual porous media can often be challenging due to their opacity. In such situations, microfluidics based porous media platforms can prove extremely advantageous, as they allow real-time and *in-situ* monitoring. In chapter 2, fabrication of the microfluidic platform, necessary steps for cell culture, and experimentation are described. Biofilm-mediated streamers and their temporal evolution were also investigated in chapter 2. The results demonstrate that the formation of streamers depends on injected flow rate. As for the flow velocity scale of  $7.1 \times 10^{-6} \text{ m/s}$ , no streamer was observed after a prolonged period of time ( $>20$  hrs). Interestingly, for higher velocity scale ( $7.1 \times 10^{-5} \text{ m/s}$ ), the streamers were formed and the time-scale of their formation was in the order of several hours. Further investigations demonstrated that the biofilm-mediated streamers originate near locations with high shear stress.

In chapter 3, we discovered a new kind of bacterial streamer formation (floc-mediated streamer) with a different physical mechanism of formation from biofilm-mediated streamers. We found that these streamers appear due to flow-induced deformation of the pre-formed bacterial flocs. For the first time, our methodology of using nanoscale fluorescent tracers allows for a direct

quantification of the evolution of the streamer morphology. We discovered that fluid flow first advects the flocs, some of which then get attached to the micropillars; subsequently, due to the hydrodynamic shear forces, even when fluid flow in a system is in the creeping flow regime, streamers can form by large deformation of flocs. The formation timescale of this floc-mediated streamer is less than a second, which is in sharp contrast to the much larger timescale witnessed for biofilm-mediated streamers. Firstly, recoverable elastic behavior of streamers at its initial stage of formation was observed by the changes in axial stretch ratio ( $\lambda(t)$ ). Next, we found that the streamers are not purely elastic structures since we observed perceptible viscous behavior at time scales larger than its formation time scale, but still far from clogging regime. At this time scale, streamers demonstrated shear thickening behavior. Moreover, due to the fact that most of the streamers originate from regions corresponding to maximum shear stress, the role of shear deformation in their formation is strongly suggested. These observations give us valuable clues about the fundamental mechanism of floc-mediated streamer formation. This was the first direct experimental observation, where the formation of a streamer and its behavior in the intermediate time-scale with respect to clogging have been demonstrated by seeding particles for very precise quantification of the biomass structures. We demonstrated that floc-mediated streamers lead to rapid clogging of the device. Thereafter, we investigated the clogging phase of floc mediated streamers in chapter 4.

In chapter 4, we investigated the clogging dynamics of mature bacterial streamer in our device. We revealed a highly nonlinear stick-slip type advance of the mature streamer structure that causes the clogging front to move in spurts rather than following a continuous advance. The onset time of stick-slip

behavior depends on the injected flow rate. We demonstrated that the stick-slip behavior was neither the result of intermittency caused by pump nor deformation of PDMS micropillars. The observation of stick-slip behavior with a different strain of bacteria (*P. aeruginosa*), demonstrated that this behavior may be a more general mechanical phenomenon and independent of the biophysical issues associated with bacterial strains. Moreover, we found that even after the onset of substantial clogging in the device, the biomass retains a highly complex dynamic state depicted by noticeable instabilities and failures. These result in extended distinct water channels in the device whose length scale was several times larger than the pore-length scale. In the time scale of our experiment, water channel formation was dependent on the injected flow rates. Furthermore, water channel formation in the channel injected with a different bacterial strain (*P. aeruginosa*) suggested a mechanical origin of these phenomena.

In chapter 5, we showed the antibacterial effect of  $\text{Mg}(\text{OH})_2$  nano-platelets on *P. fluorescens* and its consequences on streamer formation. We found that the antibacterial properties of  $\text{Mg}(\text{OH})_2$  nano-platelets can inhibit bacterial growth and consequently bacterial streamer formation. We also found that the time of incubation and the concentration of nano-platelets play an important role in antibacterial effect of  $\text{Mg}(\text{OH})_2$  nano-platelets and consequently their effects on streamer formation. Applying antibacterial effect of  $\text{Mg}(\text{OH})_2$  nano-platelets can be a promising preventive measure with regard to bacterial streamers.

## 6.2 Future work

Depending on the different applications, various designs of microfluidic devices can be considered to investigate the bacterial streamers formation and their clogging dynamics. Furthermore, the model presented in this thesis was an approximation of our real conditions. The simulation of the real scenario, where the solution contains bacterial flocs, should be taken into account in future.

In order to control and prevent streamer formation, using different types of nanoparticles with antibacterial effect is recommended. Furthermore, the fabrication method can be modified in order to coat the pillar with different nanoparticles to inhibit biofilm mediated streamers. In such circumstances, the PDMS can be mixed with the nanoparticles and then get cured and bonded to the coverslip. By this method, biofilm formation around the pillars, which is required in the case of biofilm-mediated streamers, can be prevented or delayed.

As we mentioned earlier, the formation of floc-mediated streamers begins with the flocs attachments to the micro-pillars. Therefore, applying different methods that can prevent flocs attachments can be useful to control floc-mediated streamers formation. One of these methods can be adding different types of surfactants into solution that contains bacterial flocs to change flocs surface properties, and consequently their attachments to the micro-pillars. The preliminary results demonstrated that adding Tween 80 can decrease the rate of flocs attachments to the wall of micro-pillars. Apart from type of surfactant, studies on the impact of different concentrations of selected surfactant and the effect of critical micelle concentration (CMC) on streamer formation are recommended for future studies. These studies can be extended to investigate

the effect of different environmental conditions, e.g. pH, for bacterial flocs growth and their attachments to the wall and subsequently streamers formation. These studies can be divided into 2 categories; the first one is growing flocs in pH=7, and then changing the pH to see the effect on surface properties, flocs attachment, and consequently streamers formation. The second study can be investigating the effect of media with varying pH on flocs formation, flocs' sizes, and streamer formation in the microfluidic devices. The primary studies demonstrated that the bacteria can only grow in the pH range of 5 to 9. Furthermore, the zeta potential test from the surfaces of flocs in different pH showed different zeta potential values, which demonstrated that the pH changes the surface properties of flocs.

Segregating the effect of biological phenomena from physical ones is challenging in studying bacterial streamers. Therefore, in future studies, having a closely mimicking abiotic system is desirable to study bacterial streamers. In such a study, a diluted suspension of PS nanoparticles and the aqueous solution of a high molecular weight polymer like polyacrylamide (PAM) can be selected to create an abiotic streamer. The results of this study can be helpful to better understand the bacterial floc-mediated streamers.

During this study, the breakage of streamers was observed in different phases, from the formation phase to clogging. We briefly studied the instability in the clogging phase and we recommend the study of instability in the initial phase of streamers formation, where the streamer aspect ratio is high (thin streamer). This study can give more insight about the instability of streamers at the initial phase of formation.

## References

- Arruda, Ellen M, and Mary C Boyce. 1993. "A three-dimensional constitutive model for the large stretch behavior of rubber elastic materials." *J Mech Phys Solids* no. 41 (2):389-412.
- Barathi, S., and N. Vasudevan. 2001. "Utilization of petroleum hydrocarbons by *Pseudomonas fluorescens* isolated from a petroleum-contaminated soil." *Environment International* no. 26 (5–6):413-416. doi: [http://dx.doi.org/10.1016/S0160-4120\(01\)00021-6](http://dx.doi.org/10.1016/S0160-4120(01)00021-6).
- Ben-David, O., S. M. Rubinstein, and J. Fineberg. 2010. "Slip-stick and the evolution of frictional strength." *Nature* no. 463 (7277):76-79. doi: 10.1038/nature08676.
- Berejnov, V., N. Djilali, and D. Sinton. 2008. "Lab-on-chip methodologies for the study of transport in porous media: energy applications." *Lab on a Chip* no. 8 (5):689-693. doi: Doi 10.1039/B802373p.
- Biswas, Ishita, Ranajay Ghosh, Mohtada Sadrzadeh, and Alope Kumar. 2016. "Nonlinear deformation and localized failure of bacterial streamers in creeping flows." *Scientific Reports* no. 6:32204. doi: 10.1038/srep32204.
- Brooks, Royal Harvard, and Arthur Thomas Corey. 1964. "Hydraulic properties of porous media and their relation to drainage design." *Transactions of the ASAE* no. 7 (1):26-0028.
- Busscher, Hendrik J, Anton H Weerkamp, Henny C van der Mei, AW Van Pelt, Hans P de Jong, and Joop Arends. 1984. "Measurement of the surface free energy of bacterial cell surfaces and its relevance for adhesion." *Applied and environmental microbiology* no. 48 (5):980-983.

- Chen, Hsiu-Hung, Junxiang Shi, and Chung-Lung Chen. 2013. "Wetting dynamics of multiscaled structures." *Appl. Phys. Lett.* no. 103 (17):171601.
- Chen, Yongbin, Tao Zhou, Huaxiong Fang, Simin Li, Yuting Yao, and Yang He. 2015. "A Novel Preparation of Nano-sized Hexagonal Mg(OH)<sub>2</sub>." *Procedia Engineering* no. 102:388-394. doi: 10.1016/j.proeng.2015.01.169.
- Costerton, J. W. 1999. "Bacterial Biofilms: A Common Cause of Persistent Infections." *Science* no. 284 (5418):1318-1322. doi: 10.1126/science.284.5418.1318.
- Costerton, J. W., Z. Lewandowski, D. E. Caldwell, D. R. Korber, and H. M. Lappin-Scott. 1995. "Microbial Biofilms." *Annual Review of Microbiology* no. 49 (1):711-745. doi: 10.1146/annurev.mi.49.100195.003431.
- Cunningham, Alfred B, William G Characklis, Feisal Abedeen, and David Crawford. 1991. "Influence of biofilm accumulation on porous media hydrodynamics." *Environmental science & technology* no. 25 (7):1305-1311.
- Das, Siddhartha, and Alope Kumar. 2014. "Formation and post-formation dynamics of bacterial biofilm streamers as highly viscous liquid jets." *Scientific Reports* no. 4:7126. doi: 10.1038/srep07126
- <http://www.nature.com/articles/srep07126#supplementary-information>.
- De Beer, Dirk, Paul Stoodley, Frank Roe, and Zbigniew Lewandowski. 1994. "Effects of biofilm structures on oxygen distribution and mass transport." *Biotechnology and bioengineering* no. 43 (11):1131-1138.
- De Schryver, P., R. Crab, T. Defoirdt, N. Boon, and W. Verstraete. 2008. "The basics of bio-flocs technology: The added value for

- aquaculture." *Aquaculture* no. 277 (3-4):125-137. doi: 10.1016/j.aquaculture.2008.02.019.
- Denn, M. M. 1990. "Issues in Viscoelastic Fluid-Mechanics." *Annual Review of Fluid Mechanics* no. 22:13-34.
- Denn, M. M. 2008. "Wall Slip and Extrusion Instabilities." *Polymer Melt Processing: Foundations in Fluid Mechanics and Heat Transfer*:199-216. doi: Book\_Do1 10.1017/Cbo9780511813177.
- Denn, Morton M. 2001. "Extrusion instabilities and wall slip." *Annual Review of Fluid Mechanics* no. 33 (1):265-287.
- Dong, Chunxu, John Cairney, Qunhui Sun, Orville Lee Maddan, Gaohong He, and Yulin Deng. 2009. "Investigation of Mg(OH)<sub>2</sub> nanoparticles as an antibacterial agent." *Journal of Nanoparticle Research* no. 12 (6):2101-2109. doi: 10.1007/s11051-009-9769-9.
- Dong, Chunxu, Gaohong He, Wenji Zheng, Tengfei Bian, Mo Li, and Dawei Zhang. 2014. "Study on antibacterial mechanism of Mg(OH)<sub>2</sub> nanoparticles." *Materials Letters* no. 134:286-289. doi: 10.1016/j.matlet.2014.07.110.
- Dong, Chunxu, Delong Song, John Cairney, Orville Lee Maddan, Gaohong He, and Yulin Deng. 2011. "Antibacterial study of Mg(OH)<sub>2</sub> nanoplatelets." *Materials Research Bulletin* no. 46 (4):576-582. doi: 10.1016/j.materresbull.2010.12.023.
- Drescher, K., Y. Shen, B. L. Bassler, and H. A. Stone. 2013a. "Biofilm streamers cause catastrophic disruption of flow with consequences for environmental and medical systems." *Proceedings of the National Academy of Sciences of the United States of America* no. 110 (11):4345-4350. doi: 10.1073/pnas.1300321110.
- Flemming, H. C., T. R. Neu, and D. J. Wozniak. 2007. "The EPS matrix: The "House of Biofilm cells"." *Journal of Bacteriology* no. 189 (22):7945-7947. doi: 10.1128/Jb.00858-07.

- Flemming, H. C., and J. Wingender. 2010a. "The biofilm matrix." *Nat Rev Microbiol* no. 8 (9):623-33. doi: 10.1038/nrmicro2415.
- Friedman, B. A., P. R. Dugan, R. M. Pfister, and C. C. Remsen. 1969. "Structure of Exocellular Polymers and Their Relationship to Bacterial Flocculation." *Journal of Bacteriology* no. 98 (3):1328-&.
- Fux, C. A., S. Wilson, and P. Stoodley. 2004. "Detachment characteristics and oxacillin resistance of *Staphylococcus aureus* biofilm emboli in an in vitro catheter infection model." *J Bacteriol* no. 186 (14):4486-91. doi: 10.1128/JB.186.14.4486-4491.2004.
- Gashti, Mazeyar Parvinzadeh, Julien Bellavance, Otini Kroukamp, Gideon Wolfaardt, Seyed Mohammad Taghavi, and Jesse Greener. 2015. "Live-streaming: Time-lapse video evidence of novel streamer formation mechanism and varying viscosity." *Biomicrofluidics* no. 9 (4):041101.
- Giorgi, Rodorico, Claudio Bozzi, Luigi Dei, Chiara Gabbiani, Barry W Ninham, and Piero Baglioni. 2005. "Nanoparticles of Mg (OH) 2: synthesis and application to paper conservation." *Langmuir* no. 21 (18):8495-8501.
- Hajnos, M., J. Lipiec, R. Świeboda, Z. Sokołowska, and B. Witkowska-Walczak. 2006. "Complete characterization of pore size distribution of tilled and orchard soil using water retention curve, mercury porosimetry, nitrogen adsorption, and water desorption methods." *Geoderma* no. 135:307-314. doi: <http://dx.doi.org/10.1016/j.geoderma.2006.01.010>.
- Hall-Stoodley, L., J. W. Costerton, and P. Stoodley. 2004. "Bacterial biofilms: from the natural environment to infectious diseases." *Nat Rev Microbiol* no. 2 (2):95-108. doi: 10.1038/nrmicro821.
- Hardoim, Pablo R., Leo S. van Overbeek, and Jan Dirk van Elsas. 2008. "Properties of bacterial endophytes and their proposed role in

- plant growth." *Trends in Microbiology* no. 16 (10):463-471. doi: <http://dx.doi.org/10.1016/j.tim.2008.07.008>.
- Hassanpourfard, Mahtab, Ranajay Ghosh, Thomas Thundat, and Alope Kumar. 2016. "Dynamics of bacterial streamers induced clogging in microfluidic devices." *Lab on a Chip* no. 16 (21):4091-4096. doi: 10.1039/C6LC01055E.
- Hassanpourfard, Mahtab, Zahra Nikakhtari, Ranajay Ghosh, Siddhartha Das, Thomas Thundat, Yang Liu, and Alope Kumar. 2015. "Bacterial floc mediated rapid streamer formation in creeping flows." *Scientific Reports* no. 5:13070. doi: 10.1038/srep13070  
<http://www.nature.com/articles/srep13070#supplementary-information>.
- Hassanpourfard, Mahtab, Xiaohui Sun, Amin Valiei, Partha Mukherjee, Thomas Thundat, Yang Liu, and Alope Kumar. 2014. "Protocol for Biofilm Streamer Formation in a Microfluidic Device with Micro-pillars." *JoVE (Journal of Visualized Experiments)* (90):e51732-e51732.
- Hassanpourfard, Mahtab, Amin Valiei, Thomas Thundat, Yang Liu, and Alope Kumar. 2014. Biofilm Streamer Formation in a Microfluidic Porous Media Mimic. Paper read at ASME 2014 International Mechanical Engineering Congress and Exposition.
- Henze, M. (Ed.). 2008. "Biological wastewater treatment: principles, modelling and design". IWA publishing.
- Hol, F. J. H., and C. Dekker. 2014. "Zooming in to see the bigger picture: Microfluidic and nanofabrication tools to study bacteria." *Science* no. 346 (6208):438-+. doi: 10.1126/Science.1251821.
- Jalasvuori, M., and E. V. Koonin. 2015. "Classification of prokaryotic genetic replicators: between selfishness and altruism." *Ann N Y Acad Sci* no. 1341:96-105. doi: 10.1111/nyas.12696.

- Jiao, C. M. 2006. "Flame Retardation of Ethylene-Vinyl Acetate Copolymer Using Nano Magnesium Hydroxide and Nano Hydrotalcite." *Journal of Fire Sciences* no. 24 (1):47-64. doi: 10.1177/0734904106053160.
- Karimi, A, D Karig, A Kumar, and AM Ardekani. 2015a. "Interplay of physical mechanisms and biofilm processes: review of microfluidic methods." *Lab on a Chip* no. 15:23-42. doi: 10.1039/C4LC01095G.
- Kasting, James F, and Janet L Siefert. 2002. "Life and the evolution of Earth's atmosphere." *Science* no. 296 (5570):1066-1068.
- Kim, M. K., K. Drescher, O. S. Pak, B. L. Bassler, and H. A. Stone. 2014. "Filaments in curved streamlines: rapid formation of *Staphylococcus aureus* biofilm streamers." *New Journal of Physics* no. 16:065024. doi: 10.1088/1367-2630/16/6/065024.
- Klapper, I., C. J. Rupp, R. Cargo, B. Purvedorj, and P. Stoodley. 2002. "Viscoelastic fluid description of bacterial biofilm material properties." *Biotechnology and Bioengineering* no. 80 (3):289-296. doi: 10.1002/bit.10376.
- Kochkodan, V., S. Tsarenko, N. Potapchenko, V. Kosinova, and V. Goncharuk. 2008. "Adhesion of microorganisms to polymer membranes: a photobactericidal effect of surface treatment with TiO<sub>2</sub>." *Desalination* no. 220 (1-3):380-385. doi: 10.1016/j.desal.2007.01.042.
- Kumar, A., D. Karig, R. Acharya, S. Neethirajan, P. P. Mukherjee, S. Retterer, and M. J. Doktycz. 2013. "Microscale confinement features can affect biofilm formation." *Microfluidics and Nanofluidics* no. 14 (5):895-902. doi: DOI 10.1007/s10404-012-1120-6.

- Lewandowski, Z., and P. Stoodley. 1995. "Flow induced vibrations, drag force, and pressure drop in conduits covered with biofilm." *Water Science and Technology* no. 32 (8):19.
- Lu, T. X., J. W. Biggar, and D. R. Nielsen. 1994. "Water movement in glass bead porous media: 1. Experiments of capillary rise and hysteresis." *Water Resources Research* no. 30 (12):3275-3281. doi: 10.1029/94WR00997.
- Maddan, O.L. 2014. Nanoplatelet metal hydroxides and methods of preparing same. Google Patents.
- Marty, A., C. Roques, C. Causserand, and P. Bacchin. 2012. "Formation of bacterial streamers during filtration in microfluidic systems." *Biofouling* no. 28 (6):551-62. doi: 10.1080/08927014.2012.695351.
- Marty, Aurélie, Christel Causserand, Christine Roques, and Patrice Bacchin. 2014. "Impact of tortuous flow on bacteria streamer development in microfluidic system during filtration." *Biomicrofluidics* no. 8 (1):014105.
- Mate, C. M., G. M. McClelland, R. Erlandsson, and S. Chiang. 1987. "Atomic-Scale Friction of a Tungsten Tip on a Graphite Surface." *Physical Review Letters* no. 59 (17):1942-1945. doi: DOI 10.1103/PhysRevLett.59.1942.
- Mercado-Blanco, J., and P. A. Bakker. 2007. "Interactions between plants and beneficial *Pseudomonas* spp.: exploiting bacterial traits for crop protection." *Antonie Van Leeuwenhoek* no. 92 (4):367-89. doi: 10.1007/s10482-007-9167-1.
- Mitchell, Andrew C., Adrienne J. Phillips, Randy Hiebert, Robin Gerlach, Lee H. Spangler, and Alfred B. Cunningham. 2009. "Biofilm enhanced geologic sequestration of supercritical CO<sub>2</sub>." *International Journal of Greenhouse Gas Control* no. 3 (1):90-99. doi: 10.1016/j.ijggc.2008.05.002.

- More, T. T., J. S. S. Yadav, S. Yan, R. D. Tyagi, and R. Y. Surampalli. 2014a. "Extracellular polymeric substances of bacteria and their potential environmental applications." *Journal of Environmental Management* no. 144:1-25. doi: 10.1016/j.jenvman.2014.05.010.
- Nanda, K. K., A. Maisels, F. E. Kruis, H. Fissan, and S. Stappert. 2003. "Higher Surface Energy of Free Nanoparticles." *Physical Review Letters* no. 91 (10). doi: 10.1103/PhysRevLett.91.106102.
- Neethirajan, S., D. Karig, A. Kumar, P. P. Mukherjee, S. Retterer, and M. Doktycz. 2012a. "Biofilms in Microfluidic Devices." In *Encyclopedia of Nanotechnology*, edited by B. Bhushan. New York: Springer.
- O'Toole, George A., and Roberto Kolter. 1998. "Initiation of biofilm formation in *Pseudomonas fluorescens* WCS365 proceeds via multiple, convergent signalling pathways: a genetic analysis." *Molecular Microbiology* no. 28 (3):449-461. doi: 10.1046/j.1365-2958.1998.00797.x.
- Okuda, K., T. Kato, and K. Ishihara. 2004. "Involvement of periodontopathic biofilm in vascular diseases." *Oral Diseases* no. 10 (1):5-12.
- Orejon, D., K. Sefiane, and M. E. R. Shanahan. 2011. "Stick-Slip of Evaporating Droplets: Substrate Hydrophobicity and Nanoparticle Concentration." *Langmuir* no. 27 (21):12834-12843. doi: 10.1021/la2026736.
- Pan, X., Y. Wang, Z. Chen, D. Pan, Y. Cheng, Z. Liu, Z. Lin, and X. Guan. 2013. "Investigation of antibacterial activity and related mechanism of a series of nano-Mg(OH)(2)." *ACS Appl Mater Interfaces* no. 5 (3):1137-42. doi: 10.1021/am302910q.
- Renner, L. D., and D. B. Weibel. 2011. "Physicochemical regulation of biofilm formation." *MRS Bull* no. 36 (5):347-355. doi: 10.1557/mrs.2011.65.

- Rusconi, R., M. Garren, and R. Stocker. 2014a. "Microfluidics Expanding the Frontiers of Microbial Ecology." *Annual Review of Biophysics* no. 43:65-91. doi: 10.1146/annurev-biophys-051013-022916.
- Rusconi, R., S. Lecuyer, N. Autrusson, L. Guglielmini, and H. A. Stone. 2011. "Secondary flow as a mechanism for the formation of biofilm streamers." *Biophys J* no. 100 (6):1392-9. doi: 10.1016/j.bpj.2011.01.065.
- Rusconi, R., S. Lecuyer, L. Guglielmini, and H. A. Stone. 2010a. "Laminar flow around corners triggers the formation of biofilm streamers." *Journal of the Royal Society Interface* no. 7 (50):1293-1299. doi: 10.1098/rsif.2010.0096.
- Saleh-Lakha, S., and J. T. Trevors. 2010. "Perspective: microfluidic applications in microbiology." *J Microbiol Methods* no. 82 (1):108-111. doi: 10.1016/j.mimet.2010.03.022.
- Salehizadeh, H., and S. A. Shojaosadati. 2001. "Extracellular biopolymeric flocculants: Recent trends and biotechnological importance." *Biotechnology Advances* no. 19 (5):371-385. doi: [http://dx.doi.org/10.1016/S0734-9750\(01\)00071-4](http://dx.doi.org/10.1016/S0734-9750(01)00071-4).
- Sen, R. 2008. "Biotechnology in petroleum recovery: The microbial EOR." *Progress in Energy and Combustion Science* no. 34 (6):714-724.
- Shaw, T., M. Winston, C. J. Rupp, I. Klapper, and P. Stoodley. 2004. "Commonality of Elastic Relaxation Times in Biofilms." *Physical Review Letters* no. 93 (9). doi: 10.1103/PhysRevLett.93.098102.
- Socoliuc, A., R. Bennewitz, E. Gnecco, and E. Meyer. 2004. "Transition from stick-slip to continuous sliding in atomic friction: entering a new regime of ultralow friction." *Phys Rev Lett* no. 92 (13):134301. doi: 10.1103/PhysRevLett.92.134301.
- Soleimani, S., P. J. Van Geel, O. B. Isgor, and M. B. Mostafa. 2009. "Modeling of biological clogging in unsaturated porous media." *J*

- Contam Hydrol* no. 106 (1-2):39-50. doi: 10.1016/j.jconhyd.2008.12.007.
- Stanley, Claire E., Guido Grossmann, Xavier Casadevall i Solvas, and Andrew J. deMello. 2016. "Soil-on-a-Chip: microfluidic platforms for environmental organismal studies." *Lab on a Chip* no. 16 (2):228-241. doi: 10.1039/C5LC01285F.
- Stewart, Philip S., and J. William Costerton. 2001. "Antibiotic resistance of bacteria in biofilms." *The Lancet* no. 358 (9276):135-138. doi: 10.1016/s0140-6736(01)05321-1.
- Stoodley, P., R. Cargo, C. J. Rupp, S. Wilson, and I. Klapper. 2002a. "Biofilm material properties as related to shear-induced deformation and detachment phenomena." *J. Ind. Microbiol. Biot.* no. 29 (6):361-367.
- Stoodley, P., R. Cargo, C. J. Rupp, S. Wilson, and I. Klapper. 2002b. "Biofilm material properties as related to shear-induced deformation and detachment phenomena." *J Ind Microbiol Biotechnol* no. 29 (6):361-7. doi: 10.1038/sj.jim.7000282.
- Stoodley, P., K. Sauer, D. G. Davies, and J. W. Costerton. 2002. "Biofilms as complex differentiated communities." *Annu Rev Microbiol* no. 56:187-209. doi: 10.1146/annurev.micro.56.012302.160705.
- Stoodley, Paul, John D. Boyle, Dirk DeBeer, and Hilary M. Lappin-Scott. 1999. "Evolving perspectives of biofilm structure." *Biofouling* no. 14 (1):75-90. doi: 10.1080/08927019909378398.
- Stoodley, Paul, Zbigniew Lewandowski, John D Boyle, and Hilary M Lappin-Scott. 1998. "Oscillation characteristics of biofilm streamers in turbulent flowing water as related to drag and pressure drop." *Biotechnology and bioengineering* no. 57 (5):536-544.

- Taherzadeh, D., C. Picioreanu, U. Kuttler, A. Simone, W. A. Wall, and H. Horn. 2010. "Computational Study of the Drag and Oscillatory Movement of Biofilm Streamers in Fast Flows." *Biotechnology and Bioengineering* no. 105 (3):600-610.
- Tomanek, D, W Zhong, and H Thomas. 1991. "Calculation of an atomically modulated friction force in atomic-force microscopy." *EPL (Europhysics Letters)* no. 15 (8):887.
- Ude, S., D. L. Arnold, C. D. Moon, T. Timms-Wilson, and A. J. Spiers. 2006. "Biofilm formation and cellulose expression among diverse environmental *Pseudomonas* isolates." *Environ Microbiol* no. 8 (11):1997-2011. doi: 10.1111/j.1462-2920.2006.01080.x.
- Vafai, Kambiz. 2010. *Porous media: applications in biological systems and biotechnology*: CRC Press.
- Valiei, A., A. Kumar, P. P. Mukherjee, Y. Liu, and T. Thundat. 2012a. "A web of streamers: biofilm formation in a porous microfluidic device." *Lab on a Chip* no. 12 (24):5133-5137. doi: 10.1039/C2lc40815e.
- Valiei, A., A. Kumar, P. P. Mukherjee, Y. Liu, and T. Thundat. 2012b. "A web of streamers: biofilm formation in a porous microfluidic device." *Lab Chip* no. 12 (24):5133-7. doi: 10.1039/c2lc40815e.
- Vidhyasekaran, P, and M Muthamilan. 1995. "Development of formulations of *Pseudomonas fluorescens* for control of chickpea wilt." *Plant disease* no. 79 (8):782-786.
- Vrouwenvelder, J. S., J. Buiters, M. Riviere, W. G. J. van der Meer, M. C. M. van Loosdrecht, and J. C. Kruithof. 2010a. "Impact of flow regime on pressure drop increase and biomass accumulation and morphology in membrane systems." *Water Research* no. 44 (3):689-702. doi: DOI 10.1016/j.watres.2009.09.054.
- Vrouwenvelder, J. S., J. Buiters, M. Riviere, W. G. van der Meer, M. C. van Loosdrecht, and J. C. Kruithof. 2010b. "Impact of flow

- regime on pressure drop increase and biomass accumulation and morphology in membrane systems." *Water Res* no. 44 (3):689-702. doi: 10.1016/j.watres.2009.09.054.
- Wang, S. Q., and P. A. Drda. 1996. "Superfluid-like stick-slip transition in capillary flow of linear polyethylene melts .1. General features." *Macromolecules* no. 29 (7):2627-2632. doi: Doi 10.1021/Ma950898q.
- Weaver, W. M., V. Milisavljevic, J. F. Miller, and D. Di Carlo. 2012. "Fluid flow induces biofilm formation in *Staphylococcus epidermidis* polysaccharide intracellular adhesin-positive clinical isolates." *Appl Environ Microbiol* no. 78 (16):5890-6. doi: 10.1128/AEM.01139-12.
- Weibel, D. B., W. R. Diluzio, and G. M. Whitesides. 2007. "Microfabrication meets microbiology." *Nat Rev Microbiol* no. 5 (3):209-18. doi: 10.1038/nrmicro1616.
- Whitesides, G. M. 2006. "The origins and the future of microfluidics." *Nature* no. 442 (7101):368-73. doi: 10.1038/nature05058.
- Whitesides, George M, and Abraham D Stroock. 2001. "Flexible methods for microfluidics." *Phys. Today* no. 54 (6):42-48.
- Whitfield, Chris. 1988. "Bacterial extracellular polysaccharides." *Can J Microbiol* no. 34 (4):415-420.
- Wingender, Jost, Thomas R Neu, and Hans-Curt Flemming. 1999. "What are bacterial extracellular polymeric substances?" In *Microbial extracellular polymeric substances*, 1-19. Springer.
- Wong, Gerard C. L., and George A. O'Toole. 2011. "All together now: Integrating biofilm research across disciplines." *MRS Bulletin* no. 36 (05):339-342. doi: 10.1557/mrs.2011.64.
- Wu, C., J. Y. Lim, G. G. Fuller, and L. Cegelski. 2012. "Quantitative Analysis of Amyloid-Integrated Biofilms Formed by

- Uropathogenic *Escherichia coli* at the Air-Liquid Interface." *Biophys. J.* no. 103 (3):464-471. doi: 10.1016/j.bpj.2012.06.049.
- Yazdi, S., and A. M. Ardekani. 2012a. "Bacterial aggregation and biofilm formation in a vortical flow." *Biomicrofluidics* no. 6 (4). doi: 10.1063/1.4771407.
- Yazdi, Shahrzad, and Arezoo M. Ardekani. 2012b. "Bacterial aggregation and biofilm formation in a vortical flow." *Biomicrofluidics* no. 6 (4):044114. doi: 10.1063/1.4771407.
- Yoshizawa, H., and J. Israelachvili. 1993. "Fundamental Mechanisms of Interfacial Friction .2. Stick-Slip Friction of Spherical and Chain Molecules." *Journal of Physical Chemistry* no. 97 (43):11300-11313. doi: Doi 10.1021/J100145a031.
- Zhang, S. L., and J. C. M. Li. 2003. "Slip process of stick–slip motion in the scratching of a polymer." *Materials Science and Engineering: A* no. 344 (1–2):182-189. doi: [http://dx.doi.org/10.1016/S0921-5093\(02\)00409-4](http://dx.doi.org/10.1016/S0921-5093(02)00409-4).
- Zuber, Sophie, Fiona Carruthers, Christoph Keel, Alexandre Mattart, Caroline Blumer, Gabriella Pessi, Cécile Gigot-Bonnefoy, Ursula Schnider-Keel, Stephan Heeb, and Cornelia Reimann. 2003. "GacS sensor domains pertinent to the regulation of exoproduct formation and to the biocontrol potential of *Pseudomonas fluorescens* CHA0." *Molecular plant-microbe interactions* no. 16 (7):634-644.